Analysis of Buoy Measurements in the Laboratory and Field

Zhaoxian Lin

Somerville College
University of Oxford

A thesis submitted for the degree of
Master of Science by Research

Trinity 2022

Abstract

Wave following buoys, which are widely deployed across the oceans, offer the potential to measure various wave properties. However, some aspects of buoy measurements are still not fully studied. Knowing the accuracy of buoy measurements and affecting factors of accuracy is essential. This thesis first assesses the accuracy of directional spreading estimates made using buoy measurements. The influence moorings may have on buoy measurements was then investigated.

In the first part of the thesis, directional spreading estimates are compared based on experimentally obtained buoy and wave gauge measurements. Experiments with both following (unimodal in direction) and crossing (bimodal in direction) sea states are examined. In addition to this, synthetic wave data are used to investigate the effects of wave generation and nonlinearity on spreading estimates. The results show that while directional estimates produced using buoy measurements are reasonably accurate in following sea states, they struggle to identify distinct directional peaks in crossing sea states.

The second part of the thesis looks at the effects moorings may have on buoy measurements made in the field. Sea states with similar statistics have been collected and investigated. It is found find that while moorings have no observable effects on buoy measurements for the majority of parameters, they may affect the directional spreading estimates.

Analysis of Buoy Measurements in the Laboratory and Field



Zhaoxian Lin

Somerville College

University of Oxford

A thesis submitted for the degree of

Master of Science by Research

Trinity 2022

Acknowledgements

Firstly, I would like to express my sincere gratitude to my supervisors, Prof. Thomas Adcock and Dr. Mark McAllister for their continued support and patience throughout this project. Without their help, this thesis would not have been possible.

I would also like to thank my friends for their encouragement during my studies. Finally, I am grateful for my family, whose constant love and trust keep me motivated. Thank you all for the strength you gave me.

Abstract

Wave following buoys, which are widely deployed across the oceans, offer the potential to measure various wave properties. However, some aspects of buoy measurements are still not fully studied. Knowing the accuracy of buoy measurements and affecting factors of accuracy is essential. This thesis first assesses the accuracy of directional spreading estimates made using buoy measurements. The influence moorings may have on buoy measurements was then investigated.

In the first part of the thesis, directional spreading estimates are compared based on experimentally obtained buoy and wave gauge measurements. Experiments with both following (unimodal in direction) and crossing (bimodal in direction) sea states are examined. In addition to this, synthetic wave data are used to investigate the effects of wave generation and nonlinearity on spreading estimates. The results show that while directional estimates produced using buoy measurements are reasonably accurate in following sea states, they struggle to identify distinct directional peaks in crossing sea states.

The second part of the thesis looks at the effects moorings may have on buoy measurements made in the field. Sea states with similar statistics have been collected and investigated. It is found find that while moorings have no observable

effects on buoy measurements for the majority of parameters, they may affect the directional spreading estimates.

Contents

List of Figures **viii**

Nomenclature **xiii**

1 Introduction **1**

1.1 Introduction 2

1.1.1 Linear waves 3

1.1.2 Stokes waves 4

1.2 Wave Spectrum 4

1.2.1 Frequency spectrum 5

1.2.2 Directional spectrum 7

1.3 Directional Wave Analysis Methods 11

1.3.1 Phase-Time-Path-Difference Approach (PTPD) 12

1.3.2 Maximum Entropy Method (MEM) 14

1.3.3 Bayesian Directional Method (BDM) 16

1.3.4 Extended Maximum Entropy Principle (EMEP) 17

1.3.5 Iterative Maximum Likelihood Method (IMLM) 18

1.3.6 Other Methods 20

1.4 Wave Measurement Techniques 21

1.4.1 Wave Gauges 21

1.4.2 Wave Buoys 23

1.4.3 Other Measurement Techniques 23

1.5 Comparison of Buoys and Gauges 24

1.5.1 Wave crest statistics 25

1.5.2 Directional Spreading 26

1.6 Mooring 28

1.6.1 Mooring effects 29

2 Spreading **31**

2.1 Chapter overview 31

2.2 Methods 32

2.2.1 Experimental setup 32

2.2.2 Directional estimation methods 39

2.2.3 Synthetic wave data 44

2.3 Results 47

2.3.1 Following sea states 47

2.3.2 Crossing sea states 56

2.3.3 Mooring configuration 59

2.4 Conclusions 61

3 Mooring influence on wave measurement **66**

3.1 Chapter overview 66

3.2 Introduction 69

3.2.1 Mooring configuration 69

3.2.2 Study site 69

3.2.3 Mooring distance 69

3.3 Data selection and quality control 71

3.4 Measured Wave Statistics 74

3.4.1 Spreading 78

3.5 Conclusions 84

4 Conclusion **89**

References **92**

List of Figures

1.1 Example of frequency spectrum and directional spectrum 5

1.2 Polar plots of Directional spectrum estimated by various conventional methods 19

1.3 Wave gauge array 21

1.4 DWR MKIII WAVERIDER BUOY 22

1.5 The typical mooring for buoy 29

2.1 Schematic diagram of wave basin, and gauge and mean buoy positions 32

2.2 Separation of all possible wave gauge pairs normalised by peak wavelength λ_p 34

2.3 EMEP estimates of directional spreading width σ_θ as a function of normalised frequency f/f_p, based on synthetic gauge and buoy data created using double (DSM) and single (SSM) summation wave generation 38

2.4 Estimates of directional spreading width σ_θ as a function of normalised frequency f/f_p based on synthetic buoy data, calculated using different methods 40

2.5 EMEP estimates of spreading width σ_θ as a function of normalised frequency f/f_p, calculated by two methods and spreading distribution at $f/f_p = 1.5$ 44

2.6 EMEP estimates of directional spreading width σ_θ as a function of normalised frequency f/f_p, and mean directional spreading distribution based on SSM synthetic linear and second-order gauge data 46

2.7 PTPD estimates of spreading width σ_θ as a function of normalised frequency f/f_p based on experimental gauge measurements with various degree of spreading 48

2.8 EMEP estimates of spreading for experimental gauge and buoy measurements with input $H_s = 0.225$ and degree of spreading $\sigma_\theta = 14.14°$ 50

2.9 EMEP estimates of spreading based on buoy measurements for the same experiments carried out with two values of significant wave height $H_s = 0.225$ m and $H_s = 0.175$ m 52

2.10 EMEP estimates of spreading width σ_θ as a function of normalised frequency f/f_p for synthetic buoy data with no noise and 10% noise 53

2.11 EMEP estimates of spreading for experimental gauge and buoy measurements with input $H_s = 0.225$ m and various degree of spreading 55

2.12 Polar plots of input and estimated (EMEP) directional spectra for experiments with various input directional spreading width and $H_s = 0.225$m 56

2.13 EMEP estimates of spreading for crossing experiments based on gauge and buoy measurements with input $H_s = 0.225$ m and degree of spreading $\sigma_\theta = 14.14°$ and crossing angle $\Delta\theta = 90°$ 57

2.14 Two buoy mooring configurations 58

2.15 EMEP estimates of spreading width σ_θ as a function of normalised frequency f/f_p for experimental buoy measurements made with taut and slack mooring configurations with input $H_s = 0.225$ m and various degree of spreading 60

2.16 Polar plots of input and estimated (EMEP) directional spectra for experimental buoy measurements made with taut and slack mooring configurations with various input directional spreading width and significant wave height $H_s = 0.225$m 61

3.1 Overview map of CDIP buoy deployment 67

3.2 The typical buoy and mooring package for CDIP with water depth larger than 200 m 68

3.3 Schematic diagram of the mooring distance 71

3.4 GPS path for in situ buoy measurements made using the Datawell Waverider buoy (71) moored beside Harvest in the North Pacific from 2002 to 2019 72

3.5 Crest height exceedance probability for in situ buoy measurements made using stations 94, 157, 29 and 71 with sea states $H_s \approx 3.5m$, $\theta_p \approx 300^\circ$ and $T_p \approx 10s$ 74

3.6 The root mean square differences between the probability of exceedance for Rayleigh distribution and estimated crest distribution for buoy stations 94, 157, 29 and 71 76

3.7 Skewness, kurtosis and standard deviation of horizontal displacements with in situ buoy measurements made using the station 94, 157, 29 and 71 for various mooring distances. 77

3.8 Comparison of significant wave height between in situ buoy measurements and ECMWF hindcast 79

3.9 Directional spreading for in situ buoy measurements made using the station 94, 157, 29, 71 and ECMWF hindcast from 2002 to 2019 as a time series 82

3.10 Directional spreading for in situ buoy measurements made using the station 94, 157, 29, 71 from 2002 to 2019 as a function of a time series for original data and fixed data 84

3.11 Directional spreading for in situ buoy measurements made using the station 94, 157, 29, 71 and ECMWF hindcast from 2002 to 2019 as a function of normalized mooring distance 85

3.12 The average difference between directional spreading width estimated using field and ECMWF hindcast data for buoy stations 86

3.13 The mean significant wave heights for buoy stations 87

Nomenclature

a . . . . . (m).

a_n . . . . . Lagrange multipliers.

A . . . . . Wave amplitude (m).

A_n . . . . . Fourier coefficient (rad).

b_n . . . . . Lagrange multipliers.

B_n . . . . . Fourier coefficient (rad).

d . . . . . Water depth (m).

d_m . . . . . Mooring distance (m).

$D(f, \theta)$ . . . . . Directional spreading function (rad^{-1}).

F_s . . . . . Velocity Reduction Factor.

e_i . . . . . Error.

E_0 . . . . . Total energy in wave spectrum.

$E(f)$ . . . . . Frequency spectrum $(m^2 s)$.

f_p . . . . . Peak frequency (Hz).

g . . . . . Gravity (ms^{-2}).

H . . . . . Transfer function for cross power spectrum.

H_s . . . . . Significant wave height (m).

$\imath$ . . . . . $\sqrt{-1}$.

I . . . . . Entropy (rad^{-1}).

k . . . . . Wavenumber (m^{-1}).

k_p . . . . . Wavenumber for peak period (m^{-1}).

m_n . . . . . The n_{th} spectral moment $(m^2 s^{-n})$.

N_z . . . . . Number of zero up crossing period.

R . . . . . Mooring watch radius (m).

s . . . . . Spreading parameter $(.deg^{-2})$.

$S(f, \theta)$ . . . . . Directional spectrum $(m^2 rad^{-1} s)$.

T_p . . . . . Peak period (s).

T_z . . . . . Mean zero up crossing period (s).

u . . . . . Velocity of wave in mean wave direction (ms^{-1}).

u_x . . . . . Velocity of water particles in x direction (ms^{-1}).

u_y . . . . . Velocity of water particles in y direction (ms^{-1}).

u_z . . . . . Velocity of water particles in z direction (ms^{-1}).

v . . . . . Velocity of wave in the direction perpendicular to mean wave direction (ms^{-1}).

α . . . . . Transfer parameter.

χ . . . . . Transfer parameter.

η . . . . . Free surface elevation (m).

η_c . . . . . Crest height (m).

ϕ . . . . . Velocity potential $(m^2 s^{-1})$.

ω . . . . . Angular frequency (rad s^{-1}).

ϵ . . . . . Phase (rad).

Λ . . . . . Phase difference (rad).

γ . . . . . Peak enhancement factor.

Δf . . . . . Frequency bin (s).

$\Delta\theta$ . . . . . Direction bin $(.deg)$.

γ . . . . . Peak enhancement factor.

β . . . . . Phillips constant.

θ_m . . . . . Mean wave direction $(.deg)$.

θ_p . . . . . Peak direction $(.deg)$.

$\Phi_{mn}(f)$ . . . . . Cross power spectrum of m^{th} and n^{th} wave measurements.

ρ . . . . . Density $(m^{-3}kg)$.

σ . . . . . Standard deviation.

$\overline{\sigma_\theta}$ . . . . . Mean directional spreading ($.deg$).

σ_θ . . . . . Directional spreading ($.deg$).

λ_p . . . . . Wave length for peak period.

λ_3 . . . . . Skewness.

λ_4 . . . . . Kurtosis.

List of abbreviations

BDM . . . . . Bayesian Directional Method.

CDIP . . . . . Coastal Data Information Program.

DFT . . . . . Discrete Fourier Transform.

DSM . . . . . Double Summation Method.

ECMWF . . . European Centre for Medium-range Weather Forecasts.

EMEP . . . . . Extended Maximum Entropy Principle.

EMLM . . . . Extended Maximum Likelihood Method.

IMLM . . . . . Iterative Maximum Likelihood Method.

JONSWAP . . Joint North Sea WAve Programme.

MEM . . . . . Maximum Entropy Method.

MLM . . . . . Maximum Likelihood Method.

NDCB . . . . . National Data Buoy Center.

PTPD . . . . . Phase Time Path Difference.

RMS . . . . . Root Mean Square.

SBWR . . . . Ship Borne Wave Recorder.

SSM . . . . . Single Summation Method.

SWIM . . . . . Surface Waves Investigation and Monitoring.

WFS . . . . . Weighted Fourier Series.

1 Introduction

Contents

1.1 Introduction 2
1.1.1 Linear waves 3
1.1.2 Stokes waves 4
1.2 Wave Spectrum 4
1.2.1 Frequency spectrum 5
1.2.2 Directional spectrum 7
1.3 Directional Wave Analysis Methods 11
1.3.1 Phase-Time-Path-Difference Approach (PTPD) 12
1.3.2 Maximum Entropy Method (MEM) 14
1.3.3 Bayesian Directional Method (BDM) 16
1.3.4 Extended Maximum Entropy Principle (EMEP) 17
1.3.5 Iterative Maximum Likelihood Method (IMLM) 18
1.3.6 Other Methods 20
1.4 Wave Measurement Techniques 21
1.4.1 Wave Gauges 21
1.4.2 Wave Buoys 23
1.4.3 Other Measurement Techniques 23
1.5 Comparison of Buoys and Gauges 24
1.5.1 Wave crest statistics 25
1.5.2 Directional Spreading 26
1.6 Mooring 28
1.6.1 Mooring effects 29

1.1 Introduction

Waves produce the dominant environmental forces on many offshore structures. They are one of the most important environmental factors for design. It is essential for engineers to understand wave statistics before designing and placing structures. For example, the forces exerted on slender structures like monopiles and pile-supported wharfs are related to wave-induced velocities and accelerations. The highest crest elevations are important for structures with decks where wave forces will rise dramatically if the waves impact on their decks. For floating structures, like wave energy converters, it is crucial to collect wave statistics to determine the dynamic responses and efficiency of energy conversion. To understand waves it is vital to measure their properties. This thesis looks at different wave measurement techniques. In particular, the performance of wave buoys will be thoroughly investigated.

In this thesis, a Cartesian coordinate system is chosen with the origin at the still water surface and z axis pointing vertically upwards. The classic water wave problem is formulated through the kinematic and dynamic boundary conditions applied here to Laplace's equation (Tucker and Pitt, 2001).

The kinematic boundary condition, at water surface, is that water particles on the surface should not leave the surface, which means the velocity of water particles normal to water surface is equal to that of surface,

$$u_z = \frac{\partial \eta}{\partial t} + u_x \frac{\partial \eta}{\partial x} + u_y \frac{\partial \eta}{\partial y} \quad \text{on} \quad z = \eta, \tag{1.1}$$

where η denotes the free surface, u_x, u_y and u_z are the fluid velocity in x, y and z directions. At the bottom ($z = -d$), the kinematic boundary condition states that the water particle cannot penetrate the seabed,

$$u_z = 0. \tag{1.2}$$

Finally, the dynamic boundary condition describes that the pressure at surface is constant, taking pressure p=0,

$$g\eta + \frac{\partial \phi}{\partial t} + \frac{1}{2}\left(u_x^2 + u_y^2 + u_z^2\right) = 0 \quad \text{on} \quad z = \eta, \tag{1.3}$$

where g is the gravitational acceleration and ϕ is the velocity potential.

1.1.1 Linear waves

In linear theory, the surface boundary conditions are approximated by evaluating them at $z = 0$ rather than at the true free surface, η. Considering only linear terms of the boundary conditions gives the linear solution of a propagating wave,

$$\eta(x, t) = A\cos(\mathbf{k} \cdot \mathbf{x} - \omega t), \tag{1.4}$$

where A is wave amplitude, ω and $|\mathbf{k}|$ are angular frequency and wavenumber, respectively, which follow the linear dispersion relationship,

$$\omega^2 = |\mathbf{k}| g \tanh(|\mathbf{k}| d), \tag{1.5}$$

where d is the water depth.

1.1.2 Stokes waves

The above solution linearises the nonlinear boundary conditions. This approximation is only valid for small amplitude waves. Actual surface gravity waves have taller crests and flatter troughs than purely harmonic profiles. Higher harmonics can be added to the basic linear form of a monochromatic wave (Stokes, 1880).

The second-order Stokes wave propagating in x direction can be written,

$$\eta(x,t) = A\cos(\omega t - kx) + kA^2 \frac{\cosh(kd)}{4\sinh^3(kd)}[2 + \cosh(2kd)]\cos[2(\omega t - kx)]. \tag{1.6}$$

The first term on the right hand side is fundamental harmonic wave and the second term is second-order 'correction'. The Stokes theory can be continued up to third order correction and higher correction (e.g. Fenton (1985)), or applied to multi-chromatic waves (e.g. Dalzell (1999)).

1.2 Wave Spectrum

The random phase/amplitude model can be used to describe linear multi-chromatic surface elevation η, where η is the summation of a large number of harmonic waves,

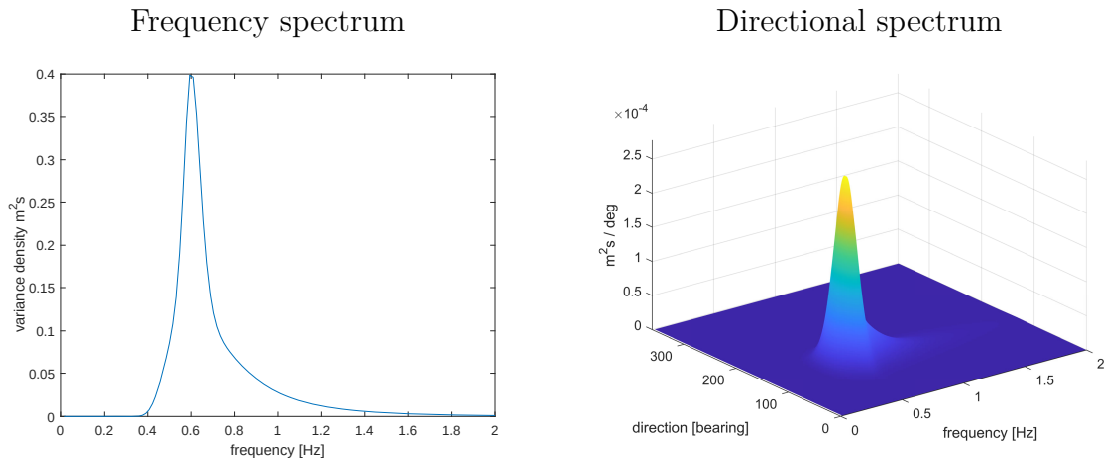


Figure 1.1: Example of frequency spectrum and directional spectrum

$$\eta(x, y, t) = \sum_{q=1}^{N} \sum_{p=1}^{M} A_{p,q} \cos\left(\varphi_{p,q}\right), \tag{1.7}$$

where

$$\varphi_{p,q} = k_p \left(x \cos\theta_q + y \sin\theta_q\right) - \omega_p t + \epsilon_{p,q}, \tag{1.8}$$

where $\epsilon_{p,q}$ is the phase chosen from a uniform distribution between 0 and 2π. ω_p is angular frequency, θ_q is direction, k_p is wavenumber and $a_{p,q}$ is the amplitude for each component. The frequency spectrum is the function of frequency, $E(f)$, showing wave energy at each frequency, whereas directional spectrum $S(f, \theta)$ describes wave energy at each frequency and direction. Figure 1.1 gives an example of these two spectra.

1.2.1 Frequency spectrum

A definition of discrete frequency spectrum $E(f)$ is given by,

$$E\left(f_n\right) = \frac{A_n^2}{2\Delta f}, \tag{1.9}$$

where Δf is the size of frequency bin in the discrete spectrum. Parameters such as peak frequency and significant wave height H_s (approximately the mean values of the highest 1/3 of wave height (Tucker and Pitt, 2001)), can be found using this spectrum. The significant wave height can be calculated as,

$$H_s = 4\sqrt{m_0}, \tag{1.10}$$

where

$$m_0 = \sum_n^M E(f_n)\Delta f, \tag{1.11}$$

M indicates the number of frequency components in the spectrum $E(f)$. A continuous frequency spectrum can be obtained by making the width of the frequency band Δf approach zero and the above parameters (H_s and m_0) can be calculated from the continuous frequency spectrum. Note that H_s is approximately equal to H_{m_0} for a sea state whose spectrum only contains a narrow band of frequency. For typical sea states, H_s is smaller than H_{m_0}.

In the real ocean, there are two typical sea states, wind seas and swell seas which have been modelled using spectra by many authors (Hasselmann et al., 1973; Pierson and Moskowitz, 1964; Gibbs and Taylor, 2005). The wind seas are generated by wind directly moving over water, whose energy spreads in a wide

frequency range. The joint North Sea wave programme (JONSWAP) spectrum is most widely used for wind sea states,

$$E(f) = \beta g (2\pi)^{-4} f_p^{-(5+n)} f^n \exp\left[\frac{n}{4}\left(\frac{f_p}{f}\right)^{-4}\right] \times \gamma^{\exp\left[-(f-f_p)^2/2\sigma^2 f_p^2\right]}, \tag{1.12}$$

where β is Phillips constant, which scales the spectrum to get the desired significant wave height H_s. γ is the peak enhancement factor, f_p is the peak frequency, $n = -5$, $\sigma\,(f \leq f_p) = 0.07$ and $\sigma\,(f > f_p) = 0.09$.

Pierson-Moskowitz spectrum is another popular spectrum approximating wind sea states and is a limiting case of the JONSWAP. Swell waves are waves that have propagated beyond the area where they were generated and typically have narrow spectral bandwidth compared to wind sea states. The measured swell spectra also can be well described by JONSWAP (Lucas and Soares, 2015).

1.2.2 Directional spectrum

The directional spectrum describes the distribution of energy as a function of direction of propagation and frequency of a given sea state. A similar definition to frequency spectrum, directional spectrum $S(f, \theta)$ can be given by,

$$S\,(f_p, \theta_q) = \frac{A_{p,q}^2}{2\Delta f \Delta\theta}, \tag{1.13}$$

where A_{pq} is the wave amplitude corresponding to frequency p and direction q. Δf and $\Delta\theta$ are sizes of frequency and direction bins in the discrete spectrum, respectively. The directional spreading function $D(f, \theta)$ is introduced here, which

represents energy distribution with θ at frequency f, which relates to the frequency spectrum and directional spectrum as,

$$S(f_p, \theta_q) = E(f_p)D(f_p, \theta_q), \tag{1.14}$$

and it follows the definition that,

$$\sum_{q}^{N} D(f_p, \theta_q)\Delta\theta = 1, \tag{1.15}$$

where N indicates all the direction components at frequency f_p.

Various forms of $D(f, \theta)$ are suggested in the literature (Cartwright, 1961; Tucker and Pitt, 2001; Veritas, 2000). A Fourier series form is one approximation used to express $D(f, \theta)$ (Tucker and Pitt, 2001),

$$D(f, \theta) = \frac{1}{\pi}\left\{\frac{1}{2} + \sum_{n=1}^{\infty}\left[A_n(f)\cos n\theta + B_n(f)\sin n\theta\right]\right\}, \tag{1.16}$$

where

$$\begin{aligned} A_n(f) &= \int_{-\pi}^{\pi} D(f, \theta)\cos n\theta \mathrm{d}\theta, \\ B_n(f) &= \int_{-\pi}^{\pi} D(f, \theta)\sin n\theta \mathrm{d}\theta. \end{aligned} \tag{1.17}$$

The averaged wave direction θ_m and directional spreading σ_θ, which is a measure of how wave energy for a given sea state is spread as a function of direction of propagation, can be expressed using above Fourier coefficients (Kuik et al., 1988),

$$\theta_m(f) = \arctan\left(\frac{A_1(f)}{B_1(f)}\right), \tag{1.18}$$

and

$$\sigma_\theta(f) = \sqrt{2\left[1 - \sqrt{A_1^2(f) + B_1^2(f)}\right]}, \tag{1.19}$$

An alternative form of $D(f,\theta)$ can be expressed in a parametric way (Cartwright, 1961),

$$D(f,\theta) = a(s)\cos^{2s(f)}\left(\frac{\theta - \theta_m(f)}{2}\right), \tag{1.20}$$

where θ_m is mean direction for each frequency, a is a scaling factor required to satisfy Eq.(1.15). s is a function of frequency and determines the level of spreading, which can be converted to σ_θ (Tucker and Pitt, 2001),

$$s = \frac{2}{\sigma_\theta^2} - 1. \tag{1.21}$$

Another expression of $D(f,\theta)$ can be given in the form of Gaussian distribution,

$$D(f,\theta) = \frac{a(\sigma_\theta)}{\sqrt{2\pi}\sigma_\theta(f)} \sum_{n=-\infty}^{\infty} \exp\left[-\frac{(\theta - \theta_m(f) + 2\pi n)^2}{2\sigma_\theta^2(f)}\right], \tag{1.22}$$

where θ_m is again mean direction and σ_θ is the frequency-dependent directional spreading.

In this thesis, the directional spreading function is assumed independent of frequency to simplify the analysis. However, this is not the case in the real ocean. The spreading typically varies with frequency and is narrower at the peak frequency and bimodal at high frequencies (Mitsuyasu et al., 1975; Hasselmann et al., 1980).

Wave Spreading Factor

The Wave Spreading Factor F_s is another parameter which can represent the directional effects on kinematics. It is the reduction in inline velocity related to a uni-directional sea state and is used in wave and structure interaction problems. It is given by (Tucker and Pitt, 2001),

$$F_s = \left[\frac{\overline{u^2}}{\overline{u^2} + \overline{v^2}}\right]^{\frac{1}{2}}, \tag{1.23}$$

where u is component horizontal velocity along the mean wave direction and v is perpendicular to it. The relationship of F_s to the spreading factor used in the standard directional spreading function can be established as below,

$$F_s(f) = \left[\frac{s^2 + s + 1}{(s+1)(s+2)}\right]^{\frac{1}{2}}, \tag{1.24}$$

where s is parameter on Eq.(1.21) and,

$$F_s(f) = \left[\frac{1}{2} + \frac{1}{2}\exp\left(-2\sigma_\theta^2\right)\right]^{\frac{1}{2}}, \tag{1.25}$$

where σ_θ is directional spreading.

Multi-modal sea states

Uni-modal sea states are characterized by the presence of only one peak of energy in the directional spectrum whereas multi-modal sea states have more than one peak. It is important to note that the form of directional spreading function (DSF)

on Eq.(1.20) and Eq.(1.22) is assumed as uni-modal. The form can be extended to bi-modal by superimposing multiple spreading functions of the same forms. The example of Eq.(1.22) is shown below,

$$D_{\sigma_{\theta 1},\theta_{m1},\sigma_{\theta 2},\theta_{m2},\lambda}(f,\theta) = \lambda D_{\sigma_{\theta 1},\theta_{m1}}(f,\theta) + (1-\lambda) D_{\sigma_{\theta 2},\theta_{m2}}(f,\theta) \quad \text{with } 0 \leq \lambda \leq 1, \tag{1.26}$$

with,

$$D_{\sigma_\theta,\theta_m}(f,\theta) = \frac{a(\sigma_\theta)}{\sqrt{2\pi}\sigma_\theta(f)} \sum_{n=-\infty}^{\infty} \exp\left[-\frac{(\theta - \theta_m(f) + 2\pi n)^2}{2\sigma_\theta^2(f)}\right] \quad \text{if } \theta \in [\theta_m - \pi; \theta_m + \pi], \tag{1.27}$$

The common approach to analyse such sea states is decomposing the observed spectrum into different wave systems and then modelling each system by using the standard spectral shapes (Boukhanovsky and Soares, 2009; Soares, 1984), and this is often the case in the real seas, where wind sea and swell occur at the same areas.

1.3 Directional Wave Analysis Methods

The conventional method to derive directional spreading function from data is to use the cross power spectrum. The fundamental relationship between above parameters can be expressed as (Isobe et al., 1984),

$$\Phi_{m,n}(f) = \int_0^{2\pi} H_m(f,\theta) H_n^*(f,\theta) E(f) D(f,\theta) \times \exp\left\{-ik\left(x_{m,n}\cos\theta + y_{m,n}\sin\theta\right)\right\} \mathrm{d}\theta, \tag{1.28}$$

where $\Phi_{m,n}(f)$ is cross power spectrum of observed properties between m^{th} and n^{th} wave measurements, $H_m(f,\theta)$ is transfer function from surface elevation to other wave properties, $E(f)$ is frequency spectrum and $*$ denotes complex conjugate. $x_{m,n}$ and $y_{m,n}$ represent the distances between m^{th} and n^{th} wave measurements. $D(f,\theta)$ is the directional spreading function, which describes the distribution of energy as a function of direction and frequency (Benoit et al., 1997). The transfer function can be expanded as,

$$H_m(f,\theta) = h_m(f)\cos^{\alpha_m}\theta \sin^{\chi_m}\theta. \tag{1.29}$$

The parameters of $h_m(f)$, α_m and χ_m are derived from linear wave potential function and those corresponding to specific wave properties are listed in table 1.1, where d is water depth, ρ is fluid density and $\imath$ is imaginary number.

1.3.1 Phase-Time-Path-Difference Approach (PTPD)

The Phase-Time-Path-Difference approach is used to calculate the wave direction (Esteva, 1977) for each frequency. The fundamental principle is that the phase difference between pairs of gauges is a function of the relative gauge locations and the frequency-dependent wavelength. Therefore, the phase difference for a given frequency f_i can be represented as,

Table 1.1: Transfer function based on linear wave theory

Measured property	Symbol	$h(f)$	α	χ
Water surface elevation	η	1	0	0
Pressure	p	$\rho g \frac{\cosh kz}{\cosh kd}$	0	0
Surface slope (x)	η_x	$\imath k$	1	0
Surface Slope (y)	η_y	$\imath k$	0	1
Water Particle velocity (x)	u_x	$\omega \frac{\cosh kz}{\sinh kd}$	1	0
Water Particle velocity (y)	u_y	$\omega \frac{\cosh kz}{\sinh kd}$	0	1
Water Particle velocity (z)	u_z	$-\omega \frac{\cosh kz}{\sinh kd}$	0	0
Displacement (x)	X	$\imath \frac{\cosh kz}{\sinh kd}$	1	0
Displacement (y)	Y	$\imath \frac{\cosh kz}{\sinh kd}$	0	1

$$\Lambda_{i,12} = k_i \left[(x_1 - x_2) \cos\theta_i + (y_1 - y_2) \sin\theta_i \right], \tag{1.30}$$

where $\Lambda_{i,12}$ is phase difference between location (x_1, y_1) and (x_2, y_2) at frequency f_i. k_i is wave number and θ_i is wave direction at given frequency f_i. Measurements at three locations allow, in principle, direction to be determined uniquely. The method as used for directional spectra requires that waves only propagate in a single direction at each frequency (Draycott et al., 2015). Directional spectra can be reconstructed by averaging over frequency bands. Wave direction is calculated using the following equation (Draycott et al., 2015),

$$\theta_{i,m} = \tan^{-1} \frac{\left[\left(x_{m,1} - x_{m,2}\right) \Lambda_{i,13} - \left(x_{m,1} - x_{m,3}\right) \Lambda_{i,12}\right] / \operatorname{sgn}\left(Q_m\right)}{\left[\left(y_{m,1} - y_{m,3}\right) \Lambda_{i,12} - \left(y_{m,1} - y_{m,2}\right) \Lambda_{i,13}\right] / \operatorname{sgn}\left(Q_m\right)}, \tag{1.31}$$

where $\theta_{i,m}$ is wave direction corresponding to each triad m and all frequency components i. $\Lambda_{i,12}$ is relative phases between two locations and Q_m is defined as,

$$Q_m = \left[\left(x_{m,1} - x_{m,2}\right)\left(y_{m,1} - y_{m,3}\right) - \left(x_{m,1} - x_{m,3}\right)\left(y_{m,1} - y_{m,2}\right)\right]. \tag{1.32}$$

Although the PTPD approach has proved to be an effective estimation method in specific experiments (Draycott et al., 2015), this method cannot be applied to conditions where waves travel in different directions at each frequency, for example in the ocean and when waves are generated using the double summation method in a wave tank.

1.3.2 Maximum Entropy Method (MEM)

The directional spreading function $D(f, \theta)$ (which satisfies Eq.(1.15)) may be regarded as a probability density function. The maximum entropy method originates in probability theory (Jaynes, 1957), and is used to determine a probability density function for a given set of observations and constraints. A solution that maximizes entropy is determined to be the best estimate of the true probability density function. The entropy I of directional spreading function is expressed as (Lygre and Krogstad, 1986),

$$I = \int_{-\pi}^{\pi} -D(f, \theta) \cdot \ln D(f, \theta) \mathrm{d}\theta, \tag{1.33}$$

where $D(f,\theta)$ is the directional spreading function. The relationship of observed wave properties and directional spreading function on Eq.(1.28) gives the constraints to determine spreading function.

The solution of the spreading function can be produced by maximising the entropy function with input data (Lygre and Krogstad, 1986),

$$D(f,\theta) = \exp\left\{a_0(f) + \sum_{n=1}^{2}\left[a_n(f)\cdot\cos(n\theta) + b_n(f)\cdot\sin(n\theta)\right]\right\}, \tag{1.34}$$

with

$$a_0(f) = -\ln\left\{\int_0^{2\pi}\exp\left\{\sum_{n=1}^{2}\left[a_n(f)\cdot\cos(n\theta) + b_n(f)\cdot\sin(n\theta)\right]\right\}\mathrm{d}\theta\right\}, \tag{1.35}$$

where a_n and b_n are unknown Lagrange multipliers determined by nonlinear equations to ensure the estimated spreading function is consistent with the measured cross spectra. It is hard to solve the above nonlinear equations analytically, so an iterative technique, namely the Newton-Raphson procedure, is applied to simplify the problem.

This estimation approach was only applied to three-quantity measurements (three measured wave properties) initially, then extended to multi-quantity measurements (Nwogu, 1989). The MEM method often provides good estimates of the spreading function, but tuning is required with field data in certain cases (Benoit, 1993). For large data sets, computation time can be an issue, and the method can be difficult to implement effectively.

1.3.3 Bayesian Directional Method (BDM)

The MEM method tries to fit a spreading function model such that it estimates the mathematical relationship between observed wave properties and the directional spectrum on Eq.(1.28) and maximize the defined entropy (see Eq.(1.33)). The limited amount of information obtained from observed wave properties makes it hard to determine various wave characteristics and many unknown factors in MEM analysis which need to solve the Eq.(1.28), which is an inherent disadvantage. Consequently, the Bayesian directional method has been developed which has a high degree of freedom in the model (Hashimoto, 1997; Hashimoto and Kobune, 1989).

The directional spreading function for BDM is assumed to be larger than zero, and treated as a piecewise-constant function over the directional range in n segments (Hashimoto and Kobune, 1989),

$$D(f,\theta) \approx \sum_{n=1}^{N} \exp\{x_n(f)\}\, L_n(\theta), \tag{1.36}$$

with

$$L_n(\theta) = \begin{cases} 1: & (n-1)\Delta\theta \le \theta < n\Delta\theta \\ 0: & \text{otherwise} \end{cases} \tag{1.37}$$

where $x_n(f) = \ln D(f,\theta)$.

The number of segments n of directional spreading function is usually in the order of 60 to 180, which is a rather high number of unknowns compared to the number of observed wave quantities and available equations given by Eq.(1.28).

An additional constraints is added to smooth the maintained directional function, which requires the difference between x_n to be close to zero, $x_n - 2x_{n-1} + x_{n-2} \approx 0$. In order to solve this regression problem under the constraints of cross spectra in Eq.(1.28) and function smoothness, Akaike's Bayesian Information Criterion (Akaike, 1998), which takes the Bayesian technique used in probability theory, is then introduced. The directional spreading function is determined as the one which minimizes Akaike's Bayesian Information Criterion.

BDM has been shown to be a very powerful estimation method though it is hard to implement (Benoit et al., 1997). However, this method works best for multi-quantity measurements, which means the performance of single-point systems or three-quantities measurements is not good.

1.3.4 Extended Maximum Entropy Principle (EMEP)

The extended maximum entropy principle extends the MEM by increasing the order of the model in Eq.(1.34) and considering errors e in the cross spectrum of observed wave properties. The directional spreading function can be assumed to be based on the solution of MEM (see Eq.(1.34)),

$$D(f,\theta) = \frac{1}{\Delta} \exp\left\{\sum_{n=1}^{N} \left[a_n(f) \cdot \cos(n\theta) + b_n(f) \cdot \sin(n\theta)\right]\right\}, \tag{1.38}$$

where

$$\Delta = \int_0^{2\pi} \exp\left\{\sum_{n=1}^{N} \left[a_n(f) \cdot \cos(n\theta) + b_n(f) \cdot \sin(n\theta)\right]\right\} \mathrm{d}\theta, \tag{1.39}$$

where n is the parameter representing the order of the model, $a_n(f)$ and $b_n(f)$ are unknown Lagrange multipliers to be determined under the restrictive conditions of Eq.(1.28).

Errors, e, contained in the observed data are taken into account. Thus, the existence of error e is added into the Eq.(1.28) after substituting Eq.(1.38) into Eq.(1.28). The directional spreading function is obtained by minimizing the error. To minimize the error, Akaike's Information Criterion (Akaike, 1997) incorporated with Newton's technique of local linearization and iteration is applied to get proper model order n and coefficients a_n, b_n.

The key advantage of EMEP lies in the fact that measured errors or statistical variability are taken into account and are not sensitive to noise. The result of this method is superior to that of MEM and comparable to that of BDM when multi-quantity measurements are applied. Also, its performance for three-quantity measurements is reliable.

1.3.5 Iterative Maximum Likelihood Method (IMLM)

Iterative Maximum Likelihood Method (IMLM) (Oltman-Shay and Guza, 1984) was developed by iteratively refining Maximum Likelihood Method (MLM) (Capon et al., 1967). The directional spreading function is first assumed as a linear combination of the cross spectra obtained from measured wave quantities for MLM,

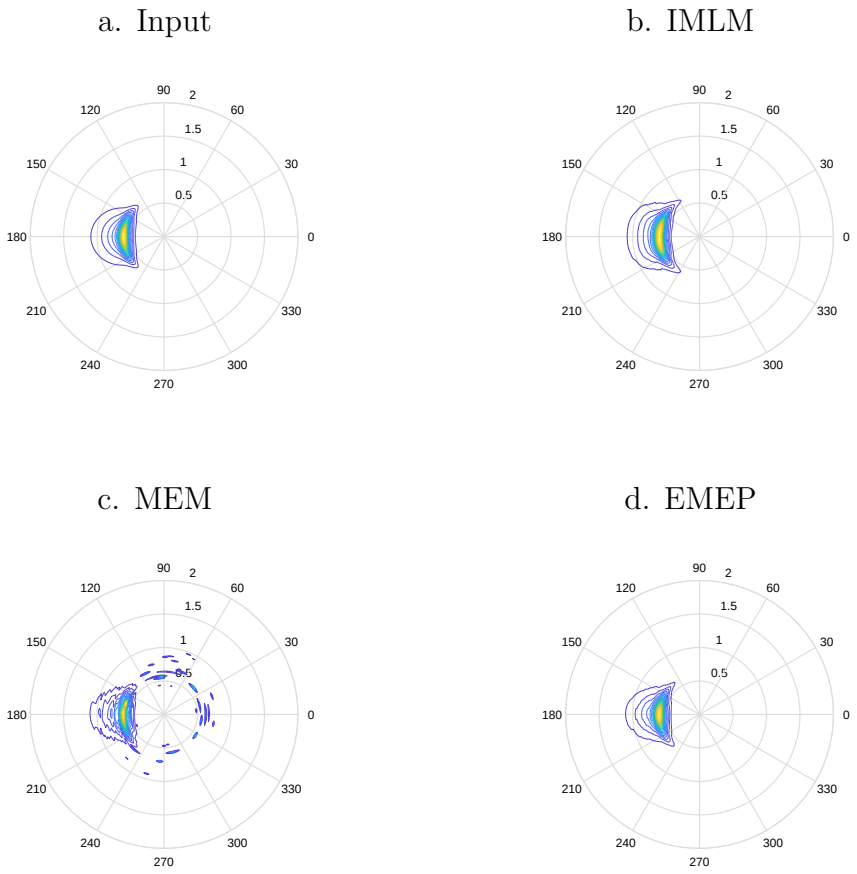


Figure 1.2: Polar plots of Directional spectrum estimated by various conventional methods. (a) Input directional spectrum, (b) IMLM, (c) MEM, (d) EMEP.

$$\hat{D}(f,\theta) = \sum_{m}\sum_{n} \tau_{m,n}(f,\theta)\Phi_{m,n}(f), \tag{1.40}$$

where $\hat{D}(f,\theta)$ is the estimated directional spreading function and $\tau_{m,n}(f,\theta)$ are unknown coefficients to be determined.

Substitution of Eq.(1.40) into Eq.(1.28) yields,

$$\hat{D}(f,\theta) = \int_{0}^{2\pi} D(f,\theta) w\left(\theta,\theta'\right) d\theta', \tag{1.41}$$

where

$$w(\theta,\theta') = \sum_m \sum_n \tau_{m,n}(f,\theta) H_m^*(f,\theta')\, H_n(f,\theta') \times \exp\left\{-ik\left(x_{m,n}\cos\theta' + y_{m,n}\sin\theta'\right)\right\}. \tag{1.42}$$

The directional spreading function is obtained by minimizing the difference between the estimated directional spreading function $\hat{D}(f,\theta)$ and the actual directional spreading function $D(f,\theta)$ in Eq.(1.41). The maximum likelihood technique used in probability theory is applied to minimize the difference and obtain the estimated directional spreading function. Oltman-Shay and Guza (1984) made iterative improvements to the original MLM estimate in order to get a more consistent estimate with the cross-spectral matrix. The n^{th} iteration of the estimated directional spreading function is obtained from the sum of the $(n-1)^{th}$ directional spreading function and a modification factor. In general, it takes 20 iterations to reach a good convergence.

1.3.6 Other Methods

There are other directional estimation methods, including weighted Fourier series decomposition (WFS) (Longuet-Higgins, 1961), Maximum likelihood method (MLM) (Krogstad, 1988) and extended maximum likelihood method (EMLM) (Isobe et al., 1984). These methods have some inherent disadvantages and poorer performance than that of approaches introduced, and will not be explained in this thesis. Figure 1.2 shows directional spectra produced using various methods with synthetic single-point measurements. Due to the fact that BDM cannot be

applied to a three-quantity system and PTPD is only suitable for specific waves, these methods are not shown here.



Figure 1.3: The example of wave gauge array in the lab (Yoon et al., 2018).

1.4 Wave Measurement Techniques

As discussed above, all the estimations are based on measured wave quantities and some of them are sensitive to the errors or noise in the data. It is important to measure these wave quantities accurately in the lab or the field. Different approaches have unique pros and cons which will be introduced below.

1.4.1 Wave Gauges

Wave gauges are used when it is possible to mount on a fixed structure or rarely on a purpose-built offshore structure. Gauge measurements are more likely to be used

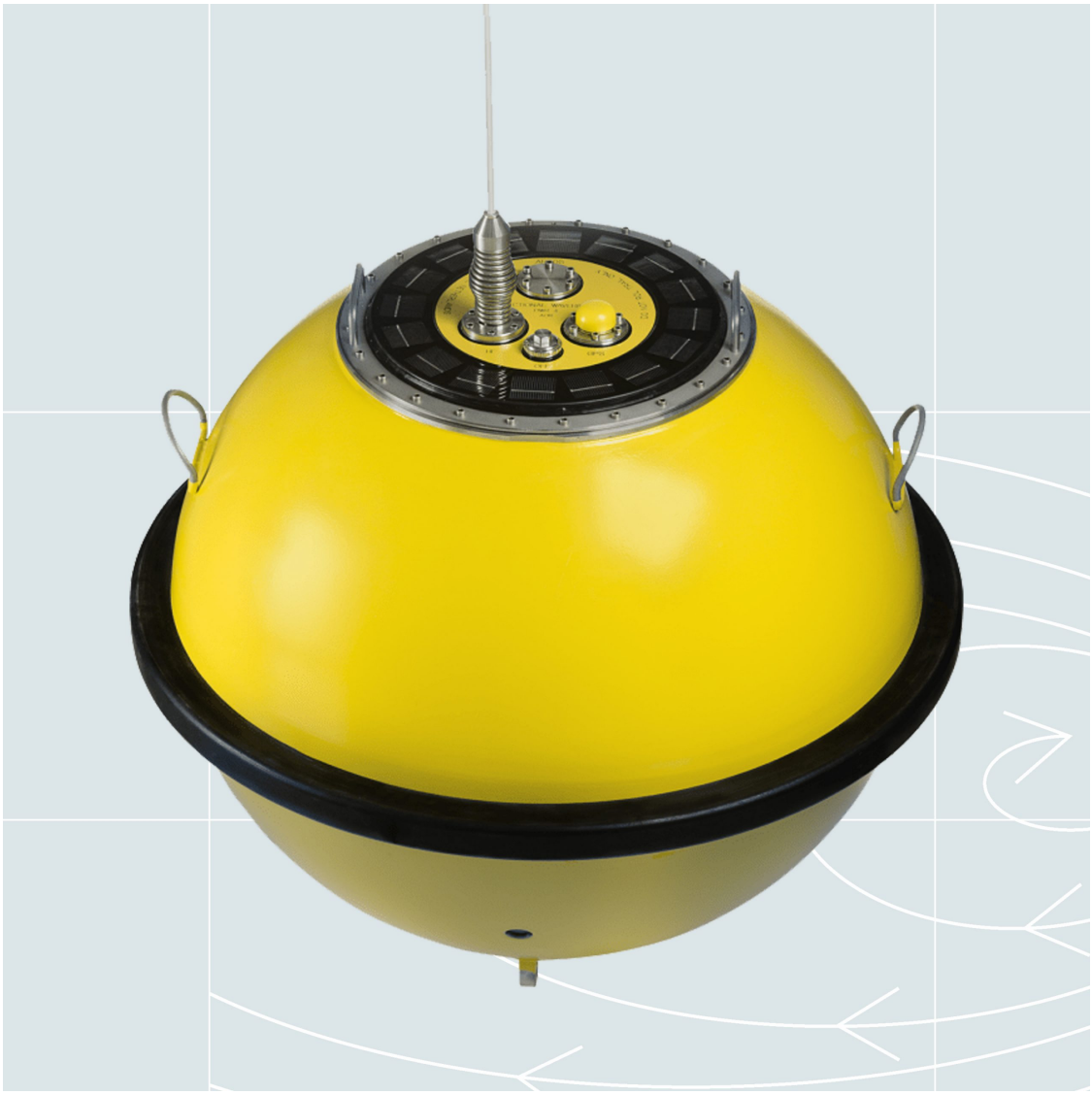


Figure 1.4: The standard MkIII Directional Waverider buoy (https://rsaqua.co.uk/product/dwr-mkiii-waverider-buoy/)

in the laboratory. The reason these are used in laboratories is the high accuracy of measured data using wave gauges. Figure 1.3 shows the example of the wave gauge array in the lab. Some common types of wave gauges are resistance-wire gauges and capacitance-wire gauges. The principles behind are similar: the resistance or capacitance across the top terminal changes with the wave elevations (Holthuijsen, 2010). One unsatisfactory property of wave gauges is that the thin films of water

form when the wave surface moves up and down, resulting in higher results than the true values for the dropping sea surface (Holthuijsen, 2010). Hence, the tools need to be calibrated and maintained regularly which again makes them difficult to use in the real ocean. It is also worth noting that the existence of a gauge sometimes changes the forms of waves when the wavelength is short, which makes results unstable (Latheef et al., 2017).

1.4.2 Wave Buoys

Compared to wave gauges, wave buoys can measure waves far offshore in deep water and are relatively easy to deploy in the ocean (see figure 1.4 for a standard wave buoy). The basic principle is that the buoys will follow the motions of sea surface or water particles (Holthuijsen, 2010; Tucker and Pitt, 2001). The acceleration can be measured, which can be integrated to get velocity or displacement in the sea. Though data measured by buoys are widely used, the behaviour of buoys in the water is not known with confidence and work is needed to validate their measurements (Forristall, 2000; Emmanuel et al., 2010).

1.4.3 Other Measurement Techniques

Shipborne wave recorders (SBWR), which are mounted on ships, are cheap to run and have high data return, though the data measured are not accurate as wave gauges and buoys (Holthuijsen, 2010; Tucker and Pitt, 2001). Remote sensing techniques like radar are built into satellites or airplanes to observe waves on a large

scale. Though it is hard to use radars to detect the waves in a short period due to the low frequency of sampling (Abdalla et al., 2013), the average sea properties can be estimated in a year or longer period.

1.5 Comparison of Buoys and Gauges

Since wave buoys are easily installed in the field, wave buoys are widely used to investigate wave properties. To explore the behaviour of wave measurement buoys, various studies have been undertaken to assess buoy measurements using different wave properties compared to wave gauges which can be regarded as truths in the lab. Liu et al. (2015) found that the spectral parameters, like peak period and significant wave height, estimated by gauges and buoys have good agreement in scaled wave conditions. McAllister and van den Bremer (2020) used experimental data to conclude similar results where the discrepancies are 2.8% and 1% for significant wave height H_s and peak period T_p, respectively. However, there is limited research comparing wave spreading for buoys and gauges. It is also found that wave buoy measurements may underestimate extreme crest height (Allender et al., 1989; Dysthe et al., 2008) compared with gauge measurements. In this section, previous works related to wave crest estimation and directional spreading by buoy and gauge are introduced.

1.5.1 Wave crest statistics

Crest height statistics are key for ocean engineering since the wave loads exerted on the designed marine structure are correlated with the wave elevation. If sea states are linear and narrow banded, the distribution of crest height is very close to a Rayleigh distribution (Longuet-Higgins, 1963). In real seas which are nonlinear and broad-banded, nonlinearity needs to be considered. Forristall (2000) proposed a second-order distribution of wave crest η based on the second-order wave model,

$$P\left(\eta_{\mathrm{c}} > \eta\right) = \exp\left[-\left(\frac{\eta}{\alpha_u H_{\mathrm{s}}}\right)^{\beta_s}\right], \tag{1.43}$$

where α_u and β_s are parameters estimated by Ursell number and steepness. H_s is again significant wave height and η_c is the crest height. Different relationships of above distribution will be applied for uni-directional and directional sea states.

Several authors also proposed second-order crest height distribution (Tayfun, 1980; Fedele and Arena, 2005). The second-order crest distributions work well for weakly nonlinear sea states. However, when the sea states become steeper, the observed distribution departs from predicted crest height distributions, especially at low exceedance probabilities due to the nonlinearity (Onorato et al., 2006). The nonlinear deviation from second-order theory was demonstrated for uni-directional and directional sea states (Shemer et al., 2010; Buchner et al., 2011). That nonlinear amplification above second-order distribution is dependent on the

spreading of sea state (Latheef and Swan, 2013), effective water depth and wave steepness (Karmpadakis et al., 2019). The amplifications reduce with wave spreading and increase with the steepness of sea states. Wave breaking occurs to dissipate the amplification when the steepness becomes larger (Karmpadakis et al., 2019). Higher-order crest distributions were also proposed to capture the effects beyond second-order (Tayfun and Fedele, 2007).

The measured crest height statistics are not only affected by actual sea-state conditions, like wave steepness and wave spreading, but also by measurement techniques. The perception is that buoy measurements will underestimate measured wave crests (Forristall, 2000; Dysthe et al., 2008). The buoy mooring effects or second-order nonlinearity cancellation due to filtering by buoys are reasons for potential underestimation (Allender et al., 1989; van Essen et al., 2018; Longuet-Higgins, 1986). McAllister and van den Bremer (2019) corrected the crest height measured by buoys, in which they proposed second-order sub-harmonic components to account for filtered frequency components.

1.5.2 Directional Spreading

Waves in the oceans are three-dimensional and comprised of components that travel in different directions. Directional spreading is a measure of how wave energy for a given sea state is spread as a function of the direction of propagation. Directional spreading affects wave kinematics, which in turn affects wave-induced forces on offshore structures and floating bodies (Isaacson and Sinha, 1986). Extreme wave

characteristics, such as nonlinearity (i.e. skewness, kurtosis) (Prevosto, 1998) and wave breaking, are also critically dependent on directional spreading (Fedele, 2015). These properties affect the likelihood of encountering extreme waves (Latheef and Swan, 2013).

Buoys and probes directly measure surface displacement at a single point in space. To perform conventional directional estimation a minimum of three concurrently measured wave properties are required. In principle, wave buoys, if appropriately moored, have 6 degrees of freedom, which may be independently measured. Wave following buoys log three of these degrees of freedom, namely x, y, z displacements. Wave gauges or similar fixed Eulerian devices generally only measure vertical displacement at a single location. Thus multiple gauges are generally required to provide directional information, whereas directional estimation may be performed using measurements from a single buoy. However, it is possible to perform indirect estimates of directional spreading using only a single Eulerian measurement by examining the magnitude of the bound harmonics (Adcock and Taylor, 2009; McAllister et al., 2017).

Although buoy measurements are widely used to measure directional spreading, to the author's knowledge, their ability to do so has not been analysed under laboratory conditions. Benoit and Teisson (1995) compared the performance of a multi-point gauge array and a single-point gauge array which mimics the behaviour of a heave-pitch-roll buoy for directional spreading. They found that the single-

point system was more effective for analysis of following sea states (unimodal in direction). Lin et al. (2020) used different quantities measured by buoys, such as displacements and velocities, to calculate spreading. They found that using velocity data resulted in the most accurate directional estimates. O'Reilly et al. (1996) used field data to compare wave buoy and fixed platform, where the directional information measured by wave buoy agreed well with that of platform. However, direct comparisons between wave buoy and gauge measurements about directional information are rare. Therefore, it is worth assessing buoy measurement based on experimental or field buoy and gauge data for directional spreading. In addition, the steepness of sea states needs to be considered, since the nonlinearity of sea states will have effects on the directionality of wave (Latheef et al., 2017). As buoys only measure three degrees of freedom they may encounter issues in crossing sea states (bimodal in direction), particular when bimodality occurs over the same range of frequencies (Benoit and Teisson, 1995). Such a study will be undertaken and introduced in chapter 2.

1.6 Mooring

Floating structures, like wave buoys, wave energy converters and platforms, are normally fastened by mooring systems (Gobat and Grosenbaugh, 2001) to mitigate the effects of drifting. Figure 1.5 shows the standard mooring layout used by CDIP for wave buoys. The single point vertical mooring is made of polypropylene

rope with a rubber cord at the top end. The rubber cord ensures small motions at low frequencies (Datawell, 2006).

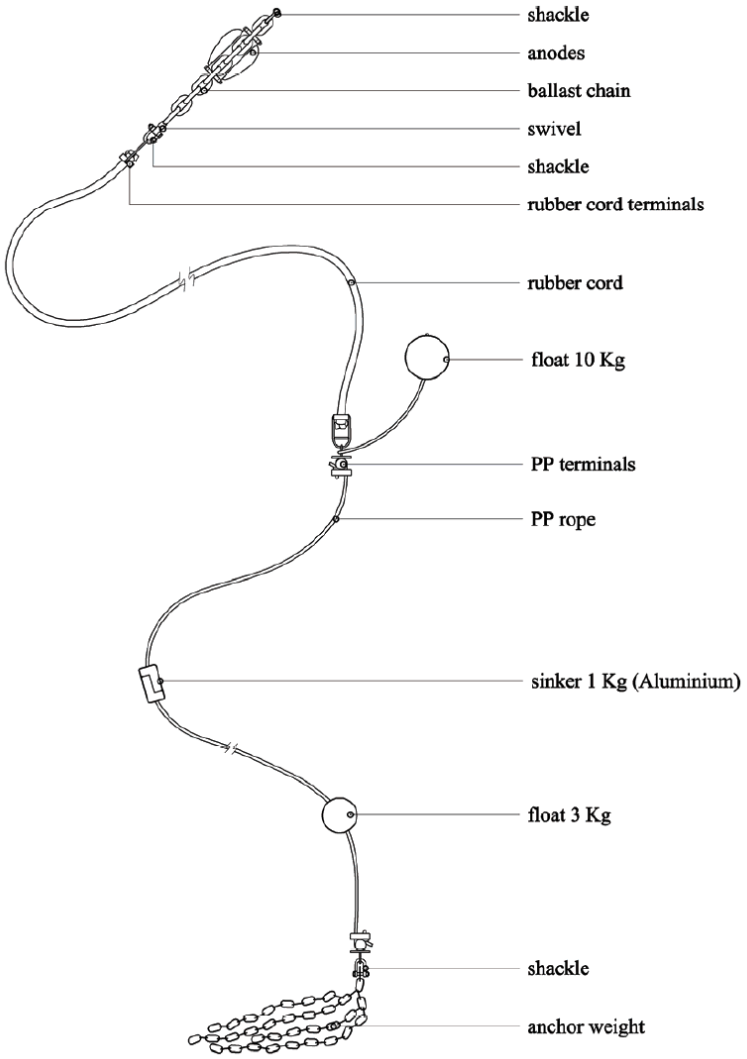


Figure 1.5: The typical mooring for CDIP buoy. Figure adapted from (Datawell, 2006)

1.6.1 Mooring effects

A great variety of moorings can be used for the floating structures, Datawell (2006) presented some preferred mooring types which depend on the size of structures, water depth, wind and current, and Joosten (2006) indicated the importance of the

sufficient elasticity in the mooring. The largest wave needs to be considered when the moorings are operated with facilities (Humphery, 1982). Walden et al. (1977) tested different mooring types with various mooring lengths to examine the mooring effects on wave measurements using experimental data. Similar research was conducted by Gould and Sambuco (1975) where they find the differences between surface moorings and moorings with subsurface flotation. More researchers then moved to investigate the dynamic behaviour of moorings (Mavrakos and Chatjigeorgiou, 1997; Zhu and Yoo, 2016) which underpin the studies of the application of wave energy converters (Johanning et al., 2007). The mooring effects on measurements of wave statistics, like significant wave height, crest distributions and directional spreading, are rarely studied, especially in the field. McAllister and van den Bremer (2019) showed there was no observable effect on wave elevations in the lab, using a simplified taught elastic mooring. However, in the field horizontal motions will accumulate over time, resulting in the changing of mooring properties, like mooring force exerts on the buoy. Niclasen and Simonsen (2007) found the semi-tidal modulations in measured wave height with a rigid mooring. Chapter 3 will discuss the mooring effects on the wave statistics based on field data.

2
Spreading

Contents

2.1 Chapter overview 31
2.2 Methods 32
2.2.1 Experimental setup 32
2.2.2 Directional estimation methods 39
2.2.3 Synthetic wave data 44
2.3 Results 47
2.3.1 Following sea states 47
2.3.2 Crossing sea states 56
2.3.3 Mooring configuration 59
2.4 Conclusions 61

2.1 Chapter overview

In this chapter, I investigate the accuracy of directional spreading estimates made using wave buoy measurements through direct comparison with estimates made using an array of wave gauges in both following and crossing conditions. This chapter is laid out as follows. First, I provide details of the experiments I use

(section 2.2.1), review state-of-the-art directional estimation methods (section 2.2.2), and use synthetic data to assess the experimental set-up and methods (section 2.2.3). The experimental data are used to perform a comparison of spreading estimates made using gauge and buoy measurements in section 2.3. Experiments with following and crossing directional spectra are assessed in sections 2.3.1 and sections 2.3.2 and the effects of mooring configuration in section 2.3.3 are examined. Finally, conclusions are provided in section 2.4. The main results of this chapter have been published in the Lin et al. (2022).

2.2 Methods

2.2.1 Experimental setup

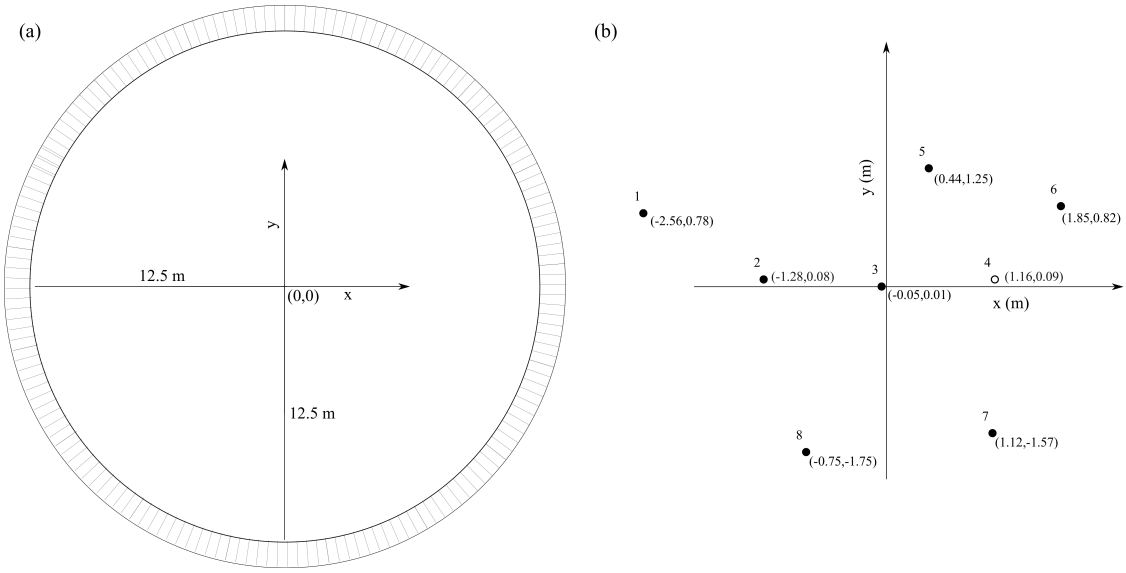


Figure 2.1: (a) Schematic diagram of wave basin (b) gauge and mean buoy positions, markers show gauge locations, and filled markers show where buoys were also located. Figure adapted from (McAllister and van den Bremer, 2020)

Full details of the experimental methods behind the data are given in McAllister and van den Bremer (2020). The experiments were carried out in the FloWave

Ocean Energy Research Facility at the University of Edinburgh. This is a circular wave basin surrounded by 168 absorbing wavemakers which enable the generation of waves in any direction. Figure 2.1 shows a schematic diagram of the wave basin, which has a 12.5 m radius and 2 m water depth.

In McAllister and van den Bremer (2020), gauge and buoy measurements were made in identical conditions at the same positions. Eight gauges and seven buoys were installed in the positions as listed in table 2.1 and shown in figure 2.1. Table 2.2 details the targeted directional conditions of the sea states examined herein which I refer to as the input directional spreading σ_θ.

The model 'buoys' were plastic spheres with a density half that of water and a diameter of 0.07 m. The buoys were positioned using an auxiliary mooring, this taut mooring was highly flexible and displayed negligible effects on measured surface elevation (see McAllister and van den Bremer, 2019). The mooring configuration will have an effect on lateral displacements, this is addressed in section 2.3.3. Buoy displacements were measured using a Qualisys motion tracking system, as opposed to any onboard instrumentation. The Qualisys system uses 8 infrared cameras, that simultaneously track the position of the buoys. The buoys were covered in a material that reflects infrared light. Resistive wave gauges were used to measure surface elevation at the positions in table 2.1. Figure 2.2 shows the separation of all possible wave gauge pairs normalised by peak wavelength λ_p, this provides an indication of the range of wavelengths over which the gauge array will

be effective. The wave gauge positions were chosen to provide uniform coverage of separations over the range of relevant wavelengths, within the constraints of what was physically realisable in the wave tank.

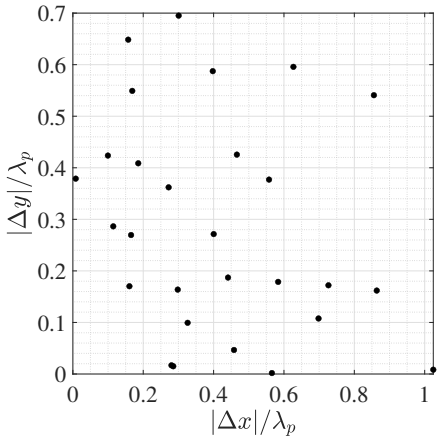


Figure 2.2: Separation of all possible wave gauge pairs normalised by peak wavelength λ_p

Wave generation

Waves are generated in the FloWave tank, using a frequency domain approach, as discrete components. The method by which this is done can affect the spatial homogeneity of the resulting waves (Latheef et al., 2017). To generate irregular directionally spread waves that fit a desired directional spectrum, the following approach is often employed. The desired surface elevation $\eta(x, y, t)$ is achieved using a double summation in frequency f and direction θ,

$$\eta(x, y, t) = \sum_{i=1}^{N} \sum_{j=1}^{M} A_{ij} \cos\left(\varphi_{ij}\right), \tag{2.1}$$

where

$$\varphi_{ij} = k_i \left(x \cos\theta_j + y \sin\theta_j\right) - \omega_i t + \epsilon_{ij}, \tag{2.2}$$

Table 2.1: gauge array and mean buoy positions

	gauge		Buoy	
No.	x (m)	y (m)	x (m)	y (m)
1	-2.56	0.78	-2.47	0.73
2	-1.28	0.08	-1.18	0.07
3	-0.05	0.01	0	0
4	1.16	0.09	—	—
5	0.44	1.25	0.55	1.21
6	1.85	0.82	1.84	0.81
7	1.12	-1.57	1.11	-1.55
8	-0.75	-1.75	-0.70	-1.76

Phase, ϵ, is sampled from a uniform distribution in the range $0 < \epsilon < 2\pi$ in the experiment. Amplitude is related to the underlying directional spectrum by

$$A = \sqrt{2S\left(f,\theta\right)\Delta f \Delta\theta}, \tag{2.3}$$

where

$$S\left(f,\theta\right) = E\left(f\right)D\left(f,\theta\right). \tag{2.4}$$

Note that Δf and $\Delta\theta$ are the resolutions of frequency and direction, which remain constant. The directional spreading function $D\left(f,\theta\right)$, follows the definition that at a given frequency f,

$$\int_{-\pi}^{+\pi} D(f,\theta)\mathrm{d}\theta = 1. \tag{2.5}$$

Table 2.2: Test matrix

H_s (m)	f_p (Hz)	water depth (m)	σ_θ $(^\circ)$	$\Delta\theta$ $(^\circ)$	realisations
			Synthetic data		
0.225	0.6	2	20	0	500
			Experimental data		
0.225	0.6	2	7.07, 14.14, 21.21	0	3
0.225	0.6	2	14.14	90	3
0.175	0.6	2	7.07, 14.14, 21.21	0	1

One issue with the double summation method (DSM) is that multiple waves of the same frequency which travel in different directions exist simultaneously. This causes the formation of partial standing waves and an inhomogeneous wave field (Miles and Funke, 1989; Jefferys, 1987), a phenomenon known as phase locking. The effects of phase-locking can be somewhat reduced by increasing the total number of wave components, which can be achieved by increasing the total duration of an experiment.

To avoid the phasing-locking problem entirely, each frequency component is only generated in one direction in the so-called single summation method (SSM),

$$\eta(x,y,t) = \sum_{i=1}^{N} A_i \cos\left[2\pi f_i t - k_i \left(x\cos\theta_i + y\sin\theta_i\right) + \epsilon_i\right], \tag{2.6}$$

where amplitude A is defined by the equation,

$$A = \sqrt{2E\left(f\right)\Delta f}. \tag{2.7}$$

For this method, directional spreading is achieved by selecting the direction θ_i randomly from a distribution with the desired form. Herein, spreading is defined using a wrapped normal distribution

$$D(\theta) = \frac{1}{\sigma_\theta \sqrt{2\pi}} \sum_{n=-\infty}^{\infty} \exp\left[-\frac{(\theta - \theta_m + 2\pi n)^2}{2\sigma_\theta^2} \right], \tag{2.8}$$

where θ_m is the mean direction, and σ_θ is the standard deviation of distribution representing the spreading width of wave energy. For crossing sea states, two wrapped normal distributions were superimposed with mean direction separated by $\Delta\theta$. In the experiments examined directional spreading is frequency independent.

The effects of phase-locking are examined in Latheef et al. (2017), which showed the maximum deviation of mean energy from expected values at some points can reach up to 30% when using DSM. In the experiments presented herein SSM was used. I assess any implications that the two wave generation methods may have on directional estimation in figure 2.3, using synthetically generated linear wave data and the EMEP (see section 2.2.2 for details of directional estimation process). For synthetic linear buoy data, directional estimates are similar and both close to input values for the two generation methods (3% lower than input value). For the synthetic gauge data, the effects of spatial inhomogeneity have an observable effect on the accuracy of directional estimation (figure 2.3(b)). This is because a single directional estimate combines input quantities from different positions, whereas an estimate made using a buoy uses measurements from approximately a single point.

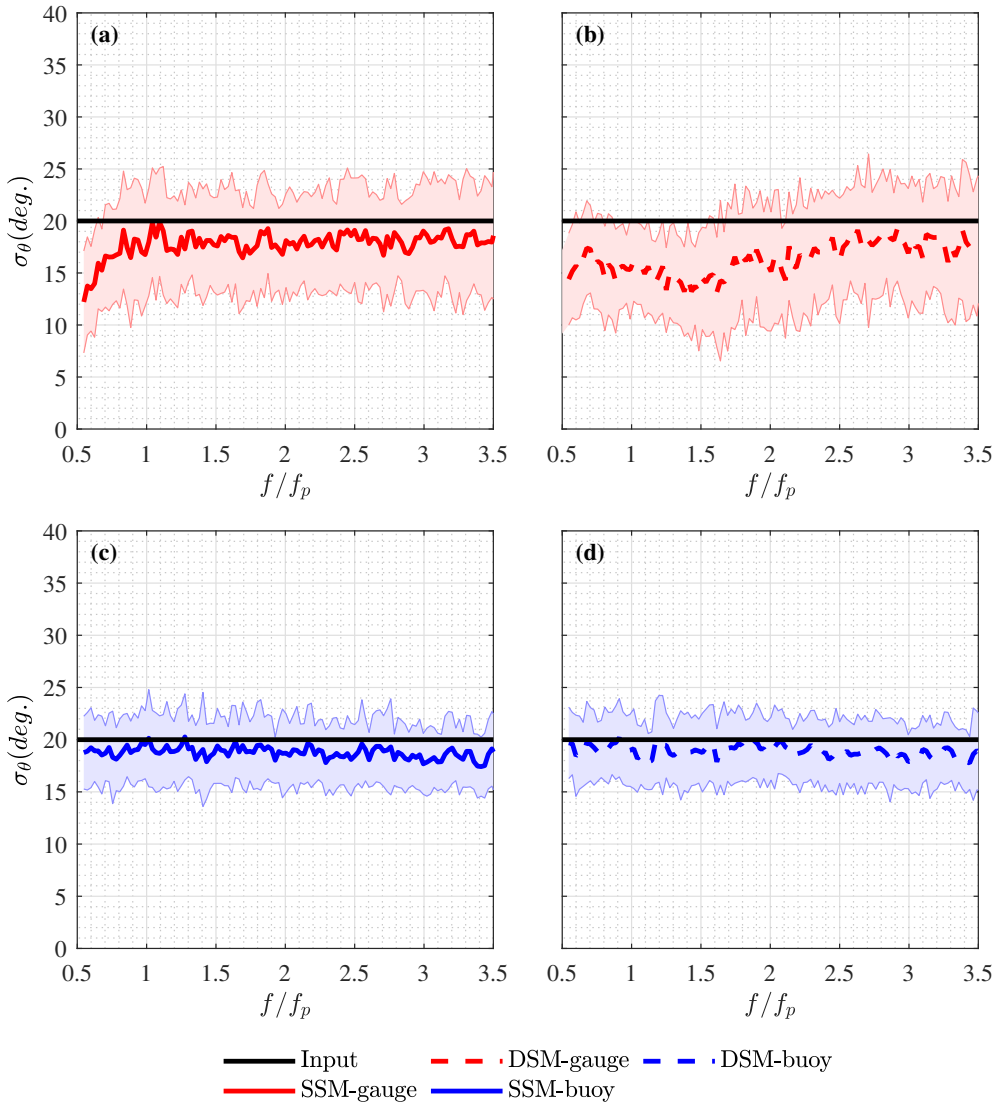


Figure 2.3: EMEP estimates of directional spreading width σ_θ as a function of normalised frequency f/f_p, based on synthetic gauge and buoy data created using double (DSM) and single (SSM) summation wave generation with an input spreading value of $\sigma_\theta = 20°$: (a) SSM for gauge array; (b) DSM for gauge array; (c) SSM for buoys; (d) DSM for buoys; Transparent envelopes show error bounds

Input Spectrum

Herein, the synthetic and experimentally generated waves were defined using a frequency spectrum $E(f)$ based on the JONSWAP spectrum (Hasselmann et al.,

1973) using Eq.(1.12). Typical values were taken for parameters in the experiments: $\gamma = 3.3$, $\sigma\,(f \leq f_p) = 0.07$ and $\sigma\,(f > f_p) = 0.09$. For all sea states synthetic and experimental, the peak frequency f_p is 0.6 Hz, which ensures the deep water condition for all the analyses.

2.2.2 Directional estimation methods

By measuring surface elevation at three or more points in space, or three wave quantities at a single point (i.e. x, y, z displacements for a buoy) it is possible to estimate directional spreading. The fundamental equation that relates directional spreading to observed quantities is presented by Eq.(1.28).

Estimating directional spectra accurately can be a challenge. There is an infinite number of unknown parameters in Eq.(1.28), which makes a unique solution for the spreading function impossible when a finite number of measured wave quantities are available. To overcome this, most estimation methods use likelihood approaches to find solutions to the under-determined problem. Common methods are the maximum likelihood method (MLM) (Capon et al., 1967), iterative maximum likelihood method (IMLM) (Oltman-Shay and Guza, 1984), the maximum entropy method (MEM) (Kobune and Hashimoto, 1986; Lygre and Krogstad, 1986), the extended maximum entropy principle (EMEP) (Hashimoto et al., 1995), and Bayesian Directional Method (BDM) (Hashimoto and Kobune, 1989). See Benoit et al. (1997) and Benoit (1993) for alternative methods such as Truncated Fourier Series (Borgman, 1969), Weighted truncated Fourier Series (Longuet-Higgins,

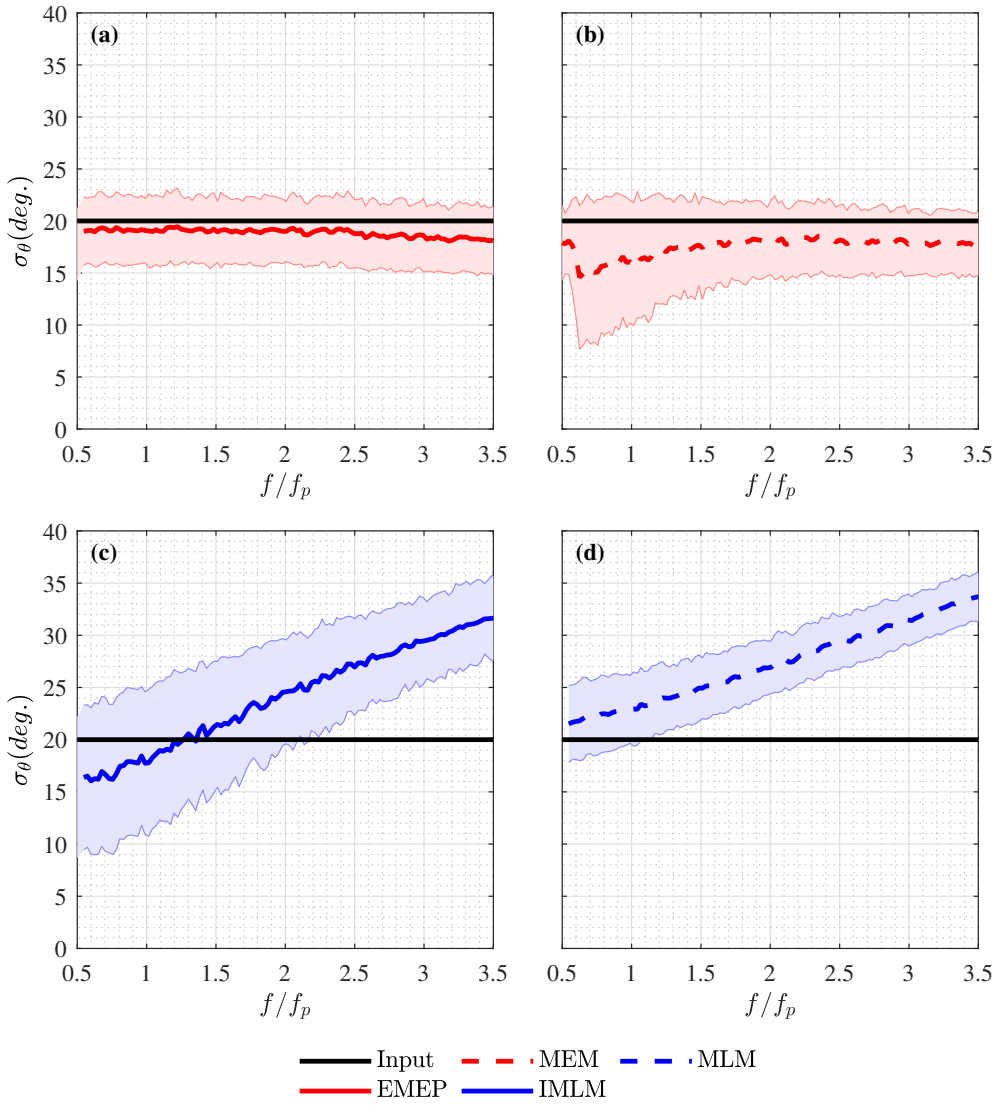


Figure 2.4: Estimates of directional spreading width σ_θ as a function of normalised frequency f/f_p based on synthetic buoy data with an input spreading value of $\sigma_\theta = 20°$, calculated using different methods: (a) EMEP; (b) MEM; (c) IMLM; (d) MLM; Transparent envelopes show error bounds.

1961), Eigenvector method (Marsden and Juszko, 1987) and Long-Hasselmann Method (Long and Hasselmann, 1979).

In figure 2.4, directional spreading widths σ_θ estimated using EMEP, MEM, IMLM, and MLM methods are compared, using 500 realisations of synthetic buoy

data, which were generated using the single summation method (see section 2.2.1). The data were generated with a spreading width $\sigma_\theta = 20°$ (see section 2.2.2 for definition). The calculated quantities for each realisation were time histories of surface elevation η, x, and y displacements, based on linear wave theory. The directional spreading and error bounds in figure 2.4 were obtained by taking the mean and standard deviation of 500 realisations.

Directional spreading estimates made using IMLM and MLM exhibit a large offset which increases with frequency. This was also found by Young (1994) who tested synthetic pitch/roll buoy data and concluded that MLM was not capable of producing accurate estimates of directional spreading. MEM and EMEP both match the true spreading value more closely. The latter is accurate over a wider frequency range and is quicker to compute. Hence, EMEP is used in the following study. To analyse the experiments I also use an additional method of directional estimation, the Phase Time Path Difference method (PTPD) (Draycott et al., 2015). The PTPD approach can be used to estimate the direction that waves are travelling in, for experiments in which single summation wave generation is used, i.e. where only a single wave component that travels in a single direction exists at each frequency. Draycott et al. (2015) showed that the PTPD method may be used to effectively estimate directional spectra for experimentally generated data. The PTPD method uses measured phase difference between triads of gauges to

infer the direction of travel of waves at each generated frequency, and may also be used to estimate the amplitude of reflected waves.

The EMEP considers errors contained in the cross spectrum when Eq.(1.28) is evaluated and minimizes these errors to produce a unique directional spectrum. The directional spreading function is calculated using Eq.(1.38). The unknown parameters $a_n(f)$ and $b_n(f)$ $(n = 1, ..., N)$ can be determined iteratively by assuming appropriate initial values. N is the order of the model chosen to minimise errors contained in the cross spectrum and Akaike's Information Criterion (Akaike, 1997). A first-order model, namely $N = 1$, is initially considered and higher-order models are sequentially added if the models meet Akaike's Information Criterion. Note that the order of model N should be within half of the number of independent equations in Eq.(1.28).

I implement EMEP spreading estimation using the WAFO Matlab toolbox (Brodtkorb et al., 2000). A Hamming window is used without overlapping to calculate cross-spectra density. The number of Discrete Fourier Transform (DFT) points and angles for the estimated directional spectra were 2048 and 180 respectively. These parameters were chosen to optimise the resolution and stability of the output directional estimates.

Herein, when referring to spreading estimates based on buoy measurements I present average values. This is the case in all figures unless stated otherwise. For each buoy spreading is estimated using measured x, y, and z displacements,

an average is then calculated based on the spreading estimates produced by all 7 buoys. As I produce 7 estimates of spreading it is also possible to assess error bounds using the standard deviation of the 7 estimates. As the wave gauges each measure only a single variable namely surface elevation η, multiple gauges are necessary to measure spreading. To understand the error bounds of the directional estimates produced using gauge measurements, bootstrapping is used. Multiple estimates of spreading are produced by using all 6 gauge combinations of the 8 gauges available. Bootstrapping gives 28 estimates of spreading from which I may calculate average values and standard deviations.

Parameter estimation

For each estimated directional spreading function $D(f,\theta)$, the widths of the spreading function σ_θ at each frequency independently are estimated. For a wrapped normal distribution, the spreading width may be estimated as the standard deviation,

$$\sigma_\theta(f) = \sqrt{\int_{-\pi}^{+\pi} (\theta - \theta_m)^2 D(f,\theta) \mathrm{d}\theta}, \tag{2.9}$$

where the mean direction is calculated using

$$\theta_m(f) = \int_{-\pi}^{+\pi} \theta D(f,\theta) \mathrm{d}\theta. \tag{2.10}$$

However, the estimated directional distribution may not be an ideal normal distribution. Where this is the case of calculating σ_θ as standard deviation is sensitive to small fluctuations at large angles from the mean, and can result in

disproportionately large values of σ_θ. As an alternative to estimating spreading width σ_θ using Eq. (2.9), σ_θ is also calculated by fitting a normal distribution to the estimated spreading function at each frequency using a least squares approach. Fitting a normal distribution to estimate spreading width provides a means of estimating σ_θ which is less sensitive to noise than calculating the standard deviation. A comparison of these two estimation methods for calculating estimated spreading width is given in section 2.2.3.

2.2.3 Synthetic wave data

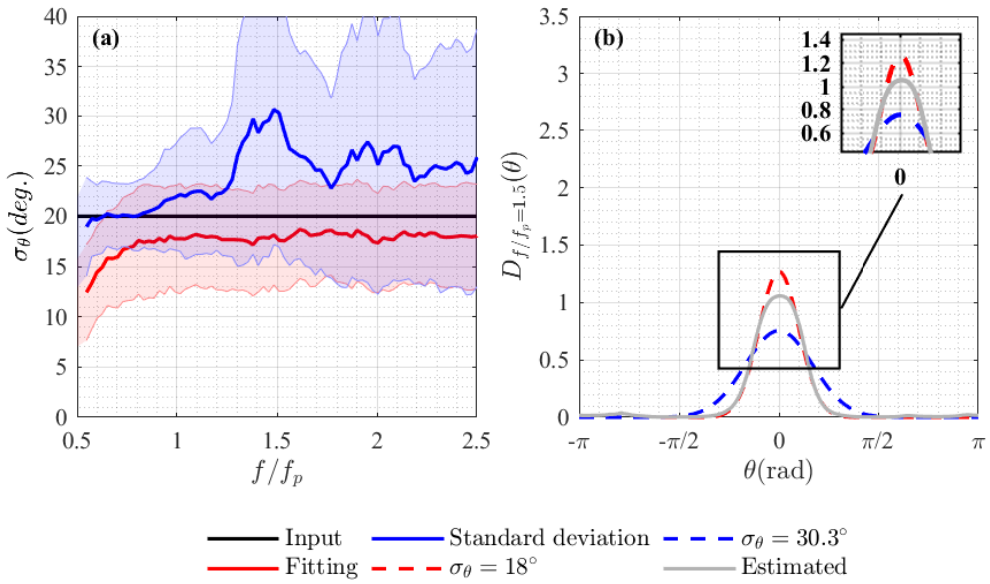


Figure 2.5: EMEP estimates of spreading width σ_θ as a function of normalised frequency f/f_p in panel (a), calculated by fitting a wrapped normal distribution and as the standard deviation in Eq.(2.9) based on SSM synthetic linear gauge data with an input spreading value of $\sigma_\theta = 20°$; in panel (b) EMEP estimated spreading distribution for $f/f_p = 1.5$, and wrapped normal distributions with $\sigma_\theta = 18°$, and $\sigma_\theta = 30.3°$ which correspond to values calculated based on fitting and standard deviation methods at $f/f_p = 1.5$ in panel (a).

The EMEP is applied to time series created using linear and second-order wave

theories (i.e. including second-order bound harmonics following Dean (1981)). The aim of this is to help identify any systematic errors in directional estimates that are associated with the methods and experimental setup I use. To replicate the experimental gauge array surface elevations with the same spatial configuration were calculated. 500 realisations with input degrees of directional spreading $\sigma_\theta = 20°$ (see table 2.2) were generated, and average values are taken across all of the realisations. Each realisation was 1024 s in duration and sampled at 32 Hz.

First, directional spectra were estimated using synthetic linear data. In figure 2.5(a) σ_θ was calculated at each frequency using standard deviation Eq. (2.9) (blue line), and by fitting wrapped normal distribution to the resulting directional spreading function $D(f_i, \theta)$ (red line). Using standard deviation to estimate σ_θ, results in large fluctuations with a significant increase near $1.5f_p$. To illustrate why this occurs, the directional spreading function at $1.5f_p$ is plotted in figure 2.5(b). Fitting gives a value of $\sigma_\theta \approx 18°$ whereas using standard deviation gives $\sigma_\theta \approx 30.3°$. Normal distributions with spreading width $\sigma_\theta = 30.3°$ and $\sigma_\theta = 18°$ are shown by the blue and red dash lines, respectively. The estimated directional spreading function (grey line) is better represented by $\sigma_\theta = 18°$ (fitting) than by $\sigma_\theta = 30.3°$ Eq.(2.9). Spreading width calculated using standard deviation is overly sensitive to noise at large angles and fitting provides more stable estimates of spreading width. Therefore, I calculate all values of σ_θ by fitting a wrapped normal distribution to estimated directional spreading functions $D(f, \theta)$ herein.

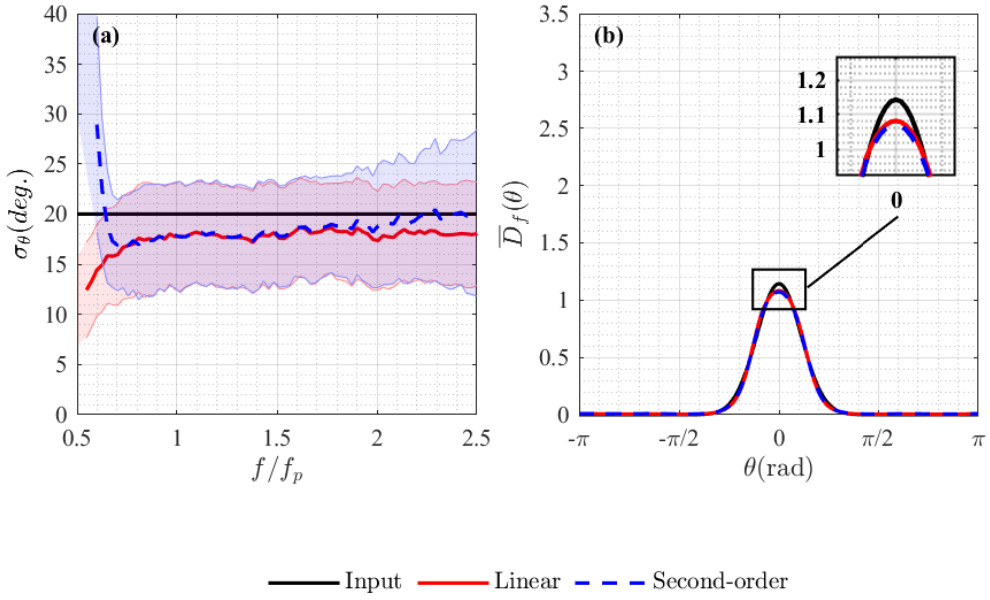


Figure 2.6: EMEP estimates of directional spreading width σ_θ as a function of normalised frequency f/f_p in panel (a), and mean directional spreading distribution in panel (b) based on SSM synthetic linear and second-order gauge data with an input spreading value of $\sigma_\theta = 20°$. Transparent envelopes show error bounds.

In figure 2.6, the estimated spreading width σ_θ and directional spreading function $D(f, \theta)$ averaged over $0.83f_p - 1.85f_p$, obtained for linear (red lines) and second-order (blue dashed lines) synthetic gauge data, are compared with the input degree of spreading (black lines). In figure 2.6(a) estimated spreading width σ_θ is plotted as a function of normalised frequency (f/f_p).

For synthetic linear data based on the experimental gauge array, the EMEP method estimates a spreading width of approximately 18.5 degrees which is stable for frequencies above $0.75f_p$. This is also the case for the second-order data across the frequency range $0.75f_p - 2f_p$, as frequency increases so does the estimated spreading width which also becomes less stable displaying larger error bounds. Therefore, the

experimental gauge array may produce less reliable directional estimates outside the range $0.75f_p - 2f_p$. For the JONSWAP spectra I examine, the amount of energy outside this range is very low (approximately 6% of the total energy).

2.3 Results

Using the experimental data measured in McAllister and van den Bremer (2020), I examine the accuracy of directional estimates made using model buoy measurements in following (unimodal in direction) and crossing (bimodal in direction) sea states, and briefly discuss potential effects of mooring configuration.

2.3.1 Following sea states

A sea state is described as following if it is directionally spread about a single mean direction. In this section, several following sea states are tested (see table 2.2). The same analysis procedures are applied to each experiment and average values are calculated across all of the available realisations. Each 1024 s experiment was partitioned into 16 sections with 2048 samples, which gives a frequency resolution of 0.0156 Hz and the angular resolution was defined as 2 degrees.

Before applying the EMEP method to the experimental data, PTPD method is used to verify the directional conditions created during the experiments and to quantify the effects of any reflections. For experiments in which SSM wave generation is used, the PTPD method can accurately estimate the direction in which each generated wave travels and verify that the directional conditions created

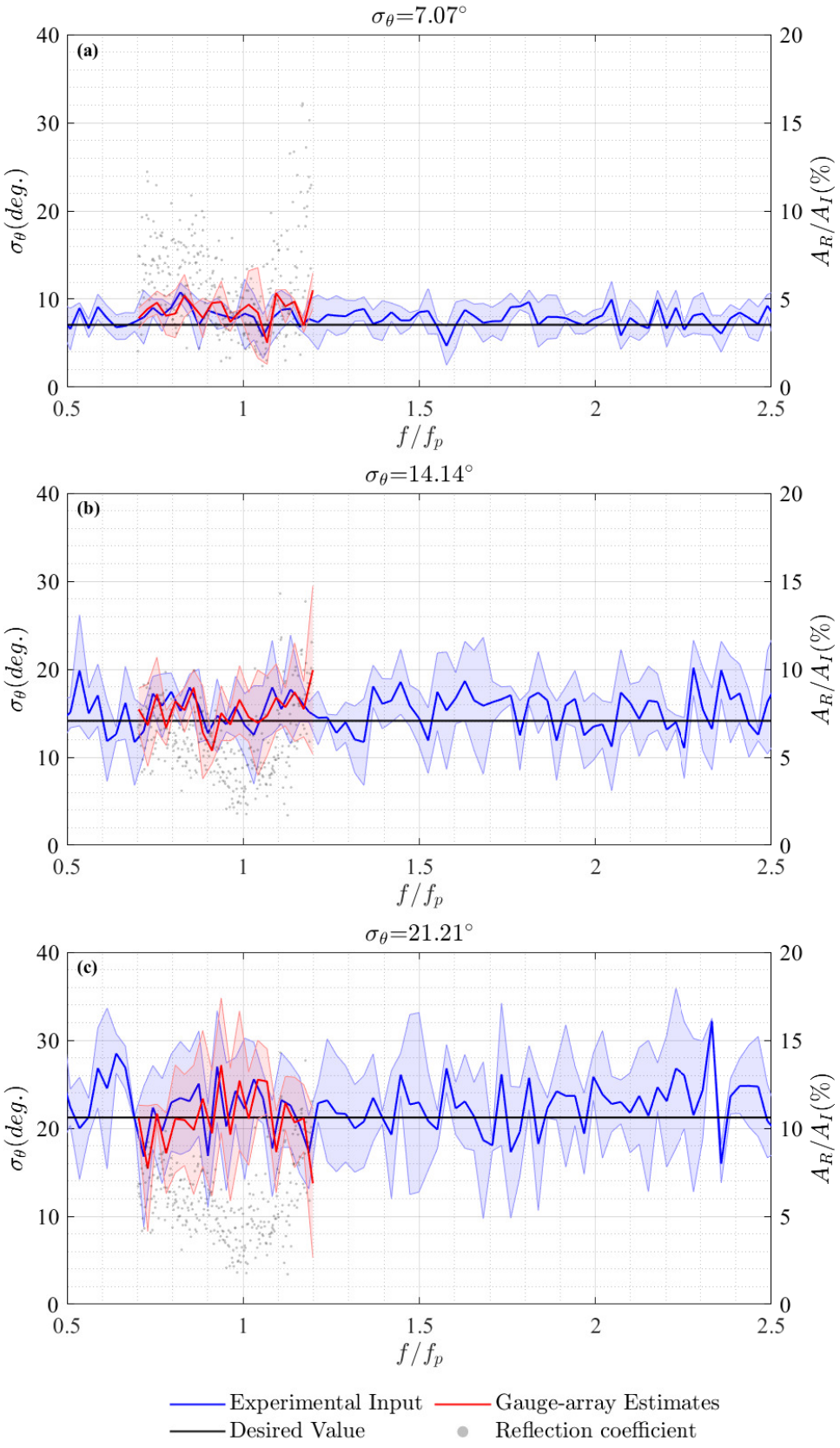


Figure 2.7: PTPD estimates of spreading width σ_θ as a function of normalised frequency f/f_p based on experimental gauge measurements with input $H_s = 0.225$ m and degree of spreading (a) $\sigma_\theta = 7.07°$, (b) $\sigma_\theta = 14.14°$ and (c) $\sigma_\theta = 21.21°$; Transparent envelopes show error bounds.

in the wave tank are as input. This method outputs wave direction $\theta(f)$ at each generated frequency, to produce directional distribution $D(f, \theta)$ I calculate average spreading over bins of 16 discrete frequency components.

Figure 2.7 shows the directional spreading calculated using the PTPD method (red lines). Owing to the spacing of the experimental gauge array, PTPD estimation is performed over a limited frequency range $0.75f_p - 1.2f_p$. When using this approach it is only possible to estimate the direction in which waves travel when the separation between gauges being used lies in the range $0.05\lambda_p$ to $0.45\lambda_p$. The reflection coefficient (amplitude of reflected waves divided by that of the incident wave) may be also estimated using the PTPD method. The degree of spreading estimated using the PTPD method shows that the desired spreading is achieved in the tank (see table 2.3). The input spreading values in table 2.3 are slightly different from those, in table 2.2, owing to the limited frequency band over which they are calculated. The estimated reflection coefficients are predominately below 10% over the range of frequencies $0.75f_p - 1.2f_p$. The estimated effects of reflections are the smallest near the peak frequency.

First, the sea states with input degrees of directional spreading $\sigma_\theta = 14.14°$ and steepness $H_s k_p/2 = 0.16$ are investigated. In figure 2.8, blue lines represent properties measured using buoys, and red lines represent those measured using the gauges. Both gauge and buoy measurements provide accurate results with slightly lower spreading than input values over the frequency range $\approx 0.7f_p - 1.8f_p$.

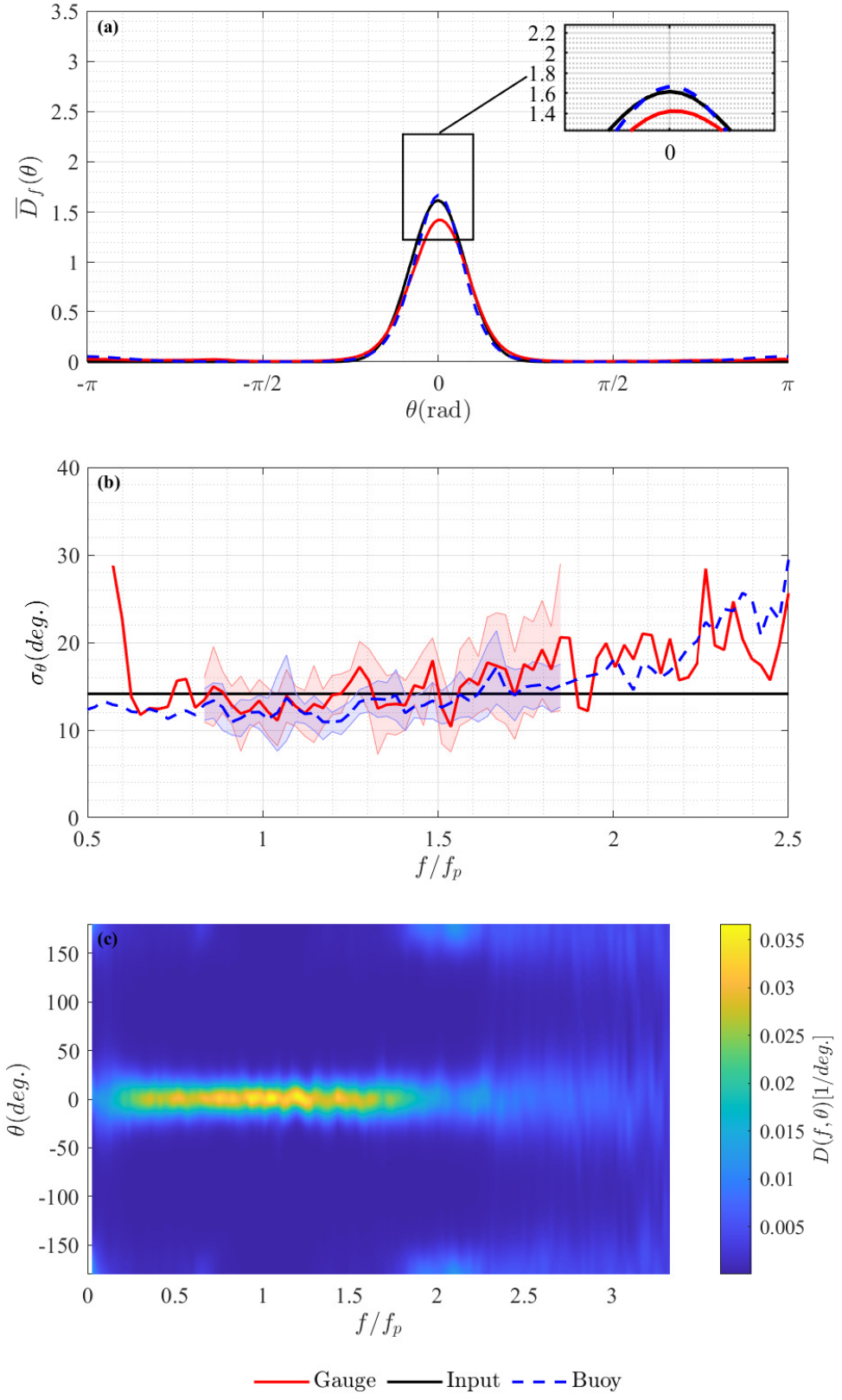


Figure 2.8: EMEP estimates of spreading for experimental gauge and buoy measurements with input $H_s = 0.225$ and degree of spreading $\sigma_\theta = 14.14°$; (a) mean directional spreading function (averaged over the range $0.83f_p - 1.85f_p$); (b) spreading width σ_θ as a function of normalised frequency f/f_p, where transparent envelopes show error bounds; (c) the directional spreading function $D(f, \theta)$ estimated for buoy measurements.

Table 2.3: Average Spreading calculated over the range $0.83f_p - 1.85f_p$ ($0.75 - 1.2f_p$ for the PTPD method)

Input (deg.)	$H_s k_p/2$ (m)	PTPD (deg.)	Gauge (deg.)	Buoy (deg.)	Slack Moored Buoy (deg.)	(Gauge-Buoy)/Input (%)
7.53	0.16	8.50	8.72	7.68	7.13	13.80
14.50	0.16	14.63	14.59	13.14	13.9	10.00
20.61	0.16	21.23	19.8	17.97	17.83	8.88
14.50	0.13	15.49	13.61	13.55	/	0.41

On average, the values estimated using the buoy measurements are 10% lower. Estimates based on buoy measurements are accurate over a slightly wider frequency range which is consistent with the results for synthetic wave data. Similar results can be also found in Benoit and Teisson (1995), which compared a single point gauge system which approximated heave, pitch, and roll to a gauge array and found that the spreading of following sea states can be estimated more effectively by the single point system.

In figure 2.8, the estimated spreading widths for both types of measurement are slightly smaller than the input values. For sea states that are steep, reductions in directional spreading width can occur as a result of nonlinearity (Latheef et al., 2017). The steepness of the sea states in figure 2.8 is $H_s k_p/2 = 0.16$, which is relativity steep. The same experiments were also carried out for reduced sea state steepness, $H_s k_p/2 = 0.13$.

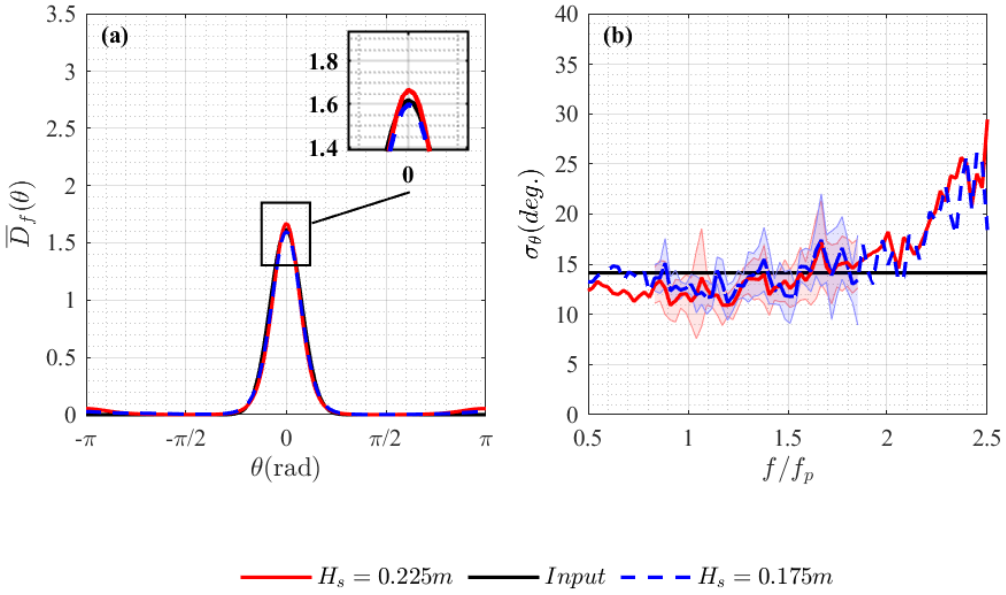


Figure 2.9: EMEP estimates of spreading based on buoy measurements for the same experiments carried out with two values of significant wave height $H_s = 0.225$ m and $H_s = 0.175$ m; (a) mean directional spreading function (averaged over the range $0.83f_p - 1.85f_p$); (b) spreading width σ_θ as a function of normalised frequency f/f_p, where transparent envelopes show error bounds.

In figure 2.9, directional properties estimated for the two experiments carried out with input steepness $H_s k_p/2 = 0.16$ and 0.13 are compared. The estimated spreading width is slightly larger (1.8% on average) for the reduced steepness sea state bringing the measured values closer to the input values. Some discrepancies between input and output may still result from nonlinearity as the second sea state is still steep. The estimated spreading width increases with frequency. In figure 2.6 It is shown that this may be a result of second-order bound nonlinearity. For experimental data, another reason may be that the signal to noise ratio becomes relatively low in both the high or low frequency tails of the spectrum making the waves at these frequencies appear more spread.

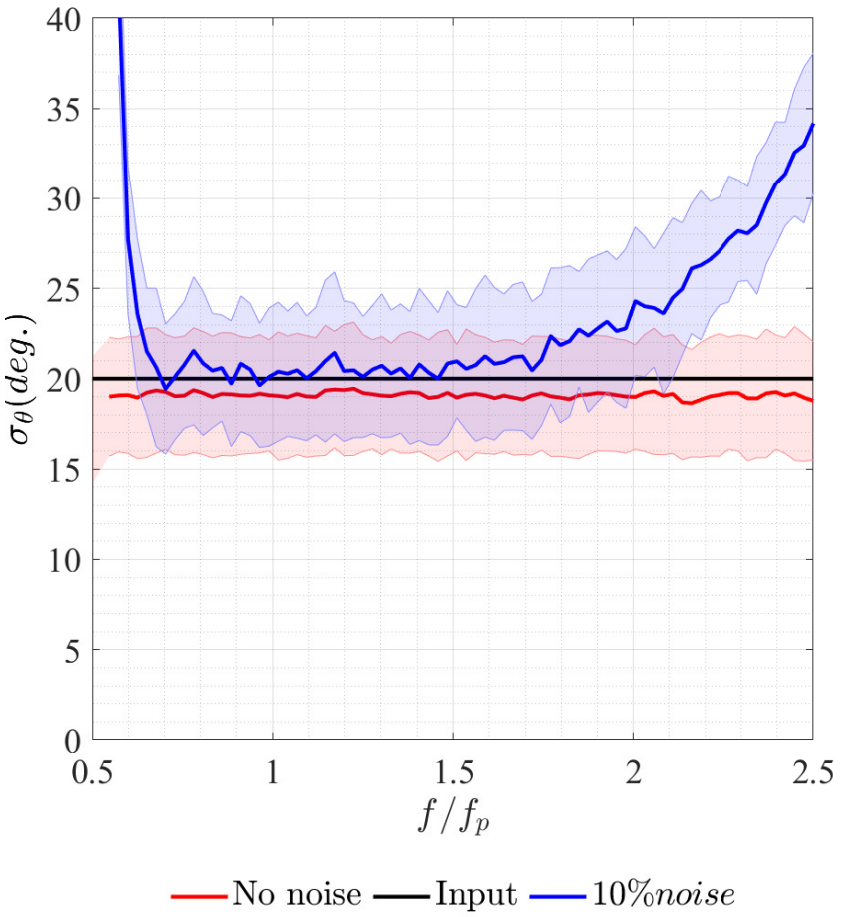


Figure 2.10: EMEP estimates of spreading width σ_θ as a function of normalised frequency f/f_p for synthetic buoy data with an input spreading value of $\sigma_\theta = 20°$; data with no noise, and data with 10% noise. Transparent envelopes show error bounds.

In figure 2.10 the effects of noise on estimated spreading width using synthetic data are examined. Noise is added to the synthetic data using a white noise spectrum, in which RMS noise amplitude is set equal to 10% of the RMS amplitude of buoy displacements. For the data with noise, estimated spreading starts to deviate from expected spreading at about twice the peak frequency, whereas the estimates based on the data without noise are stable across the frequency range. Figure 2.8 (c) shows directional spreading function over $0 - 2.5f_p$. The spectrum

becomes bimodal at high and low frequencies, which may make the estimated spreading disproportionally large as well. A similar phenomenon can be found in field data (Young et al., 1995), however in the experiments this is most likely a result of noise, aliasing or reflections rather than a result of the physics which drives this in the ocean. The reflection coefficients presented in figure 2.7 are approximately 10%.

The spreading width measured using the gauge-array is slightly larger than that measured by the buoys, in figure 2.8. Figure 2.11 shows directional estimates for all three following experiments with input degrees of directional spreading $\sigma_\theta = 7.07°$, 14.14° and 21.21°. Red solid lines show gauge measurements and blue solid lines show buoy measurements. Transparent envelopes show error bounds (over the range $0.83f_p - 1.85f_p$). The directional spreading width estimated using buoy measurements is slightly smaller than that measured using gauges for all the cases (see table 2.3). When the degree of spreading increases, the relative difference is reduced. The resulting directional spectra are illustrated as polar plots in figure 2.12.

The observations of directional spreading, show the same trend as other measured sea state parameters, such as significant wave height, skewness, and kurtosis which differ most from gauge measurements in narrowly spread conditions (McAllister and van den Bremer, 2020). In steep sea states with narrow directional spreading, increased Lagrangian transport induced by large waves may cause the apparent narrowing of the directional spectrum measured by the buoys. In table 2.3 averaged values of spreading are presented. The directional spreading estimated using

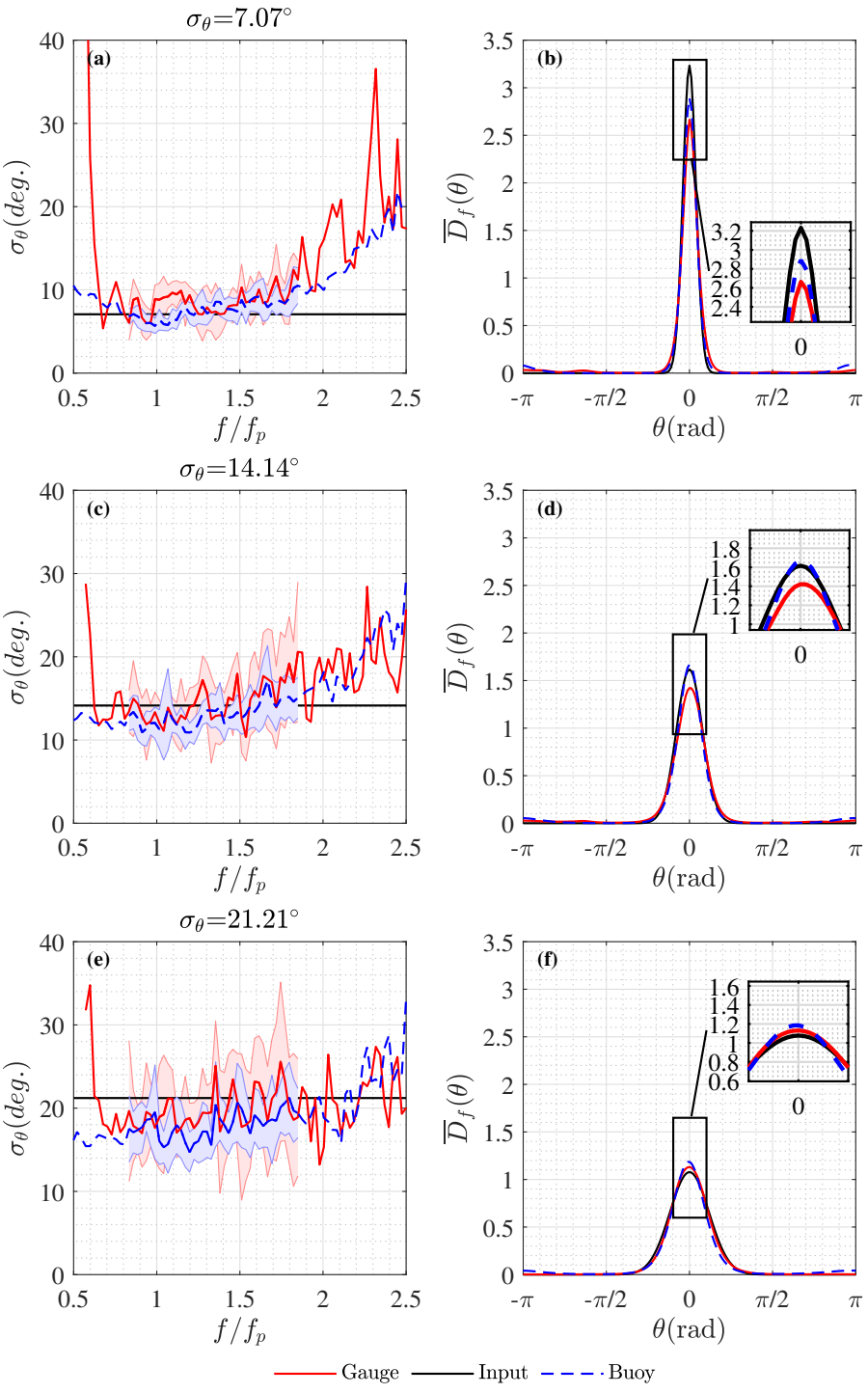


Figure 2.11: EMEP estimates of spreading for experimental gauge and buoy measurements with input $H_s = 0.225$ m and degree of spreading (a, b) $\sigma_\theta = 7.07°$, (c, d) $\sigma_\theta = 14.14°$ and (e, f) $\sigma_\theta = 21.21°$; (a), (c), (e)spreading width σ_θ as a function of normalised frequency f/f_p, where transparent envelopes show error bounds (in the range $0.83f_p - 1.85f_p$); (b), (d), (f) mean directional spreading function (averaged over the range $0.83f_p - 1.85f_p$).

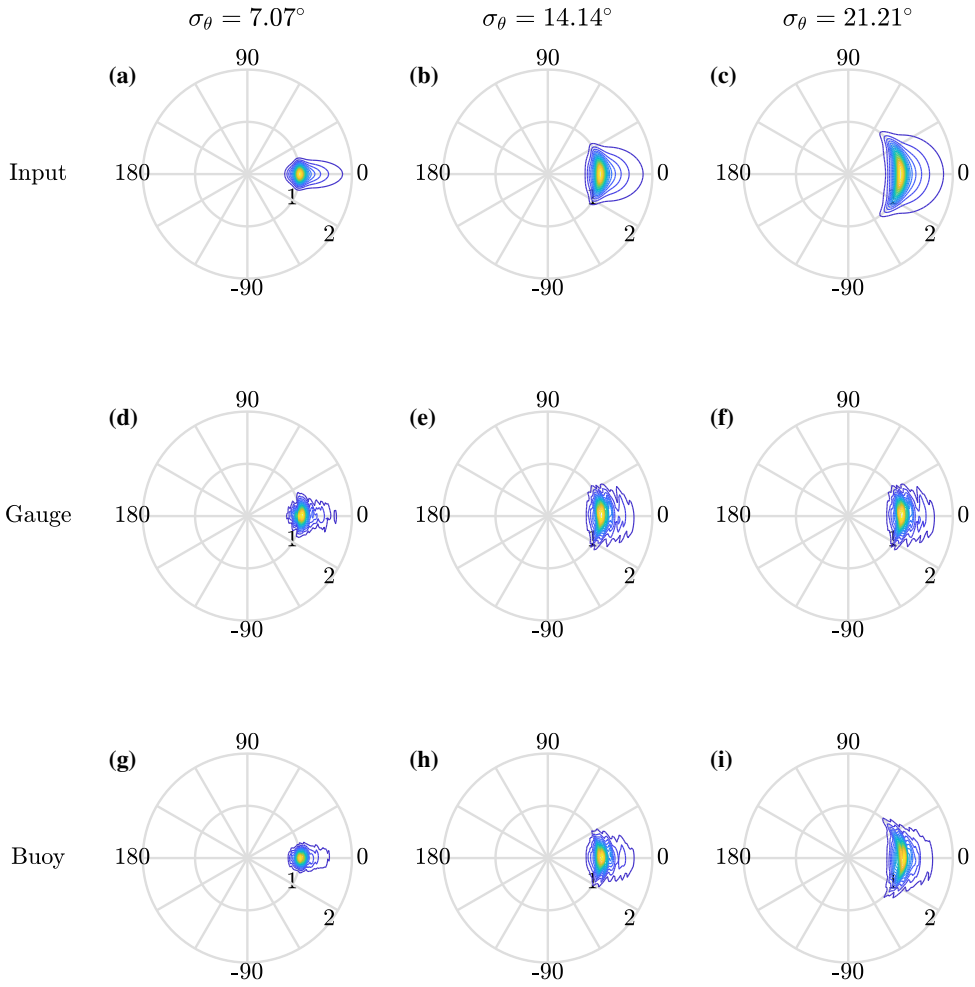


Figure 2.12: Input and estimated (EMEP) directional spectra for experiments with input directional spreading width $\sigma_\theta = 7.07°$, $14.14°$ and $21.21°$ and $H_s = 0.225$m; (a)-(c) desired directional spectra; (d)-(f) directional spectra estimated using gauge measurements; (d)-(f) directional spectra estimated using buoy measurements.

buoy measurements for experimentally generated following sea states is reasonably accurate and only differs from gauge measurements by around 10%.

2.3.2 Crossing sea states

Crossing sea states may occur when waves generated by different weather systems combine, or during highly transient systems such as tropical storms. As only

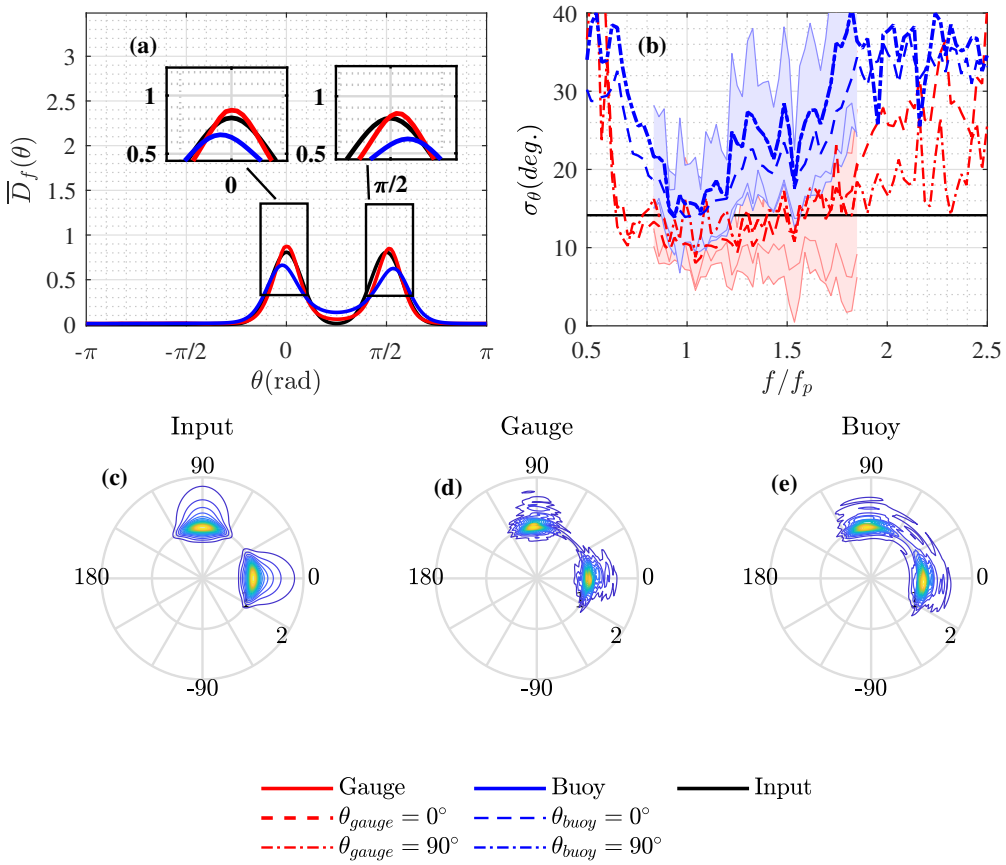


Figure 2.13: EMEP estimates of spreading for crossing experiments based on gauge (red lines) and buoy (blue lines) measurements with input $H_s = 0.225$ m and degree of spreading $\sigma_\theta = 14.14°$ and crossing angle $\Delta\theta = 90°$; (a) mean directional spreading function (averaged over the range $0.8f_p - 1.5f_p$); (b) spreading width σ_θ as a function of normalised frequency f/f_p for the two directions (0°,90°), transparent envelopes show error bounds (in the range $0.83f_p - 1.85f_p$), and the black lines shows input spreading; (c) desired directional spectra; (d) directional spectra estimated using gauge measurements; (e) directional spectra estimated using buoy measurements.

three quantities are used for directional estimates made using buoy measurements, bimodal directional distributions may present a challenge. Identifying crossing sea states is important, as they can be hazardous for seafaring vessels and potentially increase the likelihood of observing large wave crests (McAllister et al., 2019).

In figure 2.13, directional spectra are estimated using buoy and gauge mea-

surements for experiments where two sea states with the same peak frequency and directional spreading $\sigma_\theta = 14.14$ cross at an angle of $\Delta\theta = 90°$. Directional estimates made using gauge measurements perform better than those made using buoy measurements, in agreement with Benoit and Teisson (1995). The spreading of two wave systems estimated using the gauges is accurate over the range from $0.8f_p - 1.5f_p$, whereas the values estimated using the buoys are only accurate near the peak frequency and significantly overestimate the degree of spreading elsewhere. Estimates based on both types of measurement identify two peaks, but the definition of the peaks is worse for the buoy estimates, this is illustrated using polar plots in panels (c)-(e). The peaks of the mean directional spreading function measured by the buoys are also shifted away from each other, meaning each perceived mean direction is incorrect and the crossing angle is overestimated (see figure 2.13(a))

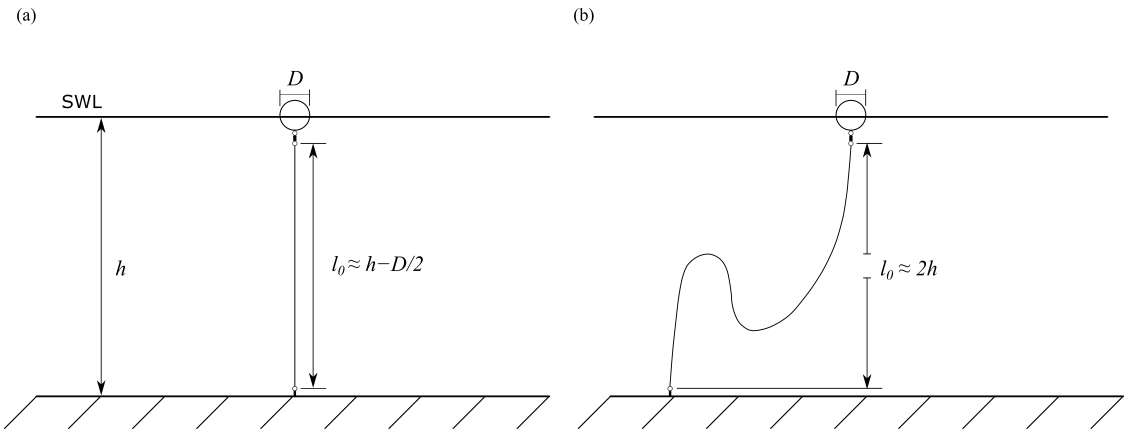


Figure 2.14: Buoy mooring configurations showing undisturbed length l_0, (a) taut mooring configuration, and (b) alternative mooring configuration adapted from (Datawell, 2006)

2.3.3 Mooring configuration

In McAllister and van den Bremer (2019) it was shown that the mooring configuration used for the experiments analysed here, had no observable effect on the vertical displacement η. However, the lateral (x, y) buoy position, which will be affected by the mooring, is important in directional estimation. In McAllister and van den Bremer (2019), additional experiments were carried out using a buoy with an alternative mooring configuration. The alternative mooring was designed to reflect more closely the type of mooring used for buoys in the ocean. The intention of this configuration, as with actual buoy moorings, is to allow for greater lateral x, y displacements. Figure 2.14 shows the taut, and alternative 'slack' mooring configurations. The standard deviation of x displacement for slack mooring was 4.2 m, whereas that of original mooring was 1.12 m indicating the different mooring had a significant effect on the lateral motion of the buoy.

In figure 2.15, directional spreading is compared for buoys with two different moorings. Directional spreading is not significantly affected by the types of mooring near the peak frequency. However, the slack-mooring appears to have an impact on the consistency of estimation, resulting in a narrower reliable frequency range (average spreading can be found in table 2.3). In figure 2.16, the polar plots which correspond to the slack moored buoy are marginally less well defined than those produced using original taut mooring.

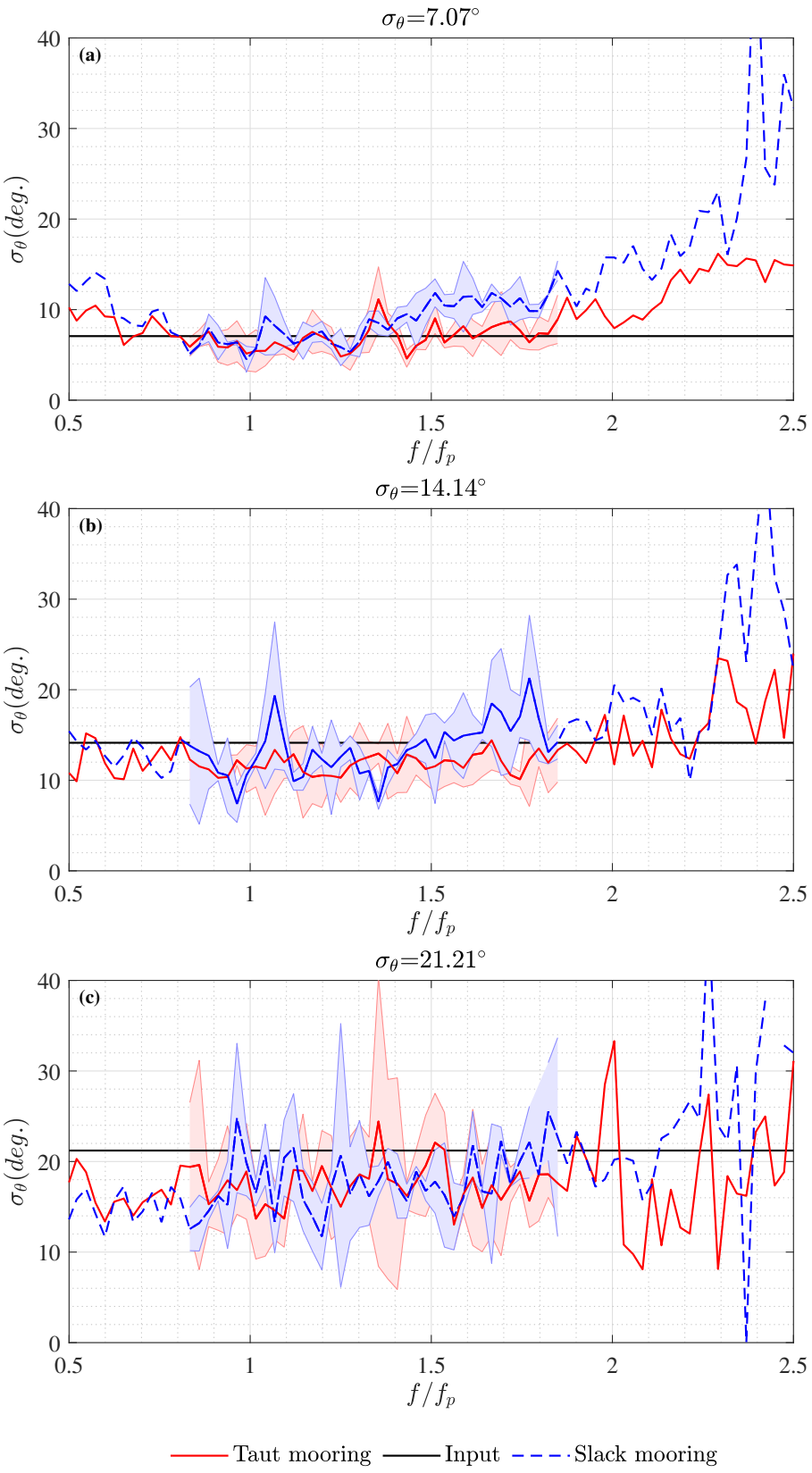


Figure 2.15: EMEP estimates of spreading width σ_θ as a function of normalised frequency f/f_p for experimental buoy measurements made with taut (red lines) and slack (blue dahs lines) mooring configurations with input $H_s = 0.225$ m and degree of spreading (a) $\sigma_\theta = 7.07°$, (b) 14.14° and (c) 21.21°. Transparent envelopes show error bounds (in the range $0.83f_p - 1.85f_p$) and the black lines show input spreading.

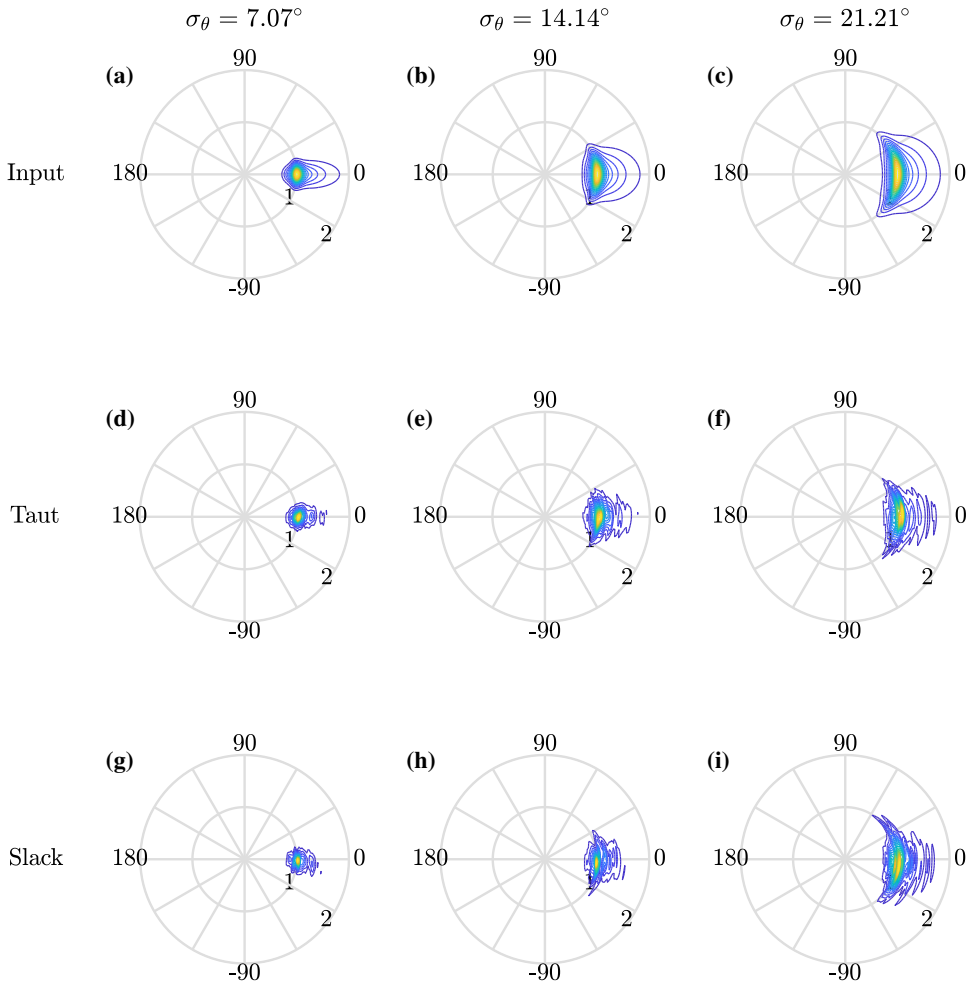


Figure 2.16: Input and estimated (EMEP) directional spectra for experimental buoy measurements made with taut and slack mooring configurations with input directional spreading width $\sigma_\theta = 7.07°$, $14.14°$, and $21.21°$ and significant wave height $H_s = 0.225$m; (a)-(c) desired directional spectra; (d)-(f) directional spectra estimated using taut moored buoy measurements; (g)-(i) directional spectra estimated using alternative slack moored buoy measurements.

2.4 Conclusions

In this chapter, directional estimates performed using an array of gauges and individual buoys are compared. To my knowledge, a direct comparison of gauge and buoy based estimates of spreading has not previously been carried out in

the lab, where unlike the field directional spreading is defined a priori. Previous experimental studies (McAllister and van den Bremer, 2019; McAllister and van den Bremer, 2020; Liu et al., 2015) have presented comparisons of measured surface elevation, extreme wave statistics and sea state parameters such as significant wave height, and peak period.

Using synthetic buoy data I compared directional estimates produced using MEM, MLM, EMEP, and IMLM methods and found that EMEP method provided the most stable and accurate results. This is consistent with Hashimoto et al. (1995) and Latheef et al. (2017) which also arrived at the same conclusion using synthetic wave data. Additionally, synthetic buoy data showed that a sharp increase in estimated spreading at high frequencies observed for experimental data is most likely a result of a low signal to noise ratio. It is demonstrated that double summation wave generation reduces the accuracy of spreading estimates made using synthetic gauge data, and showed that second-order bound nonlinearity can slightly reduce the range of frequencies over which estimates are reliable. A fitting method is proposed to estimate the spreading width σ_θ. It is shown that the fitting method is less sensitive to the small fluctuations at the end tail of the frequencies and provides more stable results than conventional standard deviation estimation.

Fitting a normal distribution to estimate spreading width provides a means of estimating σ_θ which is less sensitive to noise than calculating the standard deviation.

For following sea states based on a JONSWAP spectrum, buoy and gauge measurements produced similar estimates of directional spreading width over the frequency range $0.83f_p - 1.85f_p$ for the experiments. The buoy measurements provide stable estimates of spreading over a wider range of frequencies than the wave gauge array, owing to the finite separation of the wave gauges. On average, spreading estimates based on buoy measurements were around 10% lower than those produced using gauges. At frequencies greater than about $2f_p$ the estimated directional distributions became bimodal, which is most likely the combined effect of aliasing, noise, and reflections, but may also be influenced by bound nonlinearity. The same sharp increase in estimated directional spreading was also observed in the experiments performed by Latheef et al. (2017).

Both buoy and gauge-array estimates of directional spreading width were generally lower than the input spreading values. A reduction in directional spreading can occur as a result of nonlinearity for individual large wave events (Latheef et al., 2017). However, the values of spreading width measured using the PTPD method did not display a reduction in spreading, which may suggest the underestimation observed is a systematic issue associated with the EMEP when applied to the measurements. I also observed the underestimation of spreading width when analysing synthetic linear and second-order data. Latheef et al. (2017) also observed a reduction in spreading width around the peak frequency when using 6 synthetic measurements of surface elevation to perform EMEP directional estimation. The

experimental observations are consistent with in situ observations made by Le Merle et al. (2021), where directional spreading estimates made using NDCB buoys (National Data Buoy Center) were shown to be on average 3° narrower than estimates made using scanning radar SWIM (Surface Waves Investigation and Monitoring) measurements.

In crossing sea states buoy and gauge-array estimates of spreading were more notably different. Estimates made using the gauge-array showed two distinct directional peaks and lower spreading width than the input value. Whereas, estimates made using buoy measurements significantly overpredicted the degree of directional spreading and struggled to identify two distinct directional peaks. The position of the peaks was also shifted away from each other, meaning their mean directions and perceived crossing angle were incorrect.

The two mooring configurations I examine displayed no significant differences in estimated degree of directional spreading. However, mooring dynamics may be more influential for real ocean measurements where configurations are less compliant or biofouling occurs.

The results demonstrate that individual wave buoys are capable of producing estimates of directional spreading to a reasonable degree of accuracy in simple sea states. However, in complex crossing sea states, where multiple wave systems exist, estimates of directional spreading are significantly less accurate and should

be treated with uncertainty or validated using other measurement systems with more degrees of freedom.

3

Mooring influence on wave measurement

Contents

3.1 Chapter overview 66
3.2 Introduction 69
3.2.1 Mooring configuration 69
3.2.2 Study site 69
3.2.3 Mooring distance 69
3.3 Data selection and quality control 71
3.4 Measured Wave Statistics 74
3.4.1 Spreading 78
3.5 Conclusions 84

3.1 Chapter overview

In chapter 2, I found that there was no observable effect on the estimated directional spreading near the peak frequency, made using buoy measurements acquired in the lab with taut and slack mooring configurations. However, mooring effects may be more influential in the field owing to the different mooring configurations and

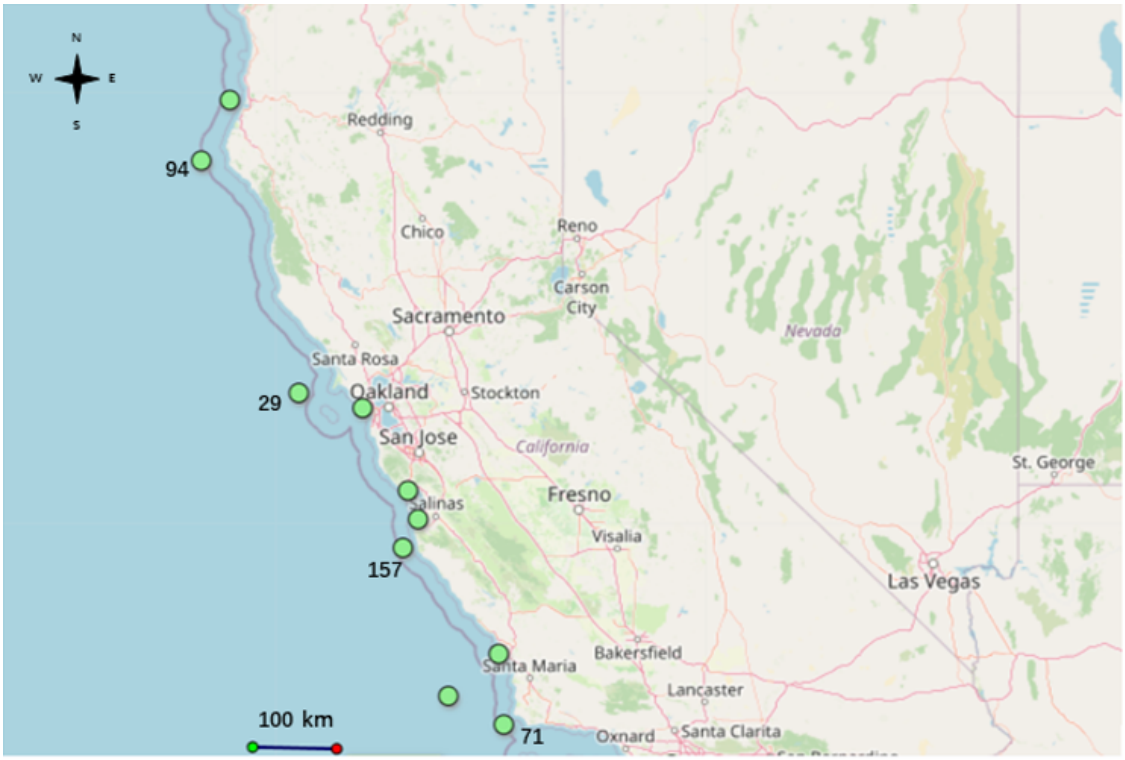


Figure 3.1: Overview map of CDIP buoy deployment (https://cdip.ucsd.edu/m/)

the large Lagrangian-mean displacements. In this chapter, a large data set from Coastal Data Information Program (CDIP) were used to investigate the potential effects of moorings for real ocean measurements. The CDIP operates an extensive network of buoys which are used for metocean monitoring along the coastlines of the United States. Figure 3.1 shows active buoy sites on along the west coast of America and table 3.1 shows information on buoy stations used in this chapter. A vast data set is provided by this program for engineers to investigate ocean-related problems. For all the data used herein, time series and wave statistics were first retrieved from the CDIP database and then analyzed after quality control.

This chapter is laid out as follows. First, I provide details of the types of buoys, moorings and study sites I analyzed (section 3.2), introduce the estimated sea

state parameters and procedures of quality control (section 3.3). I analyze the relationship between mooring distance and sea state parameters in sections 3.4. Finally, I draw conclusions in section 3.5.

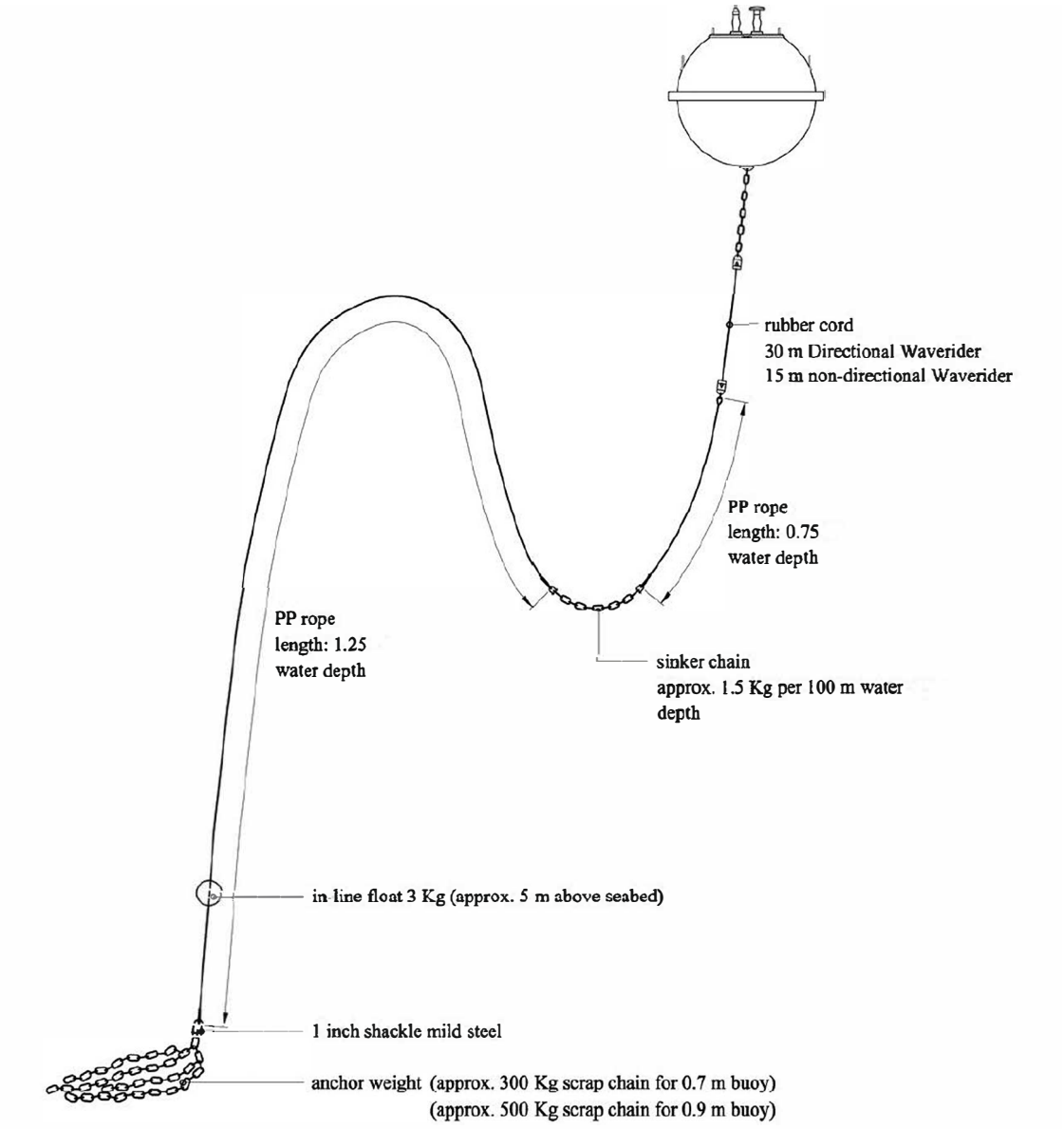


Figure 3.2: The typical mooring for a CDIP buoy installed in water depth larger than 200 m adapted from Datawell (2006)

3.2 Introduction

3.2.1 Mooring configuration

Figure 3.2 shows a typical mooring configuration for a Datawell wave buoy on a water depth larger than 200 m. The top section comprises a 30 m rubber cord which allows buoys to follow the motion of waves, to help ensure good quality wave measurements. A ballast chain attached to the mooring eye located on the bottom of the buoy connects a Datawell Directional Waverider MKIII 0.9 m diameter buoy and the mooring. The buoy follows the wave motions and measures vertical, north and west displacements which are collected at a rate of 1.28 Hz.

3.2.2 Study site

Data measured using the mooring configuration described above were collected from four stations at sites (see table 3.1) along the west coast of America, namely Cape Mendocino (40.29°N 124.73°W), Point Sur (36.33°N 122.10°W), Point Reyes (37.94°N 123.46°W) and Harvest (34.45°N 120.78°W). These stations were chosen owing to the availability of data with selected sea state conditions. Herein, field data collected between 2000 to 2019 are used.

3.2.3 Mooring distance

Before studying the potential influence of mooring compliance on buoy measurements, I define a measure of the buoy position relative to its equilibrium position in the absence of wind and waves, namely mooring distance d_m. The equilibrium

Table 3.1: Information on buoy stations used in this studies

Station Number	Name	Latitude	Longitude
94	CAPE MENDOCINO	40.294870°	-124.731770°
157	POINT SUR	36.334767°	-122.103900°
29	POINT REYES	37.936675°	-123.462920°
71	HARVEST	34.451650°	-120.779817°

position or centre of a buoy watch circle is defined using the GPS coordinates of the original deployment location provided by CDIP. Mooring distance d_m is defined as the horizontal distance from the original deployment location, which is measured using the mean GPS coordinates output for every 30 minutes of buoy measurement. Figure 3.3 presents the relationship between mooring distance and mooring length. The mooring distance, or watch circle, can be approximated by using the Pythagorean Theorem if the water depth and mooring length are known. Herein, the watch circle radius R is defined using the maximum values of mooring distance recorded for a given dataset. Figure 3.4 shows a histogram of GPS locations relative to the equilibrium position for buoy station 71 during its deployment. This visualises the watch circle of this buoy station. The buoy measurements are divided into 5 groups based on their normalised radial position d_m/R. Sea state parameters and statistics are investigated using above groups to assess the influence of mooring extension on buoy measurements.

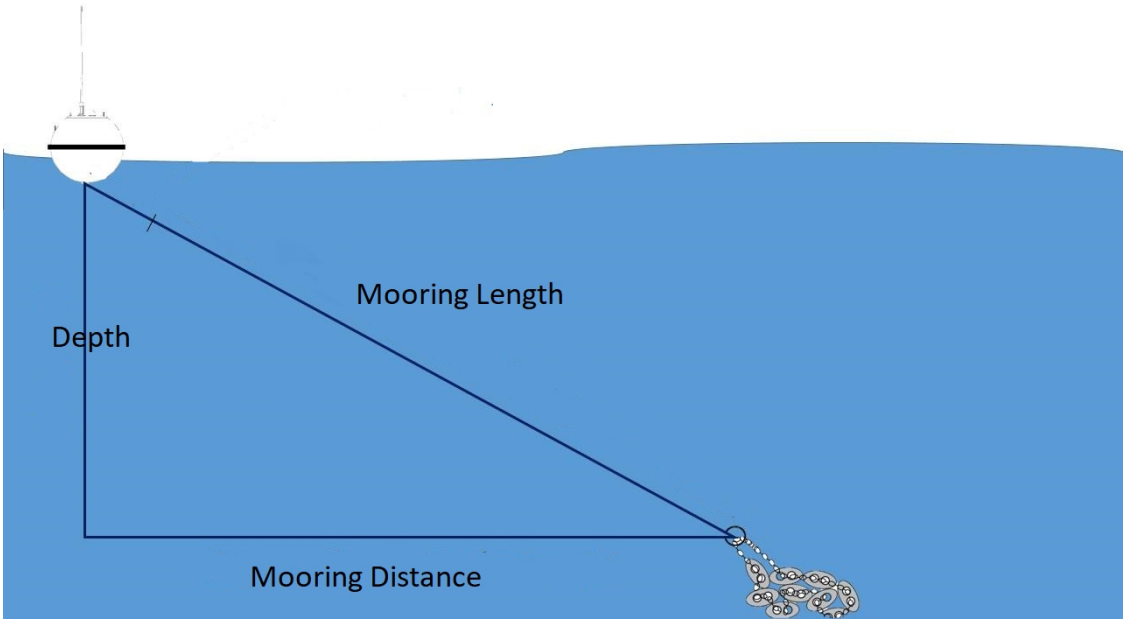


Figure 3.3: Schematic diagram of the mooring distance (adapted from https://cdip.ucsd.edu/m/documents/index.html)

3.3 Data selection and quality control

CDIP deploys buoys in various ocean environments, from coastal waters to the deep ocean which requires different mooring configurations. Only measurements from buoys deployed in deep water conditions (i.e. depths greater than 200 m) are used herein to ensure similarity between their mooring configurations and metocean conditions. To ensure similarity within the data set used, data were collected from similar sea states. Sea states with the value of significant wave height H_s of between 3 to 4 m, peak direction θ_p of between 300° to 320° and peak period T_p of between 10 to 11.5 s were selected. This was achieved using sea state parameters published for each buoy station by CDIP, which are calculated every 30 minutes prior to analysis.

Erroneous buoy data are unavoidable in the process of measuring, transferring

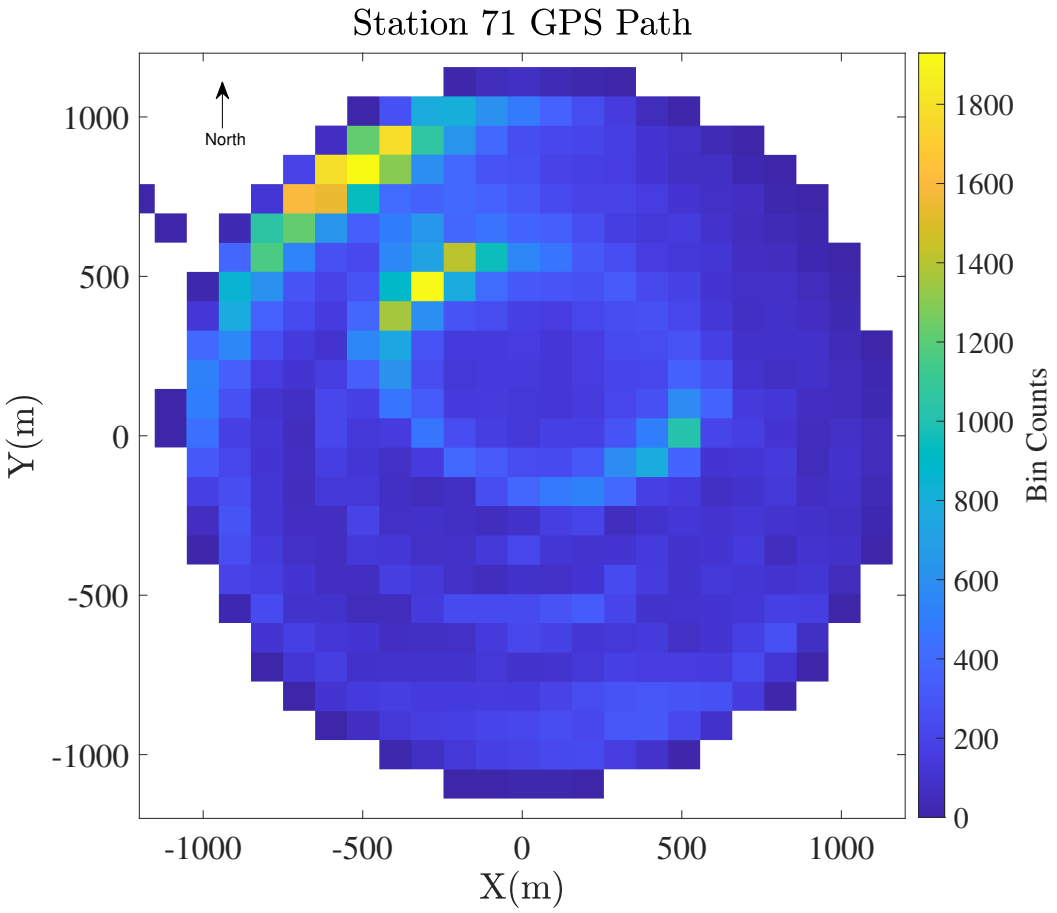


Figure 3.4: GPS path for in situ buoy measurements made using the Datawell Waverider buoy (71) moored beside Harvest in the North Pacific from 2002 to 2019. Buoy original deployment station is set as the centre (0,0) and, x and y represent the distance from original deployment. Each bin counts the number of points which shows the mean position over 30 minutes.

and reformatting. For example, outliers (spikes or out of scale data) may be due to technical defects in buoys or configuration errors. Data may be missing during transferring. Therefore, a strict quality control procedure is required to remove instrumental errors and produce a high-quality data set. First, questionable, bad and missing data flagged by CDIP were removed from the data set. Erroneous values not flagged by CDIP were identified using the strict quality control procedures presented by Christou and Ewans (2014). A number of flags were defined to check the

unrealistic values. Each flag corresponds to a specific erroneous buoy measurement. For example, the buoy signal lock-in resulting in consecutive equal values can be identified by flag 1 (see details below) and unexpectedly large elevations can be found by flags 3 and 4 (see details below). The main flags are described below (see (Christou and Ewans, 2014) for details):

- Flag 1: 10 successive points with the same value are found.
- Flag 2: Wave periods are longer than 25s.
- Flag 3: The limit rate of change of water surface elevation is exceeded. The limit is given below,

$$\frac{2\pi\sigma}{T_z}\sqrt{2\ln N_z}, \tag{3.1}$$

  where N_z is the number of zero up crossing periods and T_z is the mean zero up crossing period.
- Flag 4: Crests are greater than 4 times the standard deviation of wave crests.
- Flag 5: The energy of spectrum below 0.04Hz is larger than 5% of total energy.
- Flag 6: The energy of spectrum above 0.6Hz is larger than 5% of total energy.

Measurements were discarded if any of these flags were realised.

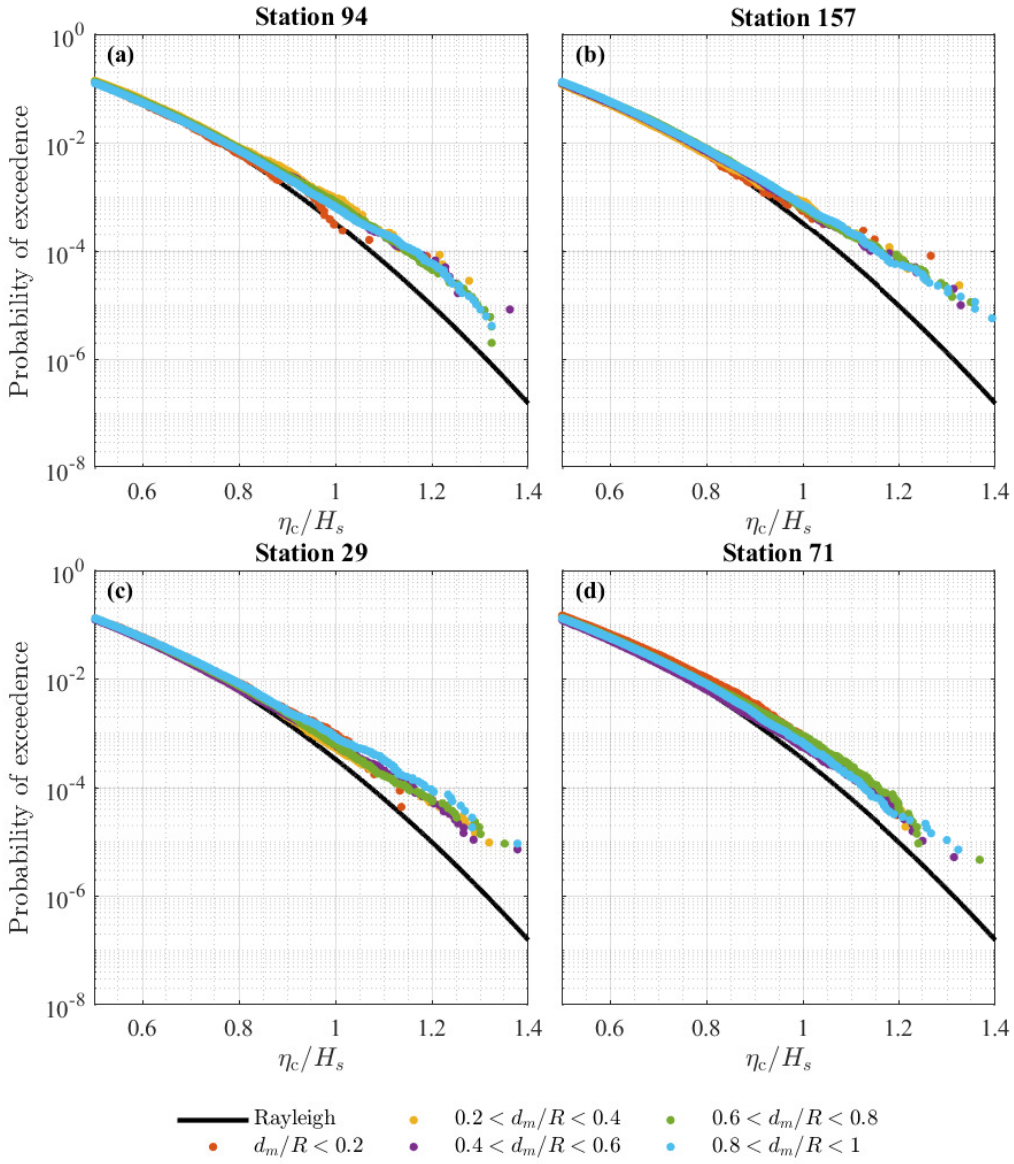


Figure 3.5: (a)-(d) Crest height exceedance probability for in situ buoy measurements made using stations 94, 157, 29 and 71 respectively. Measurements made in sea states with H_s of between 3 to 4m, θ_p of between 300° to 320° and T_p of between 10 to 11.5 s. Red, yellow, purple, green and blue markers denote normalized mooring distances from 0 to 1 in increments of 0.2. Black lines show the Rayleigh distribution (see Eq.(3.2)).

3.4 Measured Wave Statistics

Buoy stations 94, 157, 29 and 71 (see table 3.1) were chosen for analysis as their data sets contained a sufficient number of measurements from similar sea states

after data selection and quality control. Firstly, wave statistics are examined, such as skewness, kurtosis and the distribution of crest heights, for each buoy station. To reduce statistical uncertainty with the aim of isolating mooring effects, data recorded during similar sea conditions with a relatively high occurrence were selected.

Figure 3.5 shows the distribution of crest heights observed in measurements from buoy stations 94, 157, 29, and 71. The distribution of crest heights is often modelled using a Rayleigh distribution for linear and narrow banded sea states,

$$P\left(\eta_c > \eta\right) = \exp\left[-8\left(\frac{\eta}{H_s}\right)^2\right]. \tag{3.2}$$

The distribution of crest heights below values of about $\eta_c/H_s = 0.8$ are similar across mooring distances and are well described by a Rayleigh distribution (Longuet-Higgins, 1952). Discrepancies appear at the extreme tails of distributions which represent the largest crests measured at each mooring distance. To further quantify mooring influences on the measurements of these extreme crests at the tails of distribution, the root mean square differences were calculated between the Rayleigh distribution and estimated distributions in the range of normalized crests larger than 0.8. Figure 3.6 presents the root mean square differences for four buoy stations. For buoy station 71, the difference is largest at 0.2 normalized mooring distance and reaches the minimum at 0.6 normalized mooring distance. However, the difference is smallest at the same normalized mooring distance for stations 157 and 94.

There is no obvious relationship between mooring distance and crest distribution by comparing root mean square differences between various buoy stations. The

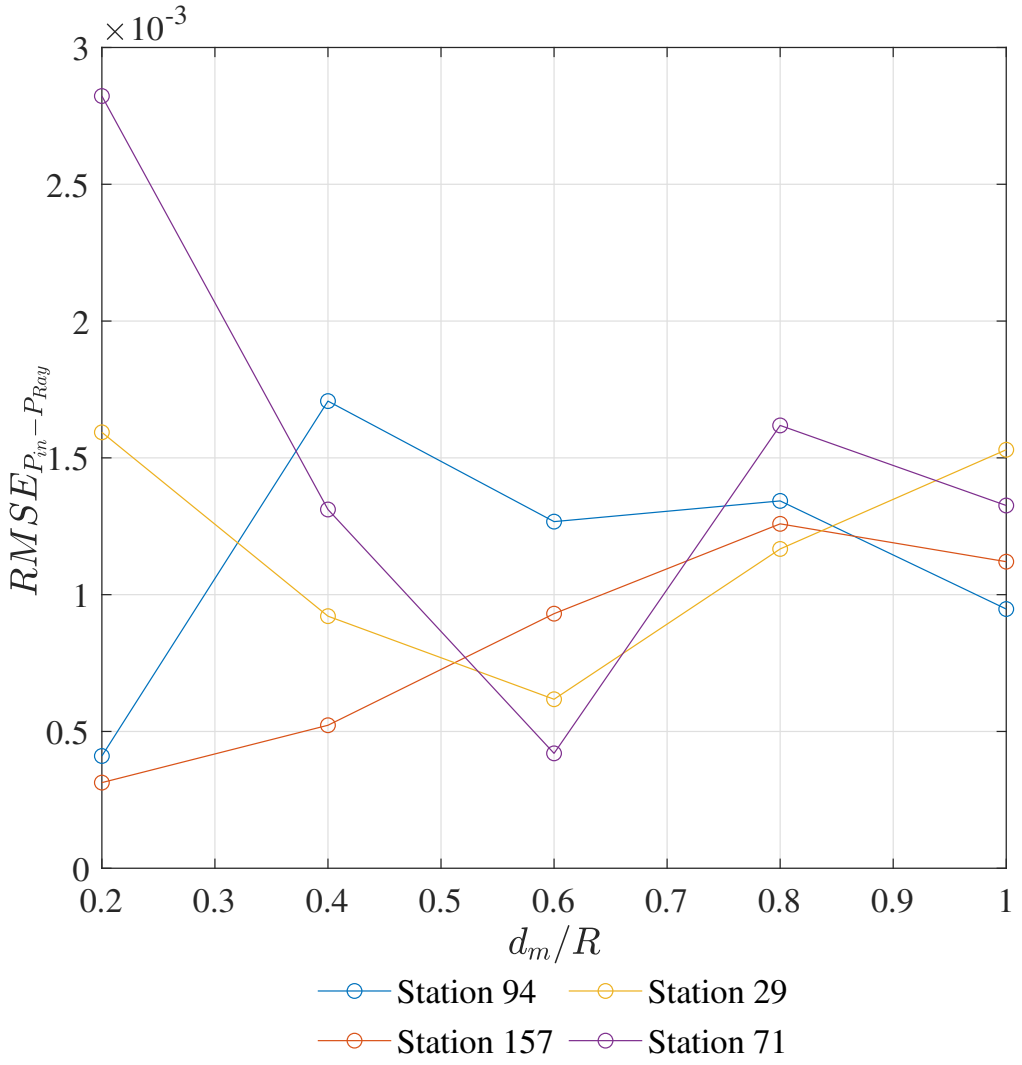


Figure 3.6: The root mean square differences between the probability of exceedance for Rayleigh distribution and estimated crest distribution for buoy stations 94, 157, 29 and 71

differences in the distribution of crest heights between different mooring distances were small which suggests that mooring effects do not significantly affect the measurements of extreme crests I have analysed. It should also be noted that the largest crests in each distribution are poorly sampled, and thus their probabilities are less reliable. Insufficient compliance in a mooring may cause buoys to be dragged under extreme crests. However, evidence of this is not clear in the data

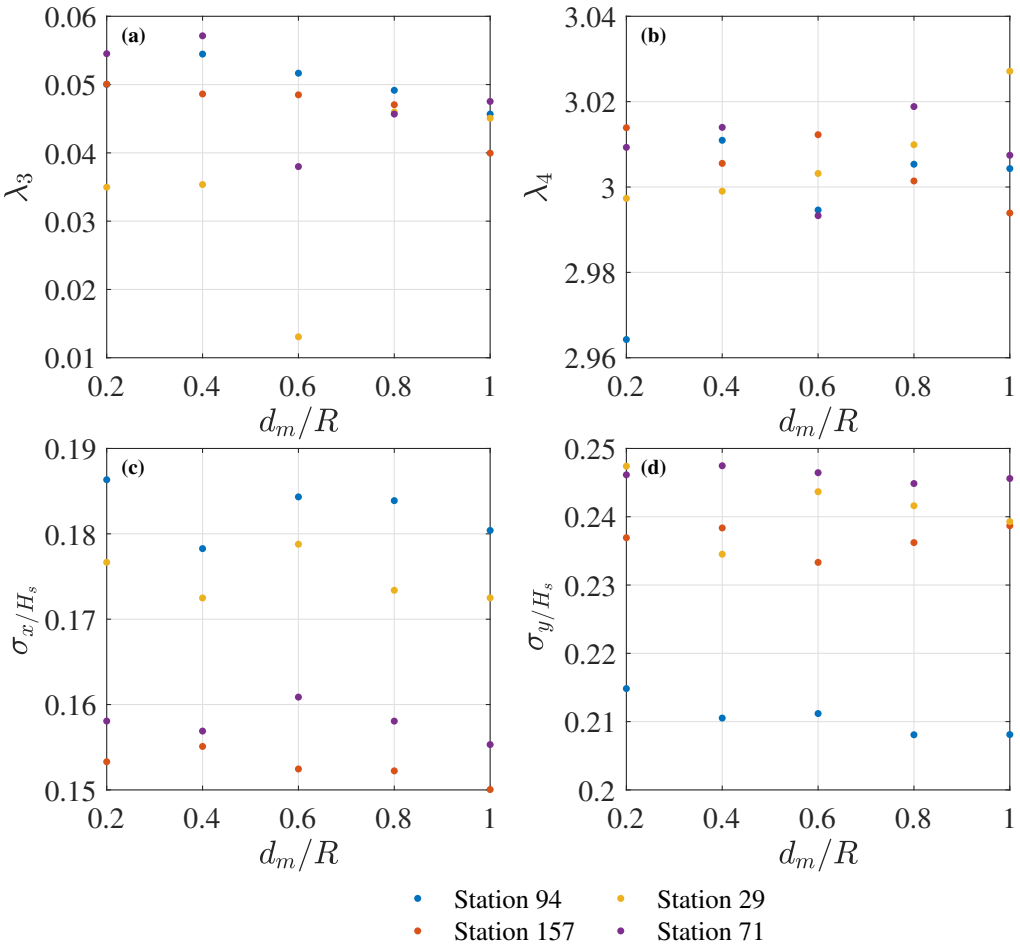


Figure 3.7: (a) Skewness, (b) kurtosis, (c) standard deviation of normalized horizontal x displacement and (d) standard deviation of normalized horizontal y displacement with in situ buoy measurements made using the station 94, 157, 29 and 71 respectively for various mooring distances. Data were in the similar sea states with H_s of between 3 to 4m, θ_p of between 300° to 320° and T_p of between 10 to 11.5 s. Blue, orange, yellow and purple markers denote stations 94, 157, 29 and 71.

I have examined. Further studies may be carried out in more severe sea states to investigate this mooring effect. The number of available data drops dramatically when the significant wave height is larger than 4m.

To further investigate if the measurements of extreme waves are influenced by mooring, skewness and kurtosis are estimated as a function of normalised mooring

distance in figure 3.7. Skewness is about 0.05 for all the cases. Skewness is always small for field buoy measurements as subharmonic bound waves are removed when the measurements of velocity or acceleration are converted to displacements (McAllister and van den Bremer, 2020). The superharmonic bound waves are presented in an Eulerian model, whereas they are not presented in a Lagrangian model. The kurtosis is about 3 for buoys with all the stations and mooring distances which indicates low nonlinearity. There is no observable difference between parameters with various mooring distances because of the low nonlinearity.

3.4.1 Spreading

In the field, Lagrangian transport and wind may cause buoys to move away from original deployment point, which results in varying mooring forces. The horizontal motion of buoys may be affected by these mooring forces. To investigate the effects of mooring forces on the horizontal motion and hence spreading estimated by buoys, the standard deviation of normalized displacements σ_x and σ_y are calculated. Displacement is normalised using significant wave height. The data are grouped by the mooring distance. Figure 3.7 shows the relationship between mooring distance and standard deviation of normalized horizontal motion. The values of normalized horizontal motion do not vary significantly in different mooring distances, in which the difference between dots is smaller than 0.01 for each buoy station. The weak trend can be found with decreasing normalized horizontal motion when the mooring distance increases.

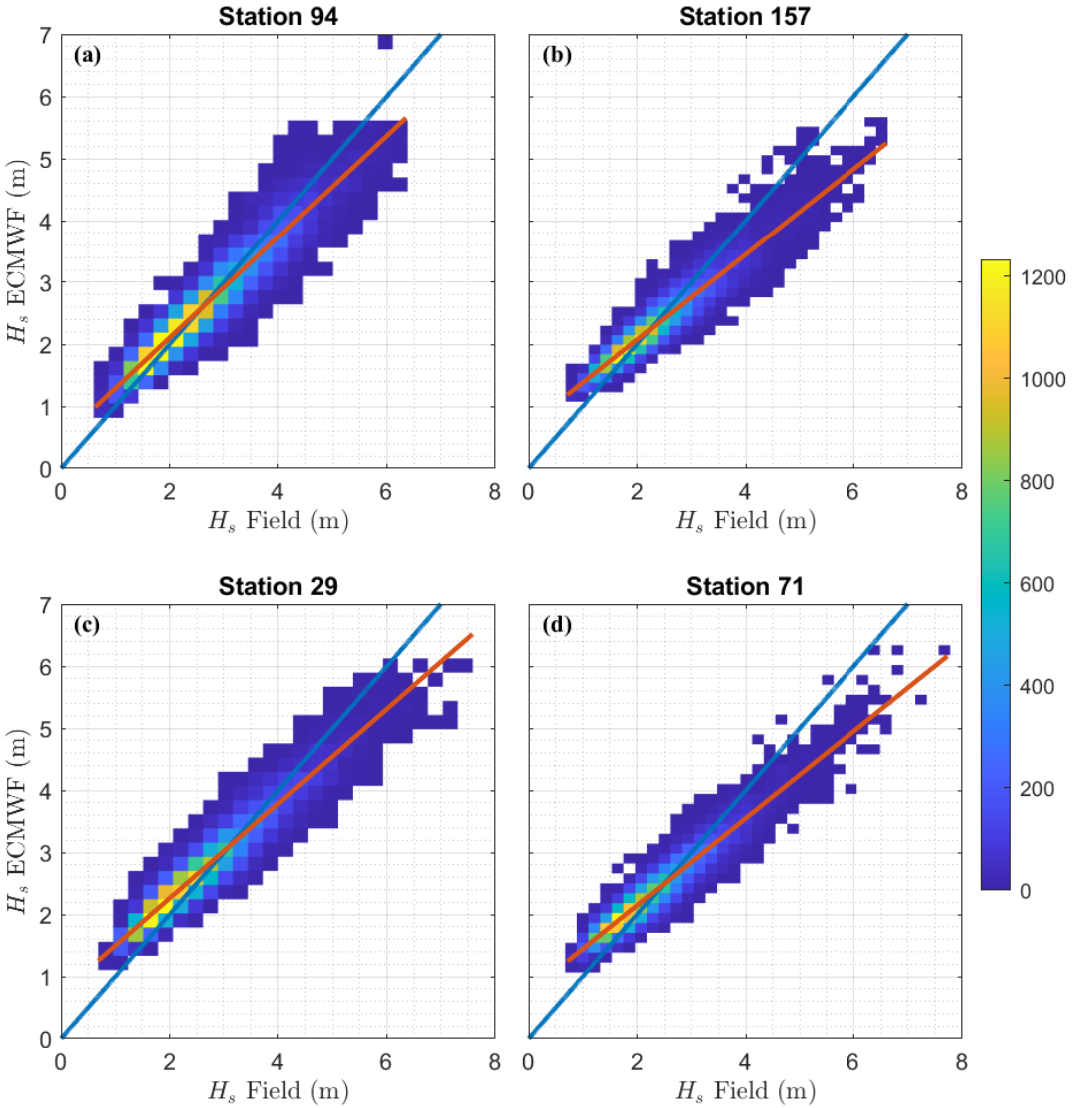


Figure 3.8: (a)-(d) Comparison of significant wave height between in situ buoy measurements made using the station 94, 157, 29, 71 and ECMWF hindcast from 2002 to 2019. The blue line represents ECMWF equal to the field. The red line presents the linear least square fitting line.

Since horizontal displacements are used to calculate directional spreading, the constrained motion may also affect the estimated spreading. To establish the influence of mooring effects on estimated spreading, estimates produced using buoy

measurements must be compared with a reliable source of spreading estimates. Here, estimates of directional spreading produced by hindcasts carried out by the European Centre for Medium-Range Weather Forecasts (ECMWF) are used to provide a comparison. ECMWF wave forecasts have been compared with estimates made using field buoy data and show good accuracy and predictive stability for bulk statistics, like significant wave height and peak period (Bidlot et al., 2002; Wang et al., 2019). The reanalysis data from ECMWF recreate past sea surface conditions over a long period by taking long period field observations into a numerical weather prediction system. The directional spreading of the wave estimated in ECMWF hindcasts is calculated as the mean directional spread $\overline{\sigma_\theta}$ given by,

$$\overline{\sigma_\theta} = \sqrt{2\,(1 - M_1)}, \tag{3.3}$$

where $M_1 = I_1/E_0$ and E_0 is the total energy. I_1 is given by,

$$I_1 = \int\int \cos(\theta - \theta_m(f))S(f,\theta)\mathrm{d}\theta\mathrm{d}f, \tag{3.4}$$

where $S(f,\theta)$ is the directional spectrum and $\theta_m(f)$ is the mean direction at frequency f presented by,

$$\theta_m(f) = \mathrm{atan}(sf(f)/cf(f)), \tag{3.5}$$

with $sf(f)$ and $cf(f)$ are given by,

$$sf(f) = \int \sin(\theta)S(f,\theta)\mathrm{d}\theta, \tag{3.6}$$

and

$$cf(f) = \int \cos(\theta) S(f, \theta) \mathrm{d}\theta. \tag{3.7}$$

To reduce the discrepancies in spreading estimates that may arise when different spreading estimation methods are used, spreading estimates made with the buoy data are performed using the same method used by ECMWF expressed in terms of the first Fourier coefficients (see Eq.(3.3) to Eq.(3.7)). It is important to stress that the hindcast data may not always accurately capture the sea states measured by the buoys. The significant wave height, which is relatively stable, is first used to assess the accuracy of ECMWF data at the given buoy locations. Figure 3.8 shows a comparison of significant wave height between measured CDIP and hindcast ECMWF data. The blue line shows a line of equality and the red line presents a line fitted to the data using the least square method. A large discrepancy between the two methods can be found for the high significant wave heights which are not considered in this study. The correlation between estimates of significant wave height for significant wave height of between 3 to 4m indicates the ECMWF model may be reasonably accurate in reproducing the conditions measured by the buoys. The measurements in this study with large differences between field and hindcast data will be excluded for directional spreading comparison. Figure 3.9 presents directional spreading estimated by CDIP and ECMWF data as time series. One reason for large differences may be that sea states can become bimodal, which will result in large estimated spreading values for buoy estimates.

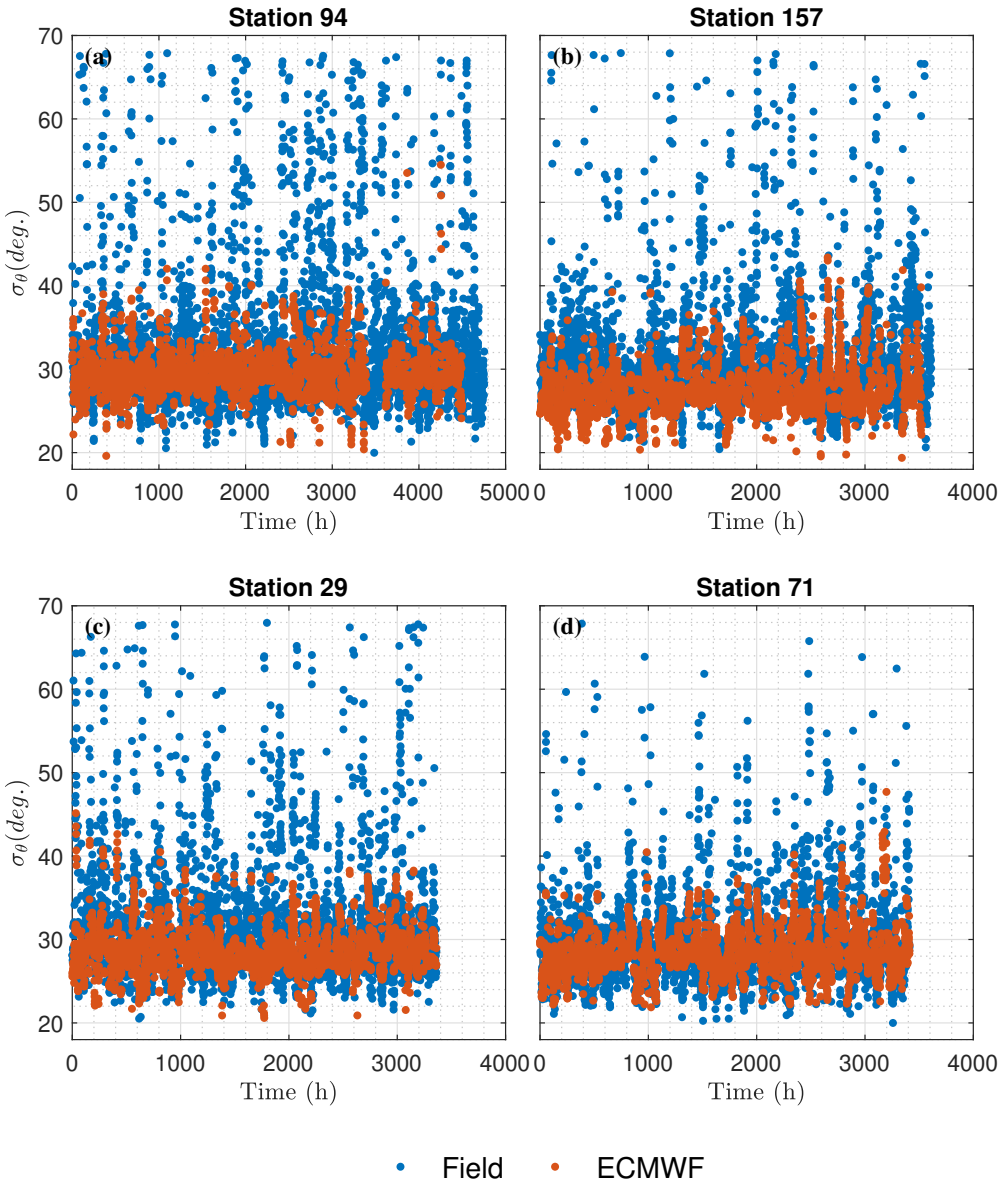


Figure 3.9: (a)-(d) Directional spreading for in situ buoy measurements made using the station 94, 157, 29, 71 and ECMWF hindcast from 2002 to 2019 as a time series. Red and blue markers denote the mean directional spreading from ECMWF hindcast and CDIP field over 30 minutes.

Figure 3.10 shows the dataset where all measurements are shown in blue and the same dataset without bimodal sea states with red markers. Bimodal sea states are identified when two distinct peaks were found in the spectrum for each buoy

measurement. Some large directional spreading indicating bimodal sea states which can not be captured by hindcast data, were detected and removed from the data set. A better correlation between the two estimates of spreading methods can be found in figure 3.11 in which measurements with bimodal sea states have been removed. There are still some large directional spreading after bimodal sea states are removed when multi-modal peaks were not large and distinct, which may not be identified and remain in the data set, causing some of these larger values.

To quantify the differences, the relative error is given by $(\sigma_{\theta F} - \sigma_{\theta E})/\sigma_{\theta E}$ where $\sigma_{\theta F}$ and $\sigma_{\theta E}$ are spreading of field data and ECMWF data respectively. Figure 3.12 shows the differences between the two estimates of spreading for all the buoy stations. Low relative differences can be found for the range of 0.2 normalized mooring distance for stations 29 and 71. The reason is that the number of data in this range is much less than that in other ranges for these stations, which results in low differences. The relative differences decrease with mooring distance. One reason is that when the mooring distances increase, the standard deviation of horizontal motions of buoy decreases which may provide more slightly stable input data for spreading calculation. Figure 3.13 provides the mean significant wave height for four buoy stations. The mean significant wave heights sightly decrease with mooring distances. The accuracy of directional spreading estimates improves with reduced significant wave heights (see section 2.3.1).

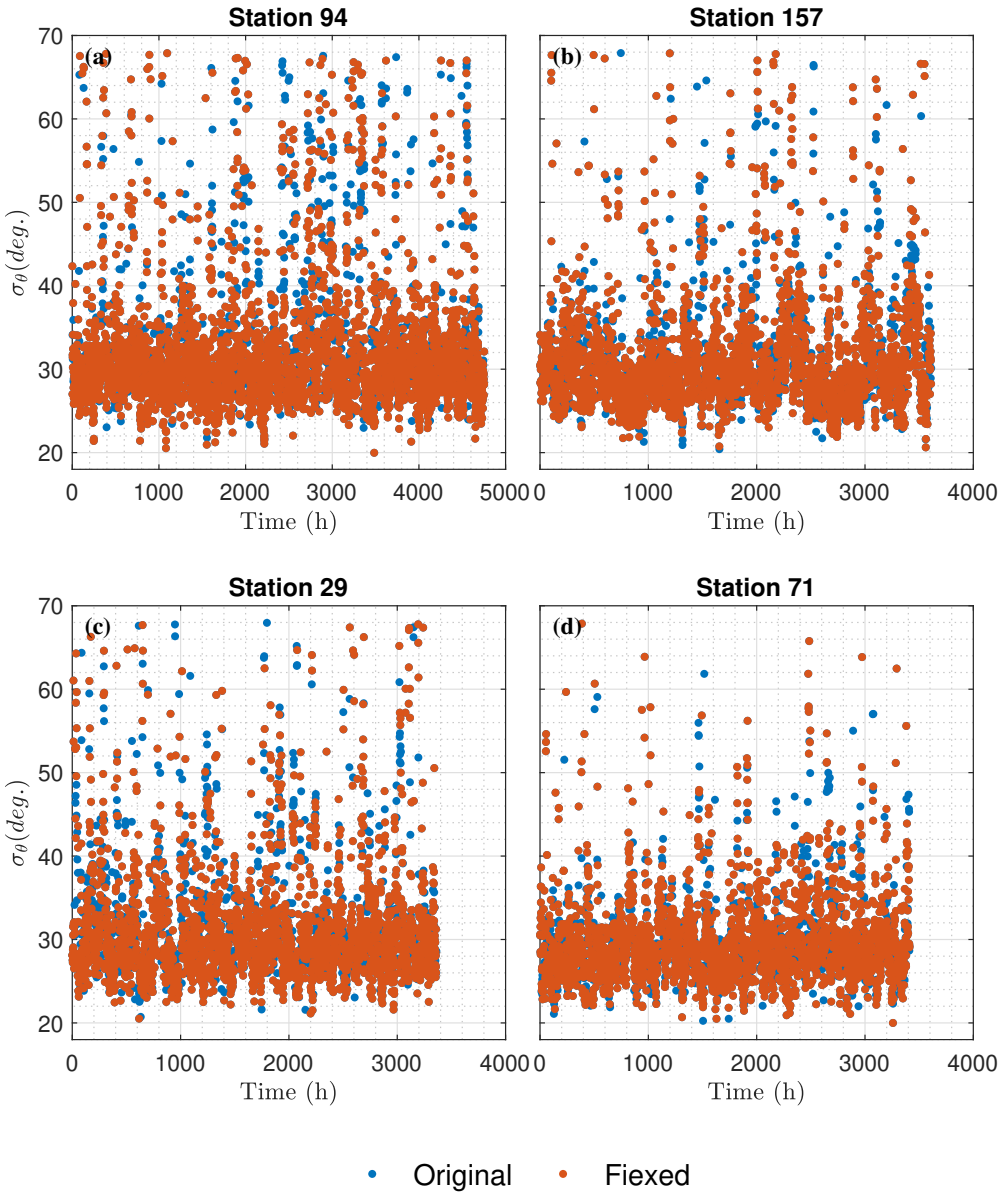


Figure 3.10: (a)-(d) Directional spreading for in situ buoy measurements made using the station 94, 157, 29, 71 from 2002 to 2019 as a function of a time series for original data and fixed data. Blue and red markers denote the original dataset and the data set excluding bimodal sea states.

3.5 Conclusions

In this chapter, I investigate the effects of mooring on measured wave parameters using field buoy data. Previous work has investigated the influence of mooring

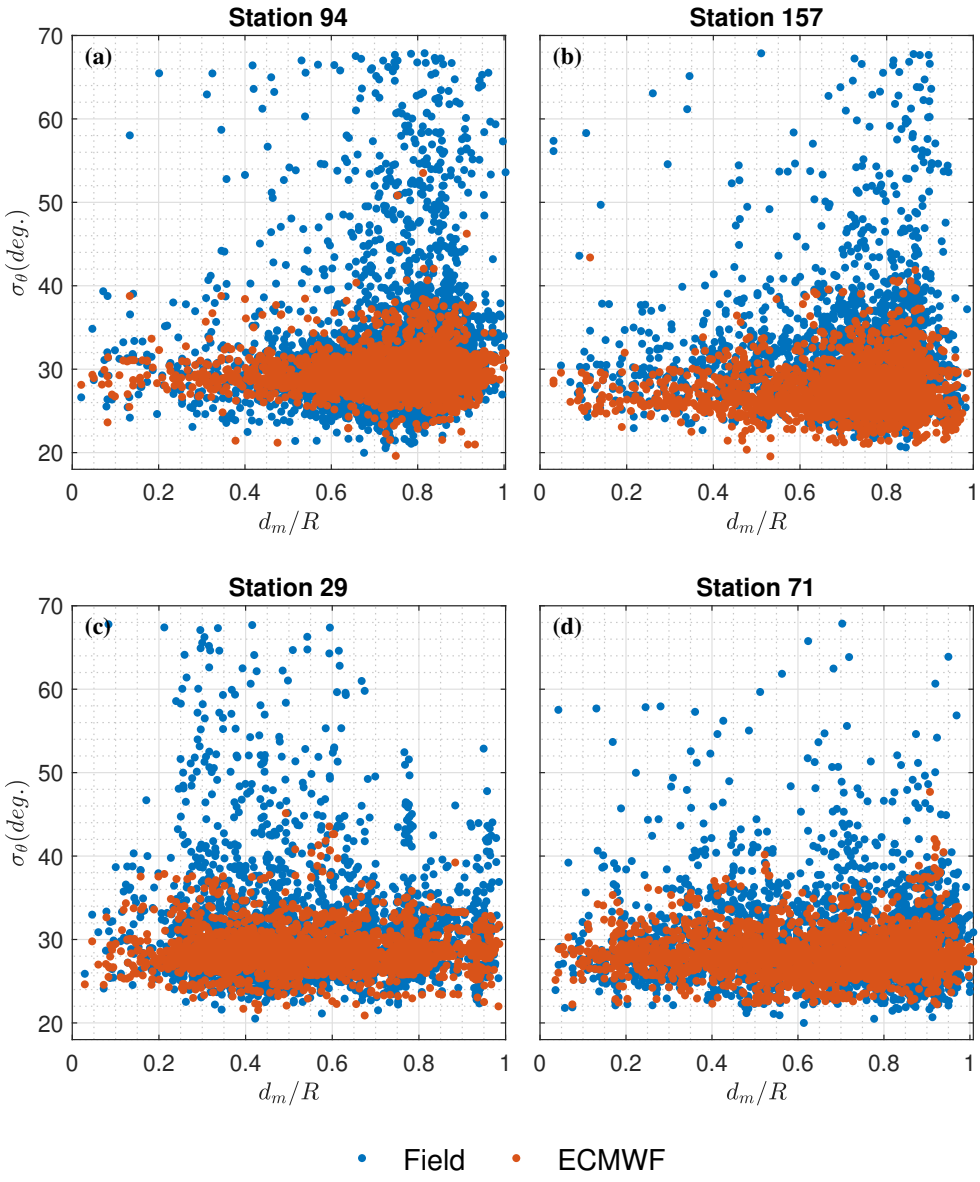


Figure 3.11: (a)-(d) Directional spreading for in situ buoy measurements made using the station 94, 157, 29, 71 and ECMWF hindcast from 2002 to 2019 as a function of normalized mooring distance. Red and blue markers denote the mean directional spreading from ECMWF hindcast and CDIP field over 30 minutes.

dynamics on wave energy converters (Mavrakos and Chatjigeorgiou, 1997; Zhu and Yoo, 2016; Johanning et al., 2007) and studied the effects of moorings on buoys in the lab (McAllister and van den Bremer, 2019; Lin et al., 2022). The

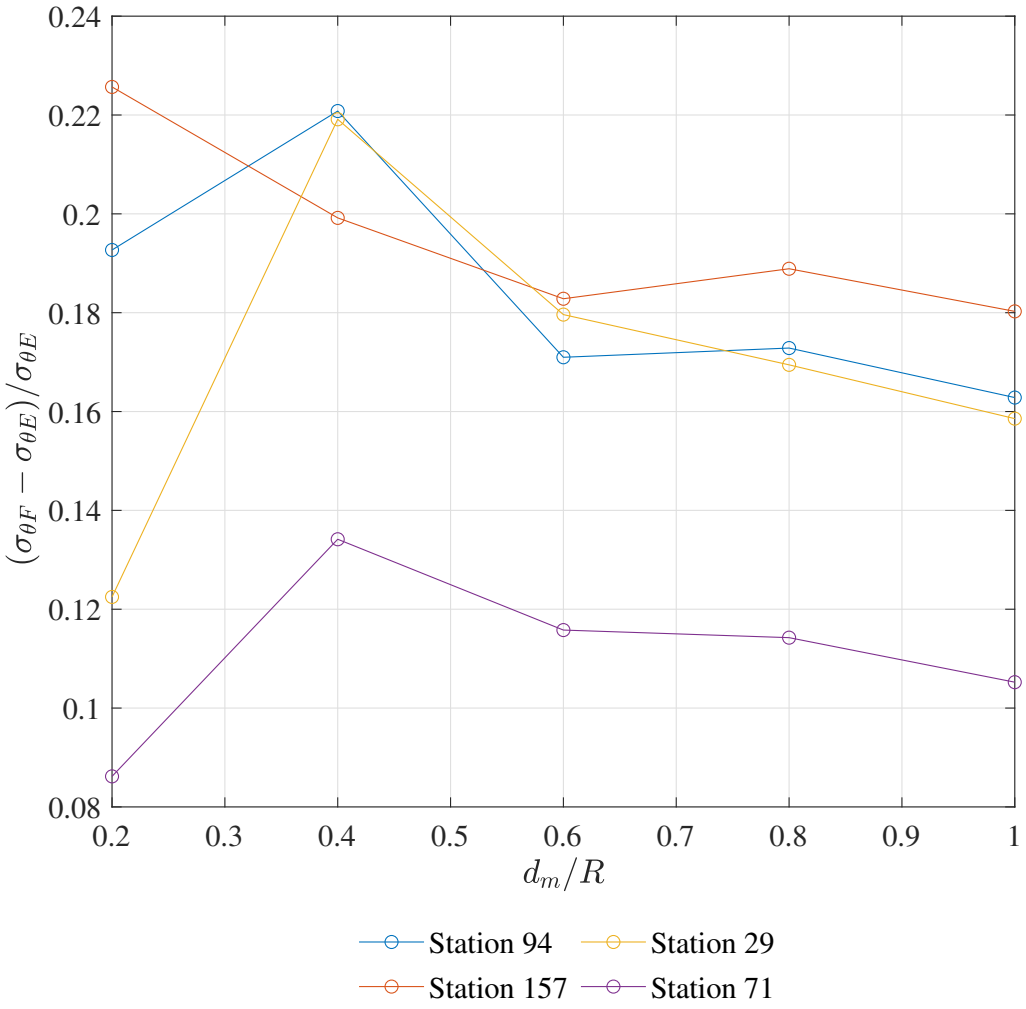


Figure 3.12: The average difference between directional spreading width estimated using field and ECMWF hindcast data for stations 94, 157, 29 and 71

effects of moorings on wave measurements have not been examined in the field. Parameters including skewness, kurtosis, crest distribution and directional spreading are studied in this chapter.

Using the GPS locations, the mooring distance from original deployment point is calculated and used to group the measured dataset into five groups based on equal increments of mooring distance. The data are chosen from similar sea states. There are no obvious relationships between mooring distance and parameters like

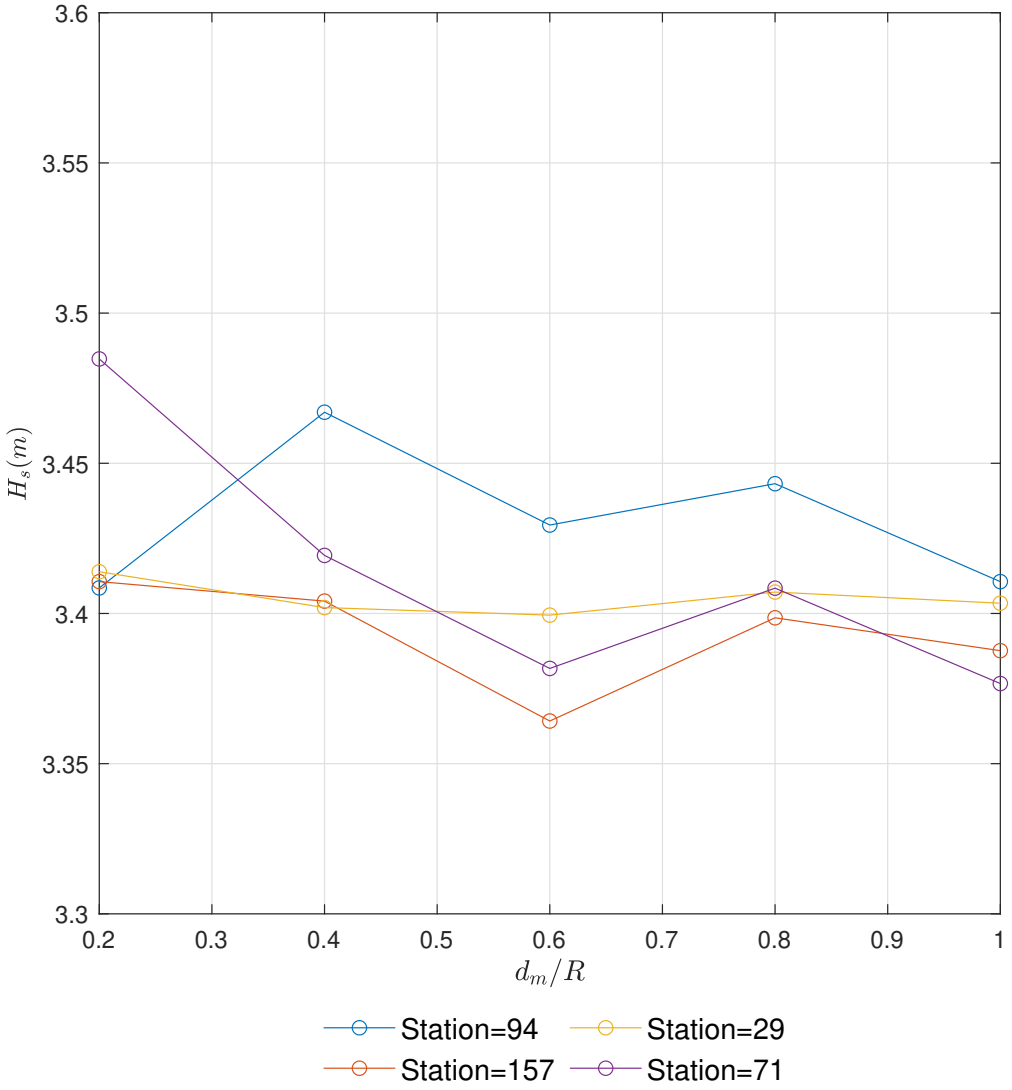


Figure 3.13: The mean significant wave heights for stations 94, 157, 29 and 71

crest distribution, skewness and kurtosis. The differences are very small, which are about 5%, between the five groups based on mooring distance. I limit my analysis using moderate sea states. It is possible that many effects are more apparent in severe sea states

For horizontal motions, the standard deviation of the displacements decreases

slightly with the mooring distance. Estimated directional spreading is then investigated which is compared to ECMWF data. The relative differences are largest at the ranges of 0.4 normalized mooring distance and decrease with mooring distance. The low relative differences at the ranges of 0.2 normalized mooring distance are due to the insufficient data set at this range.

The results demonstrate that estimates of certain wave parameters need to consider the mooring effects. The parameters like skewness and kurtosis need further investigation in severe sea states.

4
Conclusion

In this thesis, two topics related to buoy measurements are considered.

In chapter 2, the use of buoy measurements to perform directional spreading estimates is assessed by comparing gauge and buoy measurements using experimental data. A set of synthetic data are used to find the preferred method of directional analysis method before performing the experimental data. Our results show the EMEP method gives the most stable and accurate results for both gauge and buoy data. Additionally, a fitting method is proposed and applied in this study to give a better directional estimate than using standard deviation.

The analyses are carried out with experimental data in following and crossing sea states. For the following sea states, there are no notable differences between the estimates of directional spreading measured by buoys and gauges near peak frequency. Our results show the spreading estimates presented by buoy measurements are more stable over a wider range of frequencies than that of gauge-array due to the imperfect

configuration of wave gauge array. Bimodality is found at the high frequencies for both measurements, owing to the effects of aliasing, nonlinearity and reflection.

For crossing sea states, the accuracy of directional estimates measured by gauge array is better than that measured by buoys. I find that it is hard to identify two distinct directional peaks and estimate the degree of directional spreading using an individual buoy. Two distinct directional peaks can be detected using the gauge array, whereas degrees of directional spreading are lower than the true values.

The estimates of directional spreading made using buoys with two mooring configurations are examined at the end of chapter 2. We find that there was no observable effect on the directional spreading near the peak frequency between taut and slack mooring configurations, whereas estimates for taut moorings are slightly more stable over a wider range of frequency. The effects of moorings are further studied in chapter 3.

In chapter 3, the mooring influences on buoy measurements are investigated using field data. Buoy data are retrieved from CDIP which can provide sufficient buoy measurements on various positions over a long period. Bulk statistics from four buoy stations are calculated in an attempt to assess the influence of any mooring effects. Our results show there is no observable influence on skewness, kurtosis and wave crest distribution. The differences, we observe, between various mooring distances for these parameters are very small. Whereas, small differences can be found for the horizontal displacements and directional spreading. For the

normalized horizontal displacements, the differences are not very large. A weak trend was found where increasing mooring distance results in a decrease in the standard deviation of horizontal displacements. For the directional spreading, the relative differences between estimates and hindcast values will also reduce generally when the mooring distances become larger, except for the 0.2 normalized mooring distances due to the limited data in this range.

There is much still to explore in developing a good understanding of the buoy measurements of waves. Further comparison needs to be performed using gauge and buoy field data in the same locations. The directional spreading of filed data is frequency dependent which is not considered in the experiments. The additional work to investigate the mooring effects in severe sea states could also be carried out. With the increasing number of new buoys which can measure the currents and waves deployed by CDIP, it would be of considerable practical interest to investigate mooring effects considering currents. It is also worth checking the spectral data provided by SOFAR for buoys with and without moorings.

In the thesis, directional estimates produced using buoy measurements are as good as those produced from gauge measurements for following waves, whereas buoy measurements do not produce stable directional estimates for crossing waves. Mooring effects are detected in the measure of horizontal displacements and directional spreading estimates based on buoy measurements. There is no observable mooring influence on the majority of bulk statistics the work examined.

References

Abdalla, S., P. A. E. M. Janssen, M. A. Balmaseda, K. Mogensen, J.-R. Bidlot, and S. Keeley (2013). "ECMWF Experience In Global Monitoring And Validation Of Radar Altimetry Products". In: *ESA Living Planet Symposium*.

Adcock, T. A. A. and P. H. Taylor (2009). "Estimating ocean wave directional spreading from an Eulerian surface elevation time history". In: *Proc. R. Soc. A* 465.2111, pp. 3361–3381.

Akaike, H. (1997). "Information theory and an extension of the maximum likelihood principle". In: *Selected papers of hirotugu akaike*. Springer, pp. 199–213.

Allender, J., T. Audunson, S. F. Barstow, S. Bjerken, H. E. Krogstad, P. Steinbakke, L. Vartdal, L. E. Borgman, and C. Graham (1989). "The WADIC project: A comprehensive field evaluation of directional wave instrumentation". In: *Ocean Eng.* 16.5-6, pp. 505–536.

Benoit, M. (1993). "Extensive comparison of directional wave analysis methods from gauge array data". In: *Proc. 2nd Int. Symp. on ASCE*, pp. 740–754.

Benoit, M., P. Frigaard, and H. A. Schäffer (1997). "Analysing multidirectional wave spectra: a tentative classification of available methods". In: *Proc. seminar on multidirectional waves and their interaction with structures*, pp. 131–158.

Benoit, M. and C. Teisson (1995). "Laboratory comparison of directional wave measurement systems and analysis techniques". In: *Coast. Eng.* Pp. 42–56.

Bidlot, J.-R., D. J. Holmes, P. A. Wittmann, R. Lalbeharry, and H. S. Chen (2002). "Intercomparison of the performance of operational ocean wave forecasting systems with buoy data". In: *Weather Forecast* 17.2, pp. 287–310.

Borgman, L. E. (1969). "Directional spectra models for design use". In: *OTC*. OnePetro.

Boukhanovsky, A. V. and C. G. Soares (2009). "Modelling of multipeaked directional wave spectra". In: *Appl. Ocean Res.* 31.2, pp. 132–141.

Brodtkorb, P. A., P. Johannesson, G. Lindgren, I. Rychlik, J. Rydén, and E. Sjö (2000). "WAFO-a Matlab toolbox for analysis of random waves and loads". In: *10th Int. J. Offshore Polar Eng.* OnePetro.

Buchner, B., G. Forristall, K. Ewans, M. Christou, and J. Hennig (2011). "New Insights in Extreme Crest Height Distributions: A Summary of the 'CresT'JIP". In: *Int. Conf. OMAE*. Vol. 44342, pp. 589–604.

Capon, J., R. Greenfield, and R. J. Kolker (1967). "Multidimensional maximum-likelihood processing of a large aperture seismic array". In: *Proc. IEEE* 55.2, pp. 192–211.

Cartwright, D. E. (1961). "The use of directional spectra in studying the output of a wave recorder on a moving ship". In: *National Institute of Oceanography, Wormley, Surray, UK, Presented at the Conference on Wave Spectra, Easton, Maryland*.

Christou, M. and K. Ewans (2014). "Field measurements of rogue water waves". In: *J. Phys. Oceanogr.* 44.9, pp. 2317–2335.

Dalzell, J. (1999). "A note on finite depth second-order wave–wave interactions". In: *Appl. Ocean Res.* 21.3, pp. 105–111.

Datawell, B. (2006). "Datawell Waverider reference manual". In: *Datawell BV, Zumerlustraat* 4, p. 2012.

Dean, R. (1981). "Simulation of wave systems due to nonlinear directional spectra." In: *Proc. Int. Symp. on Hydrodyn. in Oc. Engrg., Norwegian Hydrodynamics Laboratory.* Pp. 1211–1222.

Draycott, S., T. Davey, D. M. Ingram, J. Lawrence, A. Day, and L. Johanning (2015). "Using a Phase-Time-Path-Difference Approach to measure directional wave spectra in FloWave". In: *EWTEC Conf. Congr.*

Dysthe, K., H. E. Krogstad, and P. Müller (2008). "Oceanic rogue waves". In: *Annu. Rev. Fluid Mech.* 40, pp. 287–310.

Emmanuel, O., J. Ruscoe, J. Side, R. Harris, S. Kerr, C. Bullen, et al. (2010). "An overview of recent technologies on wave and current measurement in coastal and marine applications". In: *JOMS* 1.1, pp. 001–010.

Esteva, D. (1977). "Wave direction computations with three gage arrays". In: *Coast. Eng.* Pp. 349–367.

Fedele, F. (2015). "On the kurtosis of deep-water gravity waves". In: *J. Fluid Mech.* 782, pp. 25–36.

Fedele, F. and F. Arena (2005). "Weakly nonlinear statistics of high random waves". In: *Phys. Fluids* 17.2, p. 026601.

Fenton, J. D. (1985). "A fifth-order Stokes theory for steady waves". In: *J. Waterw. Port, Coast.* 111.2, pp. 216–234.

Forristall, G. Z. (2000). "Wave crest distributions: Observations and second-order theory". In: *J. Phys. Oceanogr.* 30.8, pp. 1931–1943.

Gibbs, R. H. and P. H. Taylor (2005). "Formation of walls of water in 'fully' nonlinear simulations". In: *Appl. Ocean Res.* 27.3, pp. 142–157.

Gobat, J. I. and M. A. Grosenbaugh (2001). "A simple model for heave-induced dynamic tension in catenary moorings". In: *Appl. Ocean Res.* 23.3, pp. 159–174.

Gould, W. and E. Sambuco (1975). "The effect of mooring type on measured values of ocean currents". In: *Deep-Sea Res. Oceanogr. Abstr.* Vol. 22. 1. Elsevier, pp. 55–62.

Hashimoto, N. (1997). "Analysis of the directional wave spectrum from field data". In: *Adv. Coast. Ocean Eng.* 3, pp. 103–144.

Hashimoto, N. and K. Kobune (1989). "Directional spectrum estimation from a Bayesian approach". In: *Coast. Eng.* Pp. 62–76.

Hashimoto, N., T. Nagai, and T. Asai (1995). "Extension of the maximum entropy principle method for directional wave spectrum estimation". In: *Coast. Eng.* Pp. 232–246.

Hasselmann, D. E., M. Dunckel, and J. Ewing (1980). "Directional wave spectra observed during JONSWAP 1973". In: *J. Phys. Oceanogr.* 10.8, pp. 1264–1280.

Hasselmann, K., T. P. Barnett, E. Bouws, H. Carlson, D. E. Cartwright, K. Enke, J. A. Ewing, H. Gienapp, D. E. Hasselmann, and Kruseman (1973). "Measurements of wind-wave growth and swell decay during the Joint North Sea Wave Project (JONSWAP)". In: *Ergänzungsheft 8-12.*

Holthuijsen, L. H. (2010). *Waves in oceanic and coastal waters.* Cambridge university press.

Humphery, J. (1982). "Operational experiences with Waverider buoys and their moorings". In: *Inst. Oceanogr. Sci.*

Isaacson, M. d. S. Q. and S. Sinha (1986). "Directional wave effects on large offshore structures". In: *J. Waterw* 112.4, pp. 482–497.

Isobe, M., K. Kondo, and K. Horikawa (1984). "Extension of MLM for estimating directional wave spectrum". In: *Proc. Symp. on Description and modeling of directional seas*, pp. 1–15.

Jaynes, E. T. (1957). "Information theory and statistical mechanics". In: *Physical review* 106.4, p. 620.

Jefferys, E. (1987). "Directional seas should be ergodic". In: *Appl. Ocean Res.* 9.4, pp. 186–191.

Johanning, L., G. H. Smith, and J. Wolfram (2007). "Measurements of static and dynamic mooring line damping and their importance for floating WEC devices". In: *Ocean Eng.* 34.14-15, pp. 1918–1934.

Joosten, H. (2006). "Directional wave buoys and their elastic mooring". In: *Int. Ocean Syst.* 10.4, pp. 18–21.

Karmpadakis, I., C. Swan, and M. Christou (2019). "Laboratory investigation of crest height statistics in intermediate water depths". In: *Proc. R. Soc. A* 475.2229, p. 20190183.

Kobune, K. and N. Hashimoto (1986). "Estimation of directional spectra from the maximum entropy principle". In: *Int. Conf. Offshore Mech. Arct. Eng. Symposium. 5*, pp. 80–85.

Krogstad, H. E. (1988). "Maximum likelihood estimation of ocean wave spectra from general arrays of wave gauges". In: *Model. Identif. Control.* 9.2, p. 81.

Kuik, A. J., G. P. Van Vledder, and L. Holthuijsen (1988). "A method for the routine analysis of pitch-and-roll buoy wave data". In: *J. Phys. Oceanogr.* 18.7, pp. 1020–1034.

Latheef, M. and C. Swan (2013). "A laboratory study of wave crest statistics and the role of directional spreading". In: *Proc. R. Soc. A* 469.2152, p. 20120696.

Latheef, M., C. Swan, and J. Spinneken (2017). "A laboratory study of nonlinear changes in the directionality of extreme seas". In: *Proc. R. Soc. A* 473.2199, p. 20160290.

Le Merle, E., D. Hauser, C. Peureux, L. Aouf, P. Schippers, C. Dufour, and A. Dalphinet (2021). "Directional and frequency spread of surface ocean waves from SWIM measurements". In: *J. Geophys. Res.: Oceans* 126.7, e2021JC017220.

Lin, Y.-P., C.-J. Huang, and S.-H. Chen (2020). "Variations in directional wave parameters obtained from data measured using a GNSS buoy". In: *Ocean Eng.* 209, p. 107513.

Lin, Z., T. A. Adcock, and M. L. McAllister (2022). "Estimating ocean wave directional spreading using wave following buoys: a comparison of experimental buoy and gauge data". In: *J. Ocean Eng. Mar. Energy.* 8.1, pp. 83–97.

Liu, Q., T. Lewis, Y. Zhang, and W. Sheng (2015). "Performance assessment of wave measurements of wave buoys". In: *Int. J. Mar. Energy* 12, pp. 63–76.

Long, R. B. and K. Hasselmann (1979). "A variational technique for extracting directional spectra from multi-component wave data". In: *J. Phys. Oceanogr.* 9.2, pp. 373–381.

Longuet-Higgins, M. S. (1952). "On the statisticaldistribution of the height of sea waves". In: *JMR* 11, pp. 245–266.

— (1961). "Observations of the directional spectrum of sea waves using the motions of a floating buoy". In: *Ocean wave spectra*.

— (1963). "The effect of non-linearities on statistical distributions in the theory of sea waves". In: *J. Fluid Mech.* 17.3, pp. 459–480.

Longuet-Higgins, M. S. (1986). "Eulerian and Lagrangian aspects of surface waves". In: *J. Fluid Mech.* 173, pp. 683–707.

Lucas, C. and C. G. Soares (2015). "On the modelling of swell spectra". In: *Ocean Eng.* 108, pp. 749–759.

Lygre, A. and H. E. Krogstad (1986). "Maximum entropy estimation of the directional distribution in ocean wave spectra". In: *J. Phys. Oceanogr.* 16.12, pp. 2052–2060.

Marsden, R. and B. Juszko (1987). "An eigenvector method for the calculation of directional spectra from heave, pitch and roll buoy data". In: *J. Phys. Oceanogr.* 17.12, pp. 2157–2167.

Mavrakos, S. and J. Chatjigeorgiou (1997). "Dynamic behaviour of deep water mooring lines with submerged buoys". In: *Comput. Struct.* 64.1-4, pp. 819–835.

McAllister, M. L. and T. S. van den Bremer (2019). "Lagrangian measurement of steep directionally spread ocean waves: Second-order motion of a wave-following measurement buoy". In: *J. Phys. Oceanogr.* 49.12, pp. 3087–3108.

— (2020). "Experimental Study of the Statistical Properties of Directionally Spread Ocean Waves Measured by Buoys". In: *J. Phys. Oceanogr.* 50.2, pp. 399–414.

McAllister, M. L., V. Venugopal, and A. G. L. Borthwick (2017). "Wave directional spreading from point field measurements". In: *Proc. R. Soc. A* 473.2200, p. 20160781.

McAllister, M. L., S. Draycott, T. Adcock, P. Taylor, and T. Van Den Bremer (2019). "Laboratory recreation of the Draupner wave and the role of breaking in crossing seas". In: *J. Fluid Mech.* 860, pp. 767–786.

Miles, M. and E. Funke (1989). "A comparison of methods for synthesis of directional seas". In: *J. Offshore Mech. Arct. Eng.* 111, pp. 43–48.

Mitsuyasu, H., F. Tasai, T. Suhara, S. Mizuno, M. Ohkusu, T. Honda, and K. Rikiishi (1975). "Observations of the directional spectrum of ocean WavesUsing a cloverleaf buoy". In: *J. Phys. Oceanogr.* 5.4, pp. 750–760.

Niclasen, B. and K. Simonsen (2007). "Note on wave parameters from moored wave buoys". In: *Appl. Ocean Res.* 29.4, pp. 231–238.

Nwogu, O. (1989). "Maximum entropy estimation of directional wave spectra from an array of wave probes". In: *Appl. Ocean Res.* 11.4, pp. 176–182.

O'Reilly, W. C., T. H. C. Herbers, R. Seymour, and R. T. Guza (1996). "A comparison of directional buoy and fixed platform measurements of Pacific swell". In: *J. Atmos. Oceanic Technol.* 13.1, pp. 231–238.

Oltman-Shay, J. and R. Guza (1984). "A data-adaptive ocean wave directional-spectrum estimator for pitch and roll type measurements". In: *J. Phys. Oceanogr.* 14.11, pp. 1800–1810.

Onorato, M., A. R. Osborne, M. Serio, L. Cavaleri, C. Brandini, and C. T. Stansberg (2006). "Extreme waves, modulational instability and second order theory: wave flume experiments on irregular waves". In: *Eur. J. Mech. B Fluids* 25.5, pp. 586–601.

Pierson, W. J. and L. Moskowitz (1964). "A proposed spectral form for fully developed wind seas based on the similarity theory of SA Kitaigorodskii". In: *J. Geophys. Res.* 69.24, pp. 5181–5190.

Prevosto, M. (1998). "Effect of directional spreading and spectral bandwidth on the nonlinearity of the irregular waves". In: *8th Int. J. Offshore Polar Eng.* OnePetro.

Shemer, L., A. Sergeeva, and D. Liberzon (2010). "Effect of the initial spectrum on the spatial evolution of statistics of unidirectional nonlinear random waves". In: *J. Geophys. Res. Oceans* 115.C12.

Soares, C. G. (1984). "Representation of double-peaked sea wave spectra". In: *Ocean Eng.* 11.2, pp. 185–207.

Stokes, G. G. (1880). "On the theory of oscillatory waves". In: *Trans. Cambridge Philos. Soc.*

Tayfun, M. A. (1980). "Narrow-band nonlinear sea waves". In: *J. Geophys. Res. Oceans* 85.C3, pp. 1548–1552.

Tayfun, M. A. and F. Fedele (2007). "Wave-height distributions and nonlinear effects". In: *Ocean Eng.* 34.11-12, pp. 1631–1649.

Tucker, M. J. and E. G. Pitt (2001). *Waves in ocean engineering*. Vol. 5.

Van Essen, S., K. Ewans, and J. McConochie (2018). "Wave buoy performance in short and long waves, evaluated using tests on a hexapod". In: *Int. Conf. OMAE*. Vol. 51272. American Society of Mechanical Engineers, V07BT06A001.

Veritas, N. (2000). *Environmental conditions and environmental loads*. Det Norske Veritas.

Walden, R. G., D. H. DeBok, J. B. Gregory, D. G. Meggitt, and W. A. Vachon (1977). "The mooring dynamics experiment-A major study of the dynamics of buoys in the deep ocean". In: *OTC*. OnePetro.

Wang, J., B. Li, Z. Gao, and J. Wang (2019). "Comparison of ECMWF significant wave height forecasts in the China sea with buoy data". In: *Weather Forecast* 34.6, pp. 1693–1704.

Yoon, S. B., J.-I. Lee, Y.-T. Kim, and C. H. Shin (2018). "Laboratory and numerical experiments on stem waves due to monochromatic waves along a vertical wall". In: *Nonlinear Processes in Geophysics* 25.3, pp. 521–535.

Young, I. (1994). "On the measurement of directional wave spectra". In: *Appl. Ocean Res.* 16.5, pp. 283–294.

Young, I., L. Verhagen, and M. Banner (1995). "A note on the bimodal directional spreading of fetch-limited wind waves". In: *J. Geophys. Res.: Oceans* 100.C1, pp. 773–778.

Zhu, X. and W. S. Yoo (2016). "Dynamic analysis of a floating spherical buoy fastened by mooring cables". In: *Ocean Eng.* 121, pp. 462–471.